

Understanding the Momentum Risk Premium: An In-Depth Journey Through Trend-Following Strategies*

Paul Jusselin
Quantitative Research
Amundi Asset Management, Paris
paul.jusselin@amundi.com

Hassan Malongo
Quantitative Research
Amundi Asset Management, Paris
hassan.malongo@amundi.com

Thierry Roncalli
Quantitative Research
Amundi Asset Management, Paris
thierry.roncalli@amundi.com

Edmond Lezmi
Quantitative Research
Amundi Asset Management, Paris
edmond.lezmi@amundi.com

Côme Masselin
Quantitative Research
Amundi Asset Management, Paris
come.masselin@amundi.com

Tung-Lam Dao
Independent Researcher
Paris
daotunglam2001@gmail.com

September 2017

Abstract

Momentum risk premium is one of the most important alternative risk premia. Since it is considered a market anomaly, it is not always well understood. Many publications on this topic are therefore based on backtesting and empirical results. However, some academic studies have developed a theoretical framework that allows us to understand the behavior of such strategies. In this paper, we extend the model of Bruder and Gausset (2011) to the multivariate case. We can find the main properties found in academic literature, and obtain new theoretical findings on the momentum risk premium. In particular, we revisit the payoff of trend-following strategies, and analyze the impact of the asset universe on the risk/return profile. We also compare empirical stylized facts with the theoretical results obtained from our model. Finally, we study the hedging properties of trend-following strategies.

Keywords: Momentum risk premium, trend-following strategy, cross-section momentum, time-series momentum, alternative risk premium, market anomaly, diversification, correlation, payoff, trading impact, hedging, skewness, Gaussian quadratic forms, Kalman filter, EWMA.

JEL classification: C50, C60, G11.

*The authors are very grateful to Alexandre Burgues, Edouard Knockaert, Didier Maillard, Raphaël Sobotka and Bruno Taillardat for their helpful comments. Thierry Roncalli would like to thank Benjamin Bruder and Nicolas Gausset who first developed the theoretical framework in the univariate case. He is also very grateful to Tung-Lam Dao, who worked on the multivariate case during his internship in 2011 and obtained some of the formulas presented in this working paper. It was logical that Tung-Lam should be our co-author. Corresponding author: thierry.roncalli@amundi.com

1 Introduction

Momentum is one of the oldest and most popular trading strategies in the investment industry. For instance, momentum strategies are crucial to commodity trading advisors (CTAs) and managed futures (MFs) in the hedge funds industry. They also represent the basic trading rules that are described in the famous Turtle trading experiment held by Richard Dennis and William Eckhardt in the nineteen-eighties¹. Momentum strategies are also highly popular among asset managers. By analyzing the quarterly portfolio holdings of 155 equity mutual funds between 1974 and 1984, Grinblatt *et al.* (1995) found that “77% of these mutual funds were momentum investors”. Another important fact concerns the relationship between options and momentum. Indeed, it is well-known that the manufacturing of structured products is based on momentum strategies. Hedging demand from retail and institutional investors is therefore an important factor explaining the momentum style.

In practice, momentum encompasses different types of management strategies. However, trend-following strategies are certainly the main component. There is strong evidence that trend-following investing is one of the more profitable styles, generating positive excess returns for a very long time. Thus, Lempérière *et al.* (2014b) and Hurst *et al.* (2014) backtest this strategy over more than a century, and establish the existence of trends across different asset classes and different study periods. This is particularly true for equities and commodities. For these two asset classes, the momentum risk factor has been extensively documented by academics since the end of nineteen-eighties. Jegadeesh and Titman (1993) showed evidence of return predictability based on past returns in the equity market. They found that buying stocks that have performed well over the past three to twelve months and selling stocks that have performed poorly produces abnormal positive returns. Since this publication, many academic works have confirmed the pertinence of this momentum strategy (e.g. Carhart, 1997; Rouwenhorst, 1998; Grundy and Martin, 2001; Fama and French, 2012). In the case of commodities, there is an even larger number of studies². However, the nature of momentum strategies in commodity markets is different than in equity markets, because of backwardation and contango effects (Miffre and Rallis, 2007). More recently, academics have investigated momentum investing in other asset classes and also found evidence in fixed-income and currency markets (Moskowitz *et al.*, 2012; Asness *et al.*, 2013).

The recent development of alternative risk premia impacts the place of momentum investing for institutional investors, such as pension funds and sovereign wealth funds (Ang, 2014; Hamdan *et al.*, 2016). Since they are typically long-term and contrarian investors, momentum strategies were relatively rare among these institutions. However, the significant growth of factor investing in equities has changed their view of momentum investing. Today, many institutional investors build their strategic asset allocation (SAA) using a multi-factor portfolio that is exposed to size, value, momentum, low beta and quality risk factors (Cazalé and Roncalli, 2014). This framework has been extended to multi-asset classes, including rates, credit, currencies and commodities. In particular, carry, momentum and value are now considered as three risk premia that must be included in a strategic allocation in order to improve the diversification of traditional risk premia portfolios (Roncalli, 2017). However, the correlation diversification approach, which consists in optimizing the portfolio's volatility (Markowitz, 1952), is inadequate for managing a universe of traditional and alternative risk premia, because the relationships between these risk premia are non-linear. Moreover, carry, momentum and value exhibit different skewness patterns (Lempérière *et al.*, 2014).

¹See <http://www.investopedia.com/articles/trading/08/turtle-trading.asp>

²For example, we can cite Elton *et al.* (1987), Likac *et al.* (1988), Taylor and Tari (1989), Erb and Harvey (2006), Szakmary *et al.* (2010) and Gorton *et al* (2013).

This is why carry and value are generally considered as skewness risk premia³, whereas momentum is a market anomaly⁴. In this context, the payoff approach is more appropriate for understanding the diversification of SAA portfolios. More precisely, mixing concave and convex strategies is crucial for managing the skewness risk of diversified portfolios.

Since momentum investing may now be part of a long-term asset allocation, institutional investors need to better understand the behavior of such strategies. However, the investment industry is generally dominated by the syndrome of backtesting. Backtests focus on the past performance of trend-following strategies. Analyzing the risk and understanding the behavior of such strategies is more challenging. However, the existence of academic and theoretical literature on this topic may help these institutional investors to investigate these topics. We notably think that some research studies are essential to understand the dynamics of these strategies beyond the overall performance of momentum investing. These research works are Fung and Hsieh (2001), Potters and Bouchaud (2006), Bruder and Gausse (2011) and Dao *et al.* (2016).

Fung and Hsieh (2001) developed a general methodology to show that “*trend followers have nonlinear, option-like trading strategies*”. In particular, they showed that a trend-following strategy is similar to a lookback straddle option, and exhibits a convex payoff. They then deduced that it has a positive skewness. Moreover, they noticed a relationship between a trend-following strategy and a long volatility strategy. By developing a theoretical framework and connecting their results to empirical facts, this research marks a break with previous academic studies, and has strongly influenced later research on the momentum risk premium.

Potters and Bouchaud (2006) published another important paper on this topic. In particular, they derived the analytical shape of the corresponding probability distribution function. The P&L of trend-following strategies has an asymmetric right-skewed distribution. They also focused on the hit ratio (or the fraction of winning trades), and showed that the best case is obtained when the asset volatility is low. In this situation, the hit ratio is equal to 50%. However, the hit ratio decreases rapidly when volatility increases. This is why they concluded that “*trend followers lose more often than they gain*”. Since the average P&L per trade is equal to zero in their model, Potters and Bouchaud (2006) also showed that the average gain is larger than the average loss. Therefore, they confirmed the convex option profile of the momentum risk premium.

The paper of Bruder and Gausse (2011) is not focused on momentum, but is concerned more generally with dynamic investment strategies, including stop-loss, contrarian, averaging and trend-following strategies. They adopted an option-like approach and developed a general framework, where the P&L of a dynamic strategy is decomposed into an option profile and a trading impact. The option profile can be seen as the intrinsic value of the option, whereas the trading impact is equivalent to its time value. By applying this framework to a continuous-time trend-following model, Bruder and Gausse (2011) confirmed the results found by Fung and Hsieh (2001) and Potters and Bouchaud (2006): the option profile is convex, the skewness is positive, the hit ratio is lower than 50% and the average gain is larger than the average loss. They also highlight the important role of the Sharpe ratio and the moving average duration in order to understand the P&L. In particular, a necessary condition to obtain a positive return is that the absolute value of the Sharpe ratio is greater than the inverse of the moving average duration. Another important result is the behavior of the trading impact, which has a negative vega. Moreover, the loss of the trend-following strategy is bounded, and is proportional to the square of the volatility.

³A skewness risk premium is rewarded for taking a systematic risk in bad times (Ang, 2014).

⁴The performance of a market anomaly is explained by behavioral theories, not by a systematic risk.

The paper of Dao *et al.* (2016) goes one step further by establishing the relationship between trend-following strategies and the term structure of realized volatility. More specifically, the authors showed that “*the performance of the trend is positive when the long-term volatility is larger than the short-term volatility*”. Therefore, trend followers have to risk-manage the short-term volatility in order to exhibit a positive skewness and a positive convexity. Another interesting result is that the authors are able to replicate the cumulative performance of the SGA CTA Index, which is the benchmark used by professionals for analyzing CTA hedge funds. Another major contribution by Dao *et al.* (2016) concerns the hedging properties of trend-following strategies. They demonstrated that the payoff of the trend-following strategy is similar to the payoff of an equally-weighted portfolio of ATM strangles. They then compared the two approaches for hedging a long-only exposure. They noticed that the strangle portfolio paid a fixed price for the short-term volatility, whereas the trend-following strategy is directly exposed to the short-term volatility. On the contrary, the premium paid on options markets is high. The authors finally concluded that “*even if options provide a better hedge, trend-following is a much cheaper way to hedge long-only exposures*”.

Our research is based on the original model of Bruder and Gaussel (2011). The idea is to confirm the statistical results cited above using a unique framework in terms of convexity, probability distribution, hit ratio, skewness, etc. Since it is a continuous-time model, we can extend the analysis to the multivariate case, and derive the corresponding statistical properties of the trend-following strategy applied to a multi-asset universe. Contrary to the previous studies, we can analyze the impact of asset correlations on the performance of trend-following strategies. It appears that the concept of diversification in a long/short approach is different and more complex than for a long-only portfolio. Therefore, three parameters are important to understand the behavior of the momentum risk premium: the vector of Sharpe ratios, the covariance matrix of asset returns, and the frequency matrix of the moving average estimator. The sensitivity of the P&L to these three key parameters is of particular interest for investors and professionals.

Today, a significant part of investments in CTAs and trend-following programs is motivated by a risk management approach, and not only by performance considerations. In particular, some investors are tempted to use CTAs as a hedging program without paying a hedging premium (Dao *et al.*, 2016). Therefore, we extend the model by mixing long-only and trend-following exposures in order to measure the hedging quality of the momentum strategy, and to see if it can be a tool for tail risk management and downside protection.

This paper is organized as follows. In Section Two, we present the model of Bruder and Gaussel (2011). We derive new results concerning the statistical properties of the trading impact. We also analyze the impact of leverage on the ruin probability. Then, we extend the model to the multivariate case. This allows us to measure the impact of asset correlations, and the influence of the choice of the moving average. Using the multivariate model, we can also draw a distinction between time-series and cross-section momentum. In Section Three, we study the empirical properties of trend-following strategies. We show how to decompose the P&L of the strategy into low- and high-frequency components. We then study the optimal estimation of the trend frequency, and the relationship between trends and risk premia. We also replicate the cumulative performance of the SG CTA Index by using our theoretical model. Section Four deals with downside protection and the hedging properties of the trend-following strategy. We analyze the single asset case, and calculate the analytical probability distribution and the value-at-risk of the hedged portfolio. The multivariate case is also considered, and particularly the cross-hedging strategy, when we hedge one asset by another asset. Then, we illustrate the behavior of the trend-following strategy in presence of skewness events. Finally, Section Five summarizes the different results of the paper.

2 A model of a trend-following strategy

2.1 The Bruder-Gaussel framework

2.1.1 Estimating the trend with an exponential weighted moving average

Bruder and Gaussel (2011) assume that the asset price S_t follows a geometric Brownian motion with constant volatility, but with a time-varying trend:

$$\begin{cases} dS_t = \mu_t S_t dt + \sigma S_t dW_t \\ d\mu_t = \gamma dW_t^* \end{cases}$$

where μ_t is the unobservable trend. By introducing the notation $dy_t = dS_t/S_t$, we obtain:

$$dy_t = \mu_t dt + \sigma dW_t$$

We denote $\hat{\mu}_t = \mathbb{E}[\mu_t | \mathcal{F}_t]$ the estimator of the trend μ_t with respect to the filtration \mathcal{F}_t . Bruder and Gaussel (2011) show that $\hat{\mu}_t$ is an exponential weighted moving average (EWMA) estimator:

$$\hat{\mu}_t = \lambda \int_0^t e^{-\lambda(t-u)} dy_u + e^{-\lambda t} \hat{\mu}_0$$

where $\lambda = \sigma^{-1}\gamma$ is the EWMA parameter. λ is related to the average duration of the moving average filter and control the measurement noise filtering (Potters and Bouchaud, 2006).

2.1.2 P&L of the trend-following strategy

Bruder and Gaussel (2011) assume that the exposure of the trading strategy is proportional to the estimated trend of the asset:

$$e_t = \alpha \hat{\mu}_t$$

Therefore, the dynamics of the investor's P&L V_t are given by:

$$\begin{aligned} \frac{dV_t}{V_t} &= e_t \frac{dS_t}{S_t} \\ &= \alpha \hat{\mu}_t dy_t \end{aligned}$$

Bruder and Gaussel (2011) show that:

$$\ln \frac{V_T}{V_0} = \frac{\alpha}{2\lambda} (\hat{\mu}_T^2 - \hat{\mu}_0^2) + \alpha \sigma^2 \int_0^T \left(\frac{\hat{\mu}_t^2}{\sigma^2} \left(1 - \frac{\alpha \sigma^2}{2} \right) - \frac{\lambda}{2} \right) dt$$

Remark 1 An alternative specification of the exposure is:

$$e_t = \frac{\ell}{\sigma^2} \sqrt{\lambda} \hat{\mu}_t$$

where ℓ is the standardized exposure. In this case, the exposure is normalized such that dV_t/V_t is of order one and has approximatively the same volatility. This specification is a special case of the general model where $\alpha = \ell \sigma^{-2} \sqrt{\lambda}$.

2.1.3 Relationship with option trading

The return of the trend-following strategy is composed of two terms:

$$\ln \frac{V_T}{V_0} = G_{0,T} + \int_0^T g_t dt$$

where the short-run component is:

$$G_{0,T} = \frac{\alpha}{2\lambda} (\hat{\mu}_T^2 - \hat{\mu}_0^2)$$

and the long-run component is⁵:

$$g_t = \alpha \sigma^2 \left(\frac{\hat{\mu}_t^2}{\sigma^2} \left(1 - \frac{\alpha \sigma^2}{2} \right) - \frac{\lambda}{2} \right)$$

Bruder and Gaussel (2011) interpret $G_{0,T}$ as the option profile and g_t as the trading impact. This result relates to the robustness of the Black-Scholes formula. El Karoui *et al.* (1998) assume that the underlying price process is given by:

$$dS_t = \mu_t S_t dt + \sigma_t S_t dW_t$$

whereas the trader hedges the European option with the implied volatility Σ , meaning that the risk-neutral process is:

$$dS_t = rS_t dt + \Sigma S_t dW_t^\mathbb{Q}$$

They show that the value of the delta-hedging strategy is equal to:

$$V_T = G_{0,T} + \frac{1}{2} \int_0^T e^{r(T-t)} \Gamma_t (\Sigma^2 - \sigma_t^2) S_t^2 dt$$

where $G_{0,T}$ is the payoff of the European option and Γ_t is the gamma sensitivity coefficient. It follows that a positive P&L is achieved by overestimating the realized volatility if the gamma is positive, and underestimating the realized volatility if the gamma is negative.

In Figure 1, we have reported the option profile $G_{0,T}$ of the trend-following strategy with respect to the final trend $\hat{\mu}_T$ when the parameters are the following: $\alpha = 25$ and $\hat{\mu}_0 = 30\%$. In Appendix A.4.4 on page 72, we show that λ is related to the average duration τ of the EWMA estimator:

$$\lambda = \frac{1}{\tau}$$

For instance, if the average duration of the moving average is equal to three months, λ is equal to 4. Figure 1 illustrates that the option profile of the trend-following strategy is convex. This confirms the result found by Fung and Hsieh (2001), who suggested that the payoff of trend followers is similar to a long exposure on a straddle. However, the convexity of the payoff depends highly on the average duration of the moving average. In particular, short-term strategies exhibit less convexity than long-term strategies. To understand this result, we recall that τ is the ratio between the asset volatility and the trend volatility:

$$\tau = \frac{\sigma}{\gamma}$$

It follows that a high value of τ implies that the volatility of the asset dominates the volatility of the trend. This means that the observed trend is relatively less noisy. In this case, it is rational to use a longer period for estimating the trend.

⁵We notice that the Markowitz solution $\alpha \propto \sigma^{-2}$ is equivalent to use the normalized exposure:

$$g_t = \ell \sqrt{\lambda} \left(\frac{\hat{\mu}_t^2}{\sigma^2} \left(1 - \frac{\ell \sqrt{\lambda}}{2} \right) - \frac{\lambda}{2} \right)$$

Figure 1: Option profile of the trend-following strategy

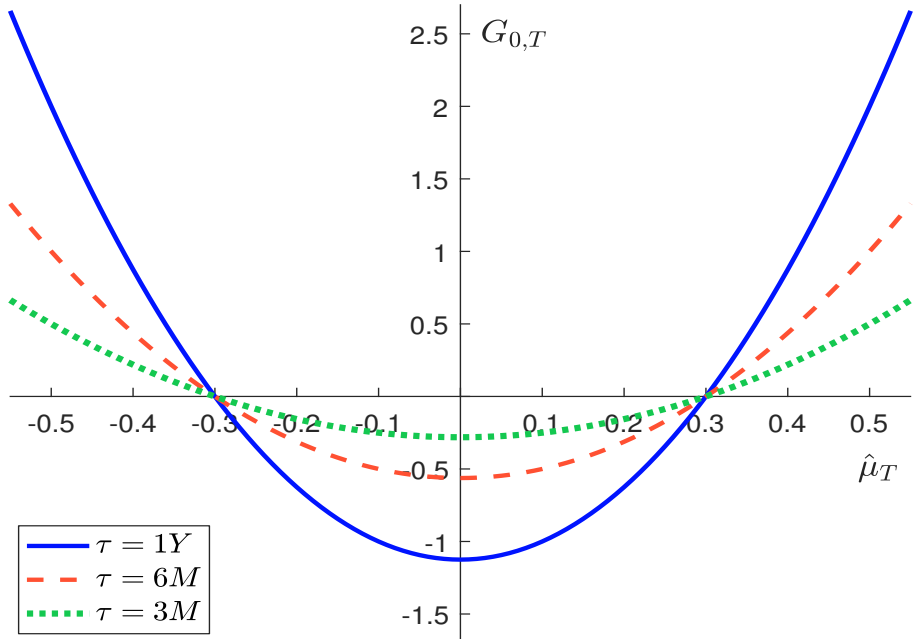
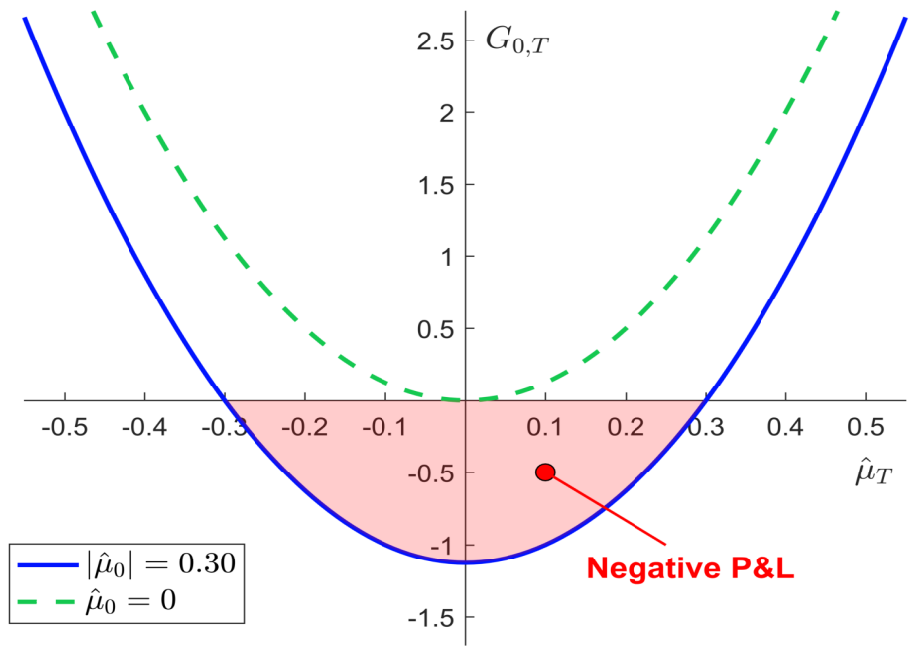


Figure 2: Impact of the initial trend when τ is equal to one year



It is remarkable that only the magnitude of the trend, and not the direction, is important. This symmetry property holds because the trend-following strategy makes sense in a long/short framework. We also notice that the option profile of the trend-following strategy also depends on the relative position between the initial trend $\hat{\mu}_0$ and the final trend $\hat{\mu}_T$. When the initial trend is equal to zero, the option profile is always positive. This is also the case when the final trend is larger than the initial trend in absolute value. The worst case scenario appears when the final trend is equal to zero. In this case, the loss is bounded:

$$G_{0,T} \geq -\frac{\alpha}{2\lambda} \hat{\mu}_0^2$$

Figure 2 summarizes these different results⁶. We also notice that the maximum loss is a decreasing function of λ , or equivalently an increasing function of the average duration of the moving average. This implies that short-term momentum is less risky than long-term momentum. This result is obvious since long-term momentum is more sensitive to reversal trends, and short-term momentum is better to capture a break in the trend.

2.1.4 Statistical properties of the trend-following strategy

In Appendix A.4.3 on page 71, we show that g_t is a linear transformation of a noncentral chi-square random variable, where the degree of freedom is 1 and the noncentrality parameter is $\zeta = s_t^2/\lambda$:

$$\Pr \{g_t \leq g\} = \mathbb{F} \left(\frac{2g + \lambda\alpha\sigma^2}{\lambda\alpha\sigma^2(2 - \alpha\sigma^2)}; 1, \frac{s_t^2}{\lambda} \right)$$

where s_t is the Sharpe ratio of the asset at time t . In Figures 3 and 4, we report the cumulative distribution function of the trading impact g_t for different moving average windows when the parameters are $\sigma = 30\%$ and $\alpha = 1$. In the first figure, we set the Sharpe ratio equal to zero. In this case, the probability of loss is larger than the probability of gain. However, the expected value of gain is larger than the expected value of loss. Here we face a trade-off between loss/gain frequency and loss/gain magnitude. As explained by Potters and Bouchaud (2006), the trend-following strategy loses more frequently than it gains, but the magnitude of gain is more important than the magnitude of loss. This theoretical result is backed by practice. Most of the time, there are noisy trends or false signals. During these periods, the trend-following strategy posts zero or negative returns. Sometimes, the financial market exhibits a big trend. In this case, the return of the trend-following strategy may be very large, but the probability of observing a big trend is low.

In Appendix A.4.5 on page 73, we derive the hit ratio of the strategy:

$$\mathcal{H} = \Pr \{g_t \geq 0\}$$

We have reported the relationship between \mathcal{H} and the Sharpe ratio s_t in Figure 5 using the previous parameters ($\sigma = 30\%$ and $\alpha = 1$) and a one-year moving average. It follows that when the Sharpe ratio is lower than 0.35, the hit ratio of the trend-following strategy is lower than 50%. If we consider the expected loss and the expected gain⁷, we obtain the results given in Figure 6. We confirm that the average loss is limited. The expected gain is an increasing concave function of the absolute value of the Sharpe ratio, meaning that the effect of the Sharpe ratio is amplified by the trend-following strategy.

⁶We use the same parameter values as for Figure 1.

⁷Analytical formulas are given in Appendix A.4.6 on page 73.

Figure 3: Cumulative distribution function of g_t ($s_t = 0$)

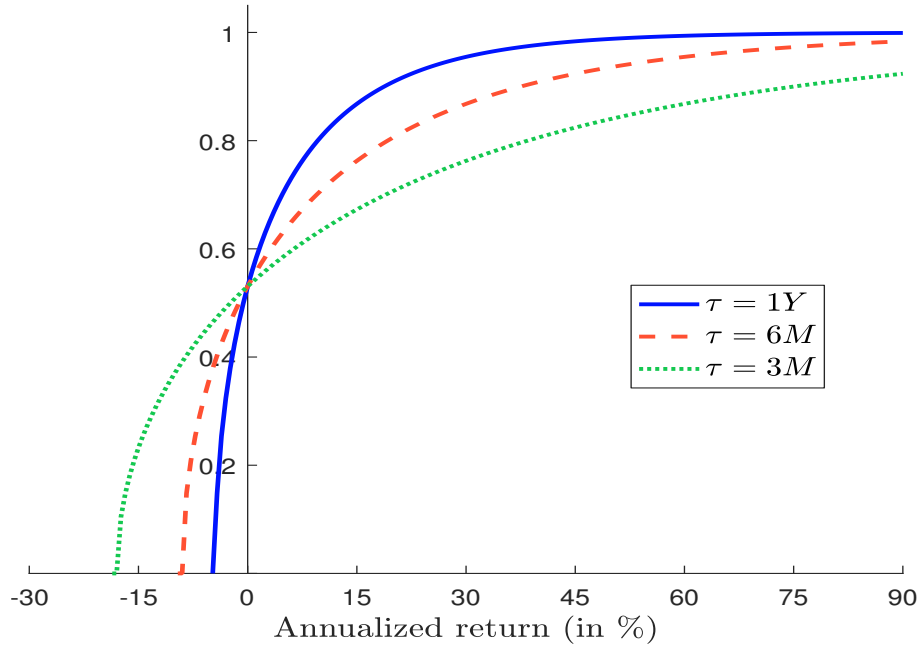


Figure 4: Cumulative distribution function of g_t ($|s_t| = 2$)

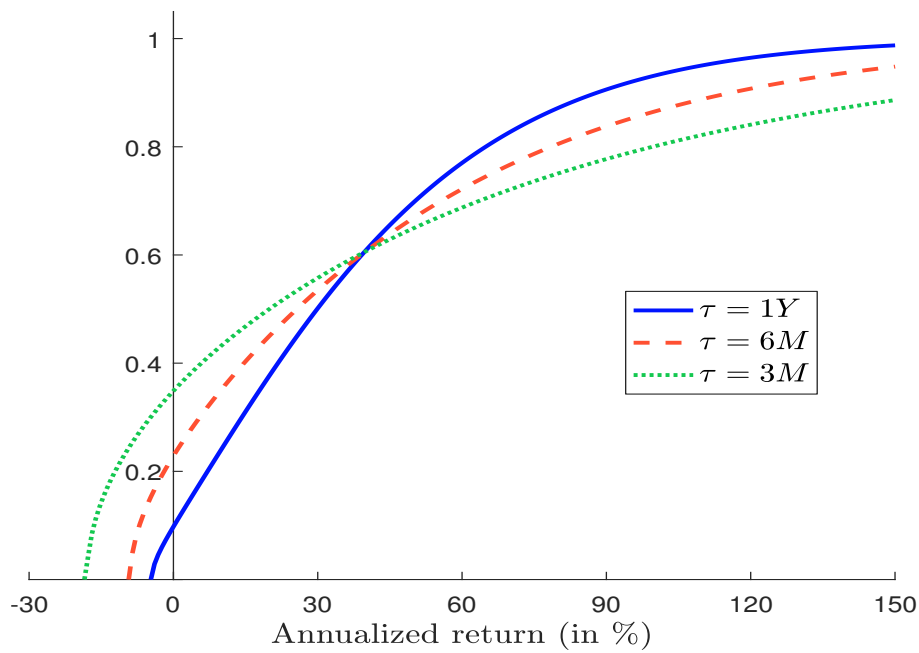


Figure 5: Hit ratio \mathcal{H} of the trend-following strategy

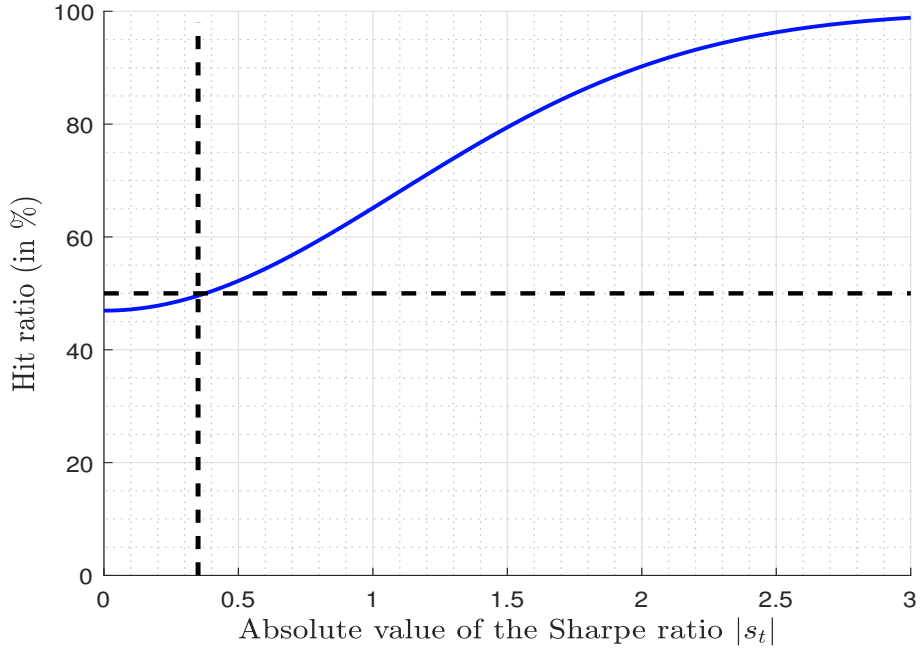
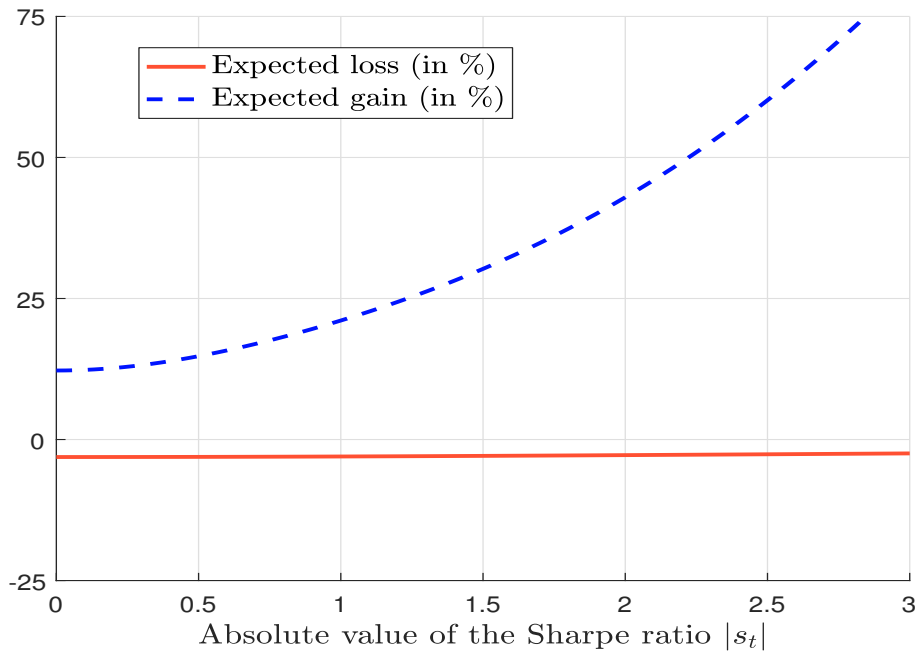


Figure 6: Expected loss and gain of the trend-following strategy



We show here the statistical moments of g_t computed by Hamdan *et al.* (2016):

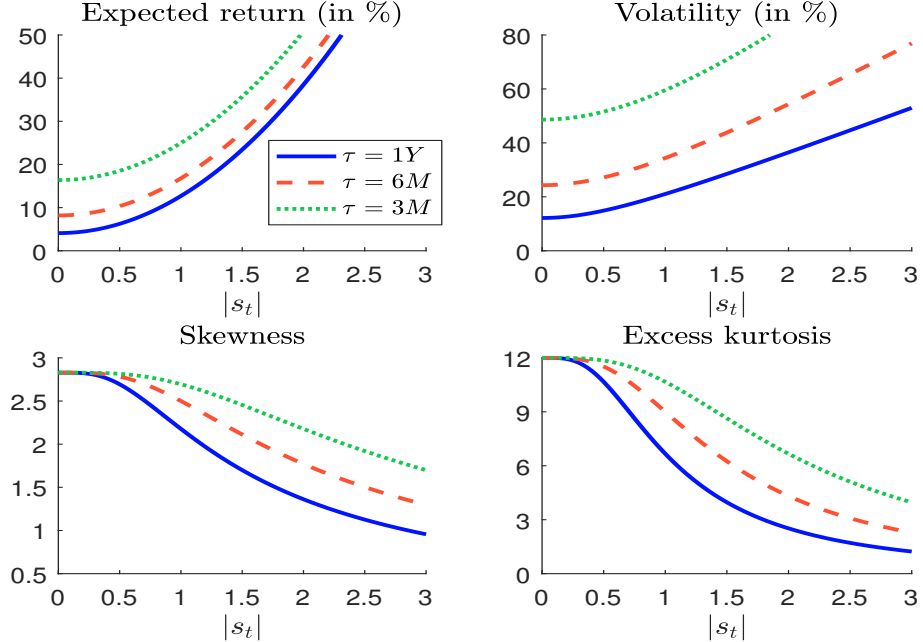
$$\begin{aligned}\mu(g_t) &= \frac{\alpha\sigma^2(2-\alpha\sigma^2)}{2}s_t^2 + \frac{\lambda\alpha\sigma^2}{2}(1-\alpha\sigma^2) \\ \sigma(g_t) &= \left| \frac{\lambda\alpha\sigma^2(2-\alpha\sigma^2)}{2} \right| \sqrt{\frac{2\lambda+4s_t^2}{\lambda}} \\ \gamma_1(g_t) &= (2\lambda+6s_t^2) \sqrt{\frac{2\lambda}{(\lambda+2s_t^2)^3}} \\ \gamma_2(g_t) &= \lambda \frac{12\lambda+48s_t^2}{(\lambda+2s_t^2)^2}\end{aligned}$$

These statistical moments⁸ are reported in Figure 7. Generally, we have $\alpha\sigma^2 \ll 1$, implying that:

$$\mu(g_t) \approx \alpha\sigma^2 \left(s_t^2 + \frac{\lambda}{2} \right)$$

This explains that $\mu(g_t)$ depends on the frequency parameter λ as illustrated in the first panel in Figure 7. We also notice that the volatility and the kurtosis coefficients are a decreasing function of the moving-average duration (second and fourth panels). This means that a short-term trend-following strategy is more risky than a long-term trend-following strategy. In contrast, the skewness is positive and not negative (third panel). This is due to the convex payoff of the strategy.

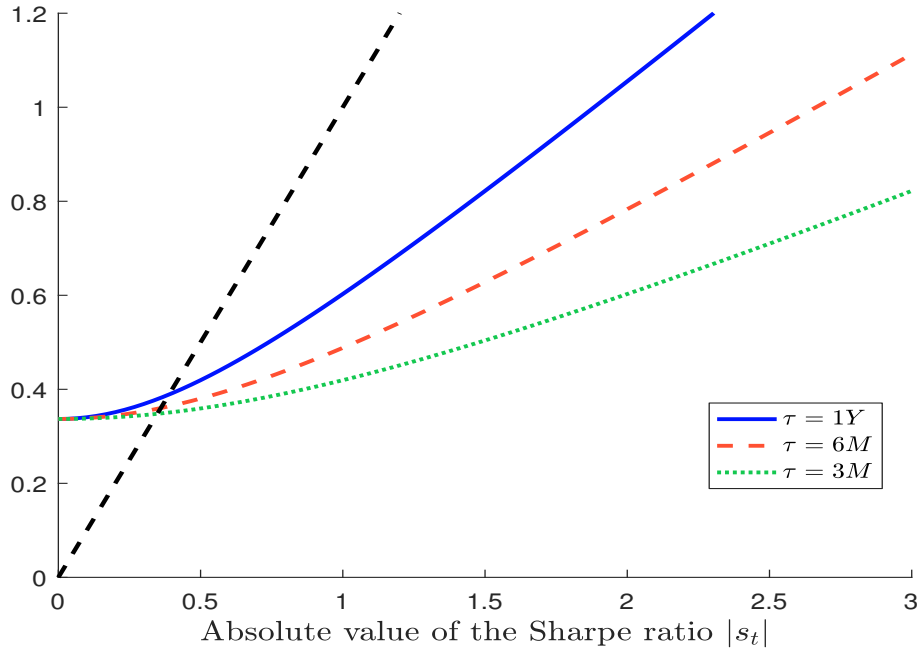
Figure 7: Statistical moments of g_t



⁸We again consider the previous parameters $\sigma = 30\%$ and $\alpha = 1$.

Remark 2 The Sharpe ratio of the trend-following strategy is represented in Figure 8. When the Sharpe ratio of the asset is low (lower than 0.40), the Sharpe ratio of the strategy is higher. However, it is lower than a buy-and-hold portfolio when the Sharpe ratio of the asset is high. Moreover, we note that long-term momentum strategies have a higher Sharpe ratio than short-term momentum strategies.

Figure 8: Sharpe ratio of g_t



2.1.5 The importance of the realized Sharpe ratio

The previous analysis highlights the role of the Sharpe ratio s_t . In this paragraph, we focus on the estimated Sharpe ratio, which can be viewed as the realized Sharpe ratio thanks to Kalman filtering.

We have seen that the P&L of the trend-following strategy can be decomposed in a similar way to the robustness formula of the Black-Scholes model. In this case, we have the following correspondence between the parameters:

Delta-hedging	$\Gamma_t S_t^2$	Σ^2	σ_t^2
Trend-following	$\alpha\sigma^2$	\hat{s}_t^2	λ

At first sight, the parameters of the trend-following strategies seem to be non-homogenous with respect to those of the delta-hedging strategy. However, there is a strong correspondence. For instance, $\Gamma_t S_t^2$ measures the residual nominal exposure of the delta-hedging strategy while $\alpha\sigma^2$ measures the normalized nominal exposure once the trend has been normalized by the variance of asset return. Indeed, we have:

$$e_t = \alpha' \hat{\mu}'_t$$

where $\alpha' = \alpha\sigma^2$ and $\hat{\mu}'_t = \sigma^{-2}\hat{\mu}_t$. We will see later what the rationale of such formulation may be. The Sharpe ratio \hat{s}_t plays the role of the implied volatility. It is the main risk factor of the trend-following strategy, exactly like volatility is the main risk factor of the delta-hedging strategy. Therefore, the trade-off between implied volatility and realized volatility takes an original form in the case of the trend-following strategy⁹:

$$\begin{aligned} g_t &\simeq \alpha\sigma^2 \left(\hat{s}_t^2 - \frac{1}{2} \text{var}(\hat{s}_t^2) \right) \\ &= \underbrace{\alpha\sigma^2 \hat{s}_t^2}_{\text{Gamma gain}} - \underbrace{\frac{1}{2} \alpha\sigma^2 \text{var}(\hat{s}_t)}_{\text{Gamma cost}} \end{aligned}$$

The trade-off is now between the squared Sharpe ratio and its half-variance. This result must be related to Equation (8) found by Dao *et al.* (2016), who show that the performance of the trend-following strategy depends on the difference between the long-term volatility (gamma gain) and the short-term volatility (gamma cost).

The robustness formula also tells us a very simple rule. If we want to obtain a positive P&L, we must hedge the European option using an implied volatility that is higher than the realized volatility if the gamma of the option is positive. In the case of the trend-following strategy, this rule becomes:

$$\begin{aligned} g_t \geq 0 &\Leftrightarrow \alpha\sigma^2 \left(\hat{s}_t^2 \left(1 - \frac{\alpha\sigma^2}{2} \right) - \frac{\lambda}{2} \right) \geq 0 \\ &\Leftrightarrow |\hat{s}_t| \geq (1 - \alpha\sigma^2/2)^{-1/2} \frac{1}{\sqrt{2\tau}} \\ &\Rightarrow |\hat{s}_t| \geq \frac{1}{\sqrt{2\tau}} \end{aligned}$$

We obtain the result of Bruder and Gaußel (2011). In Figure 9, we report the admissible region in order to obtain a positive trading impact. We notice that a low duration implies a high Sharpe ratio. For instance, if we use a three-month EWMA estimator, the absolute value of the Sharpe ratio must be larger than 1.41 in order to observe a positive trading impact. In the case of a one-year moving average, the bound is 0.71 (see Table 1).

Table 1: Upper and lower bounds of the admissible region

Duration	1W	1M	3M	6M	1Y
Bounds	± 5.10	± 2.45	± 1.41	± 1.00	± 0.71

The reason is that the estimator depends on the duration. In Figure 10, we have reported the probability density function of the Sharpe ratio estimator \hat{s}_t when the true value of s_t is equal to 0.5. We observe that the standard deviation is wide, even if we consider a ten-year period. This is why the Sharpe ratio estimate must be significant in order to generate a positive P&L. Since gamma costs increase with the frequency of the moving average, it is perfectly normal that the estimate must be higher for low duration than for high duration.

Remark 3 All these results confirm that short-term momentum strategies must exhibit more cross-section variance than long-term momentum strategies. Another implication is the importance of trading costs induced by gamma trading in particular for short-term momentum strategies.

⁹We assume that $\alpha\sigma^2 \ll 1$.

Figure 9: Admissible region for positive trading impact

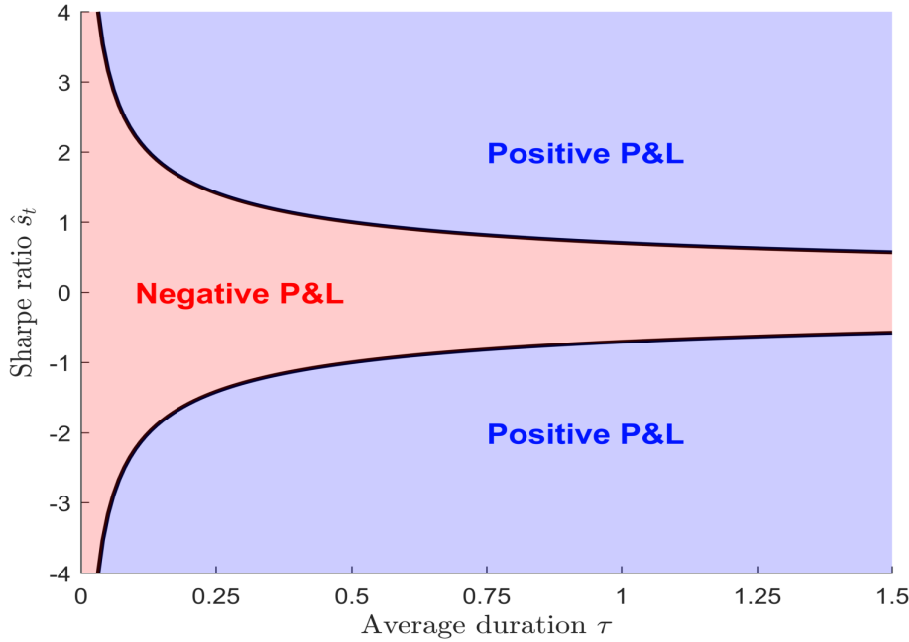
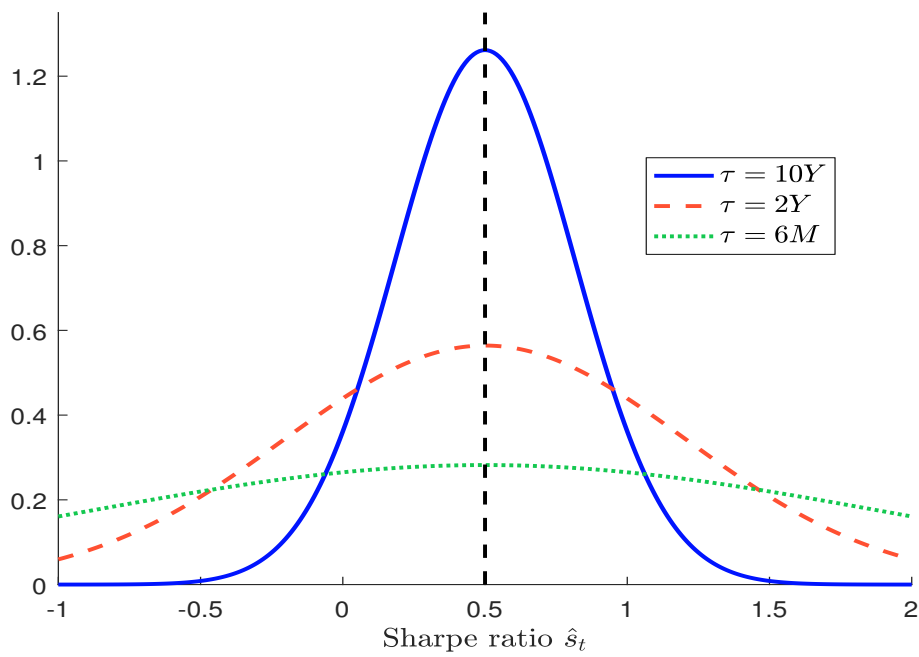


Figure 10: Probability density function of the Sharpe ratio estimator



2.1.6 The leverage effect and the ruin probability

Bruder and Gaußel (2011) propose using the optimal Markowitz allocation:

$$\alpha = \frac{m}{\sigma^2}$$

Since this rule is simple and seems to be natural, it is not obvious that it is the optimal leverage. In Figure 11, we have reported the relationship between the leverage α and the trading impact g_t when the Sharpe ratio is equal to 2. We notice that g_t is concave function of α (panel 1). In particular, the P&L decreases when α is higher than a certain value α^* . The maximization of the trading impact implies that the optimal leverage α^* is equal to¹⁰:

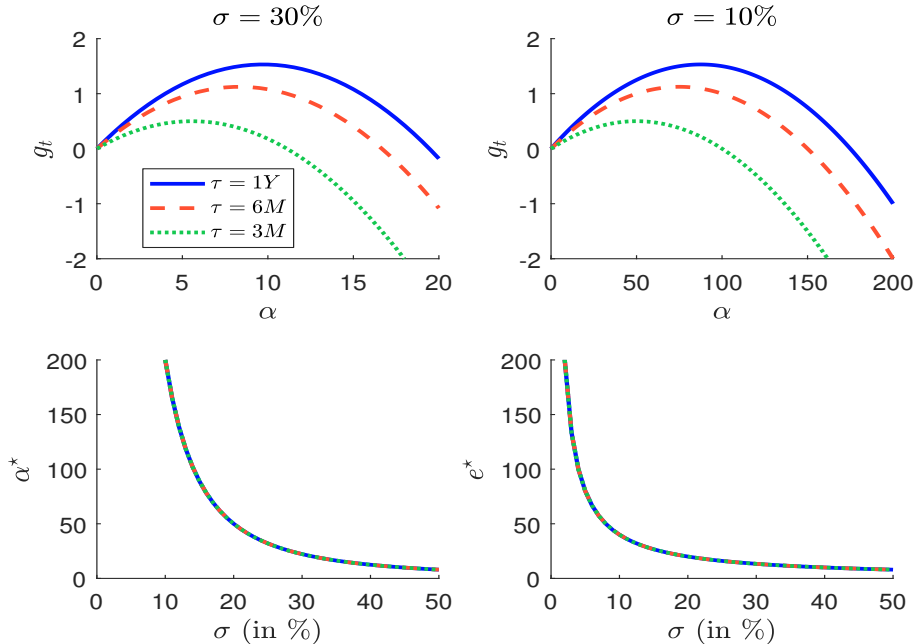
$$\alpha^* = \max \left(\min \left(\frac{2\hat{s}_t^2 - \lambda}{\sigma^2}, \frac{2}{\sigma^2} \right), 0 \right)$$

We have reported the value of α^* and also the corresponding exposure e^* in the third and fourth panels. These results show that the exposure must be an increasing function of the Sharpe ratio and also a decreasing function of the asset volatility. However, this conclusion must be contrasted, because too high an exposure can destroy the strategy. In the previous paragraphs, we have always assumed that $\alpha\sigma^2 \ll 1$. Otherwise, we obtain:

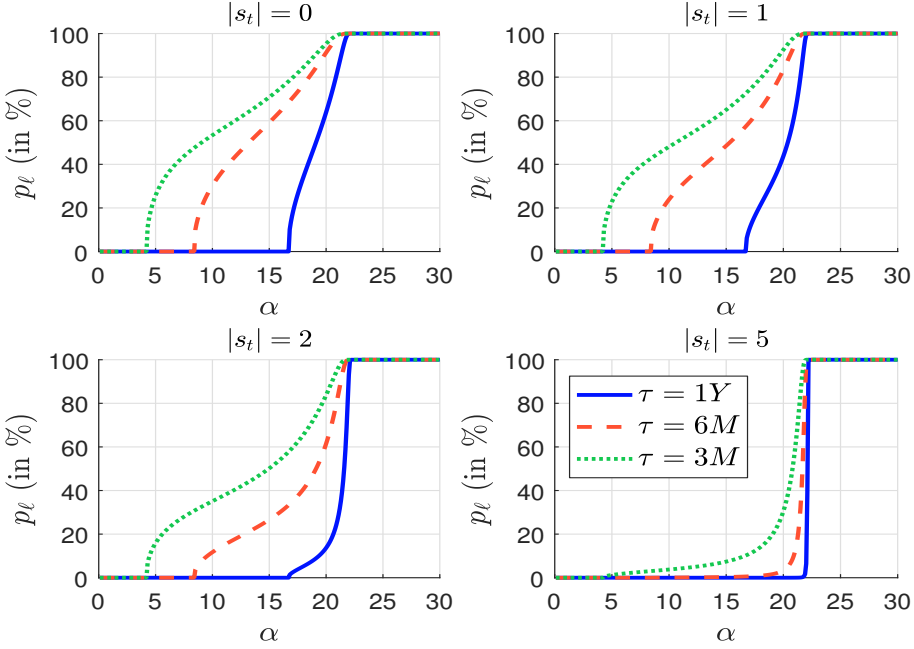
$$g_t = \underbrace{\alpha\sigma^2\hat{s}_t^2}_{\text{Gamma gain}} - \underbrace{\frac{1}{2}\alpha\sigma^2 \text{var}(\hat{s}_t) + \frac{1}{2}\alpha^2\sigma^4\hat{s}_t^2}_{\text{Gamma cost}}$$

It follows that gamma costs can be prohibitive in this case.

Figure 11: The leverage effect



¹⁰This result is valid if we assume that \hat{s}_t^2 is relatively constant.

Figure 12: Ruin probability ($\ell = -75\%$)


Remark 4 In Figure 12, we have reported the ruin probability $p_\ell = \Pr \{g_t \leq -\ell\}$ when ℓ is set to 75%. We verify that it is an increasing function of the leverage α . We also notice that the ruin probability is larger for short-term momentum than long-term momentum. This result is counter-intuitive, because we could think that a short-term momentum may react quickly if it has a false signal. Here our analysis assumes that we annualize the return and does not take into account the final payoff that may be extremely negative for long-term momentum.

2.2 Extension to the multivariate case

Here we discuss the general case when the momentum strategy invests in n risky assets:

$$\begin{cases} d\mathbf{S}_t = \mu_t \odot \mathbf{S}_t dt + (\sigma \odot \mathbf{S}_t) \odot dW_t \\ d\mu_t = \sigma^* \odot dW_t^* \end{cases}$$

where \mathbf{S}_t , μ_t , σ and σ^* are four $n \times 1$ vectors. We also assume that $\mathbb{E}[W_t W_t^\top] = \mathcal{C}$ and $\mathbb{E}[W_t^* W_t^{*\top}] = \mathcal{C}^*$ where \mathcal{C} and \mathcal{C}^* are two square matrices, and $\mathbb{E}[W_t^* W_t^\top] = \mathbf{0}$. We denote Σ the covariance matrix of asset returns and Γ the covariance matrix of trends¹¹.

The portfolio is a weighted sum of the asset returns:

$$\frac{dV_t}{V_t} = \sum_{i=1}^n e_{i,t} \frac{dS_{i,t}}{S_{i,t}}$$

where $e_{i,t}$ is the exposure on Asset i at time t . Let $\mathbf{S}_t = (S_{1,t}, \dots, S_{n,t})$ and $\mathbf{e}_t = (e_{1,t}, \dots, e_{n,t})$ be the vectors of asset prices and exposures. The matrix form of the pre-

¹¹We have $\Sigma_{i,j} = \mathcal{C}_{i,j} \sigma_i \sigma_j$ and $\Gamma_{i,j} = \mathcal{C}_{i,j}^* \sigma_i^* \sigma_j^*$.

vious equation is:

$$\frac{dV_t}{V_t} = \mathbf{e}_t^\top \frac{d\mathbf{S}_t}{\mathbf{S}_t}$$

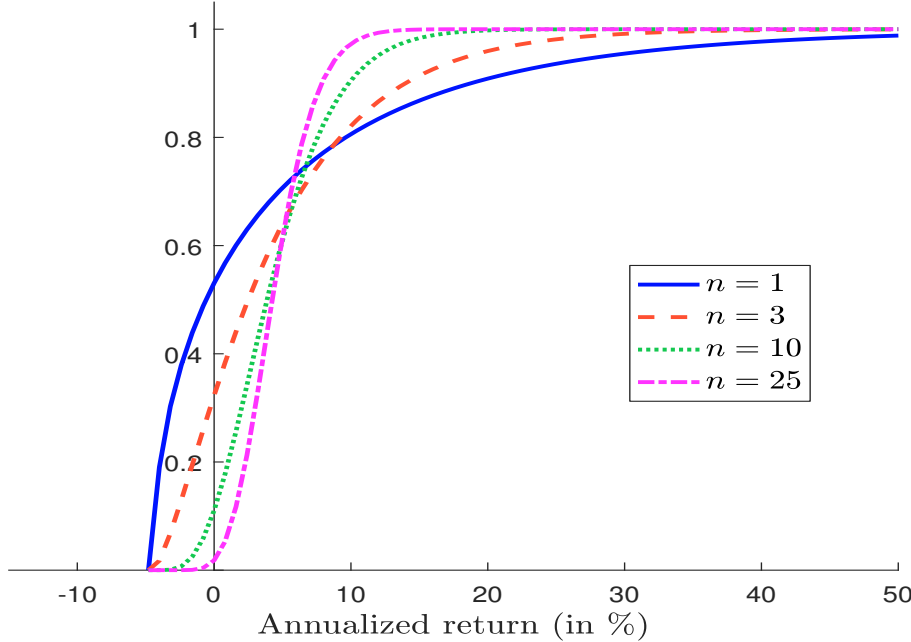
The momentum strategy is defined by:

$$\mathbf{e}_t = A\hat{\mu}_t$$

where A is the allocation matrix and $\hat{\mu}_t = (\hat{\mu}_{1,t}, \dots, \hat{\mu}_{n,t})$ is the vector of estimated trends.

In this section, we will see that the generalization to the multi-dimensional case is very natural, and also that correlations have a big impact on the strategy.

Figure 13: Cumulative distribution function of g_t ($s_t = 0, \mathcal{C}_{i,j} = 0$)



2.2.1 Uncorrelated assets

If we assume that the matrix A is diagonal¹² and the assets are uncorrelated ($\mathcal{C} = \mathbf{0}$ and $\mathcal{C}^* = \mathbf{0}$), the expression of the P&L becomes:

$$\begin{aligned} \ln \frac{V_T}{V_0} &= \sum_{i=1}^n \frac{\alpha_i}{2\lambda_i} (\hat{\mu}_{i,T}^2 - \hat{\mu}_{i,0}^2) + \int_0^T \sum_{i=1}^n \alpha_i \sigma_i^2 \left(\frac{\hat{\mu}_{i,t}^2}{\sigma_i^2} \left(1 - \frac{\alpha_i \sigma_i^2}{2} \right) - \frac{\lambda_i}{2} \right) dt \\ &= G_{0,T} + \int_0^T g_t dt \end{aligned}$$

We obtain the decomposition between the option profile and the trading impact.

¹²We have:

$$A = \text{diag}(\alpha_1, \dots, \alpha_n)$$

In Appendix A.5.3 on page 75, we show that g_t is a Gaussian quadratic form of random variables:

$$\Pr \{g_t \leq g\} = \mathbb{Q}_1 \left(g + \frac{1}{2} \sum_{i=1}^n \lambda_i \alpha_i \sigma_i^2; a, b \right)$$

where $a = (a_i)$, $b = (b_i)$ and:

$$\begin{aligned} a_i &= \frac{\lambda_i \alpha_i \sigma_i^2 (2 - \alpha_i \sigma_i^2)}{2} \\ b_i &= \frac{s_{i,t}}{\sqrt{\lambda_i}} \end{aligned}$$

Let us illustrate the impact of the asset number n on the cumulative probability distribution. We use the same parameters for all the assets: the Sharpe ratio is equal to 0, the volatility is equal to 30% and the average duration of the moving average is set to one year. In order to compare the results, the exposure α_i is equal to $1/n$, where n is the number of assets. The cumulative distribution function is shown in Figure 13. The number of uncorrelated assets changes its shape. In particular, it reduces the loss probability, but also the gain probability. These effects are due to the diversification effect, and are close to those observed with the equally-weighted long-only portfolio. When the Sharpe ratio of assets is equal to zero, we also notice that:

$$\lim_{n \rightarrow \infty} g_t = 0$$

There is no miracle: the trading impact tends to zero when the number of assets is large. In Figure 14, we consider the case where the absolute value of the Sharpe ratio is equal to 2. As before, the cumulative distribution function shifts towards the right.

Figure 14: Cumulative distribution function of g_t ($|s_t| = 2, C_{i,j} = 0$)

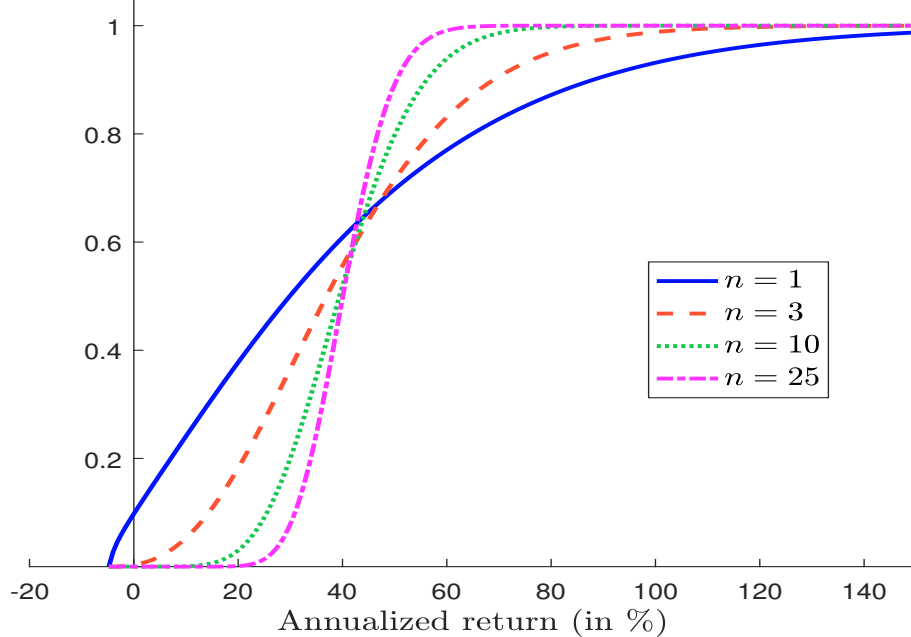
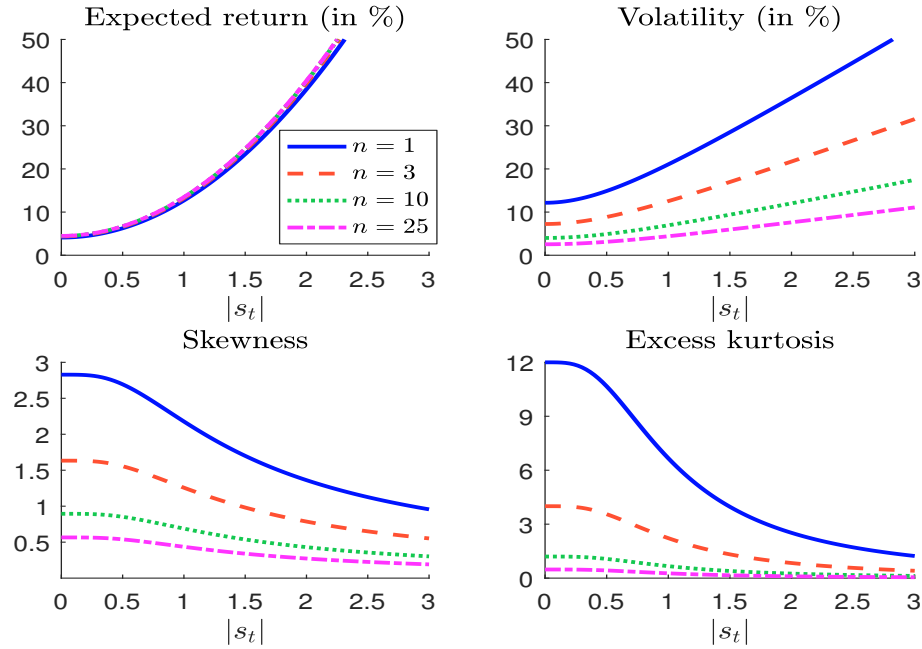
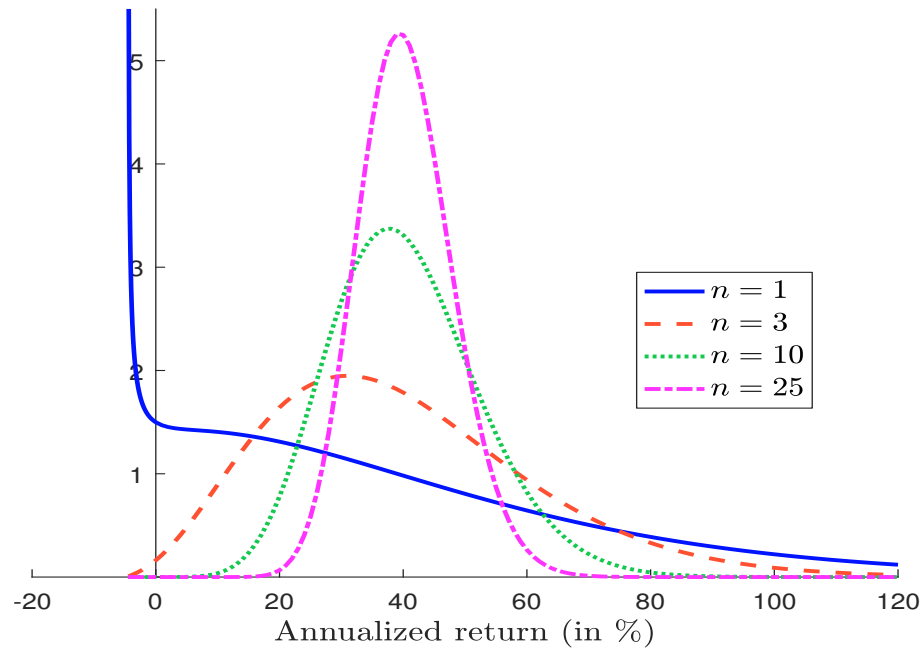


Figure 15: Statistical moments of g_t with respect to the number of uncorrelated assets

 Figure 16: Probability density function of g_t ($|s_t| = 2, \mathcal{C}_{i,j} = 0$)


The statistical moments¹³ of g_t for a one-year EWMA are given in Figure 15. The number of uncorrelated assets has no impact on the mean, but dramatically reduces the other moments. Since the volatility decreases, the Sharpe ratio of the momentum strategy increases with the number of uncorrelated assets. Moreover, skewness and excess kurtosis coefficients tend to zero when n tends to ∞ . Therefore, the probability distribution tends to be Gaussian as shown in Figure 16 – the corresponding cumulative distribution functions are those given in Figure 14.

2.2.2 Correlated assets

We now turn to the general case. The optimal estimator of the trend becomes:

$$\hat{\mu}_t = \int_0^t e^{-(t-u)\Lambda} \Lambda dy_u + e^{-t\Lambda} \hat{\mu}_0$$

As previously, we obtain an exponentially-weighted moving average, but it is multi-dimensional¹⁴ and depends on the matrix $\Lambda = \Upsilon_\infty \Sigma^{-1}$.

In Appendix A.5.2 on page 74, we show that the expression of the P&L is equal to:

$$\begin{aligned} \ln \frac{V_T}{V_0} &= \frac{1}{2} (\hat{\mu}_T^\top A^\top \Lambda^{-1} \hat{\mu}_T - \hat{\mu}_0^\top A^\top \Lambda^{-1} \hat{\mu}_0) + \\ &\quad \int_0^T \left(\hat{\mu}_t^\top A^\top \left(\mathbf{I}_n - \frac{1}{2} \Sigma A \right) \hat{\mu}_t - \frac{1}{2} \text{tr}(A^\top \Sigma \Lambda^\top) \right) dt \end{aligned}$$

We again obtain a decomposition of the performance between an option profile and a trading impact¹⁵. Since g_t is a Gaussian quadratic form, we deduce that¹⁶:

$$\Pr \{ g_t \leq g \} = \mathbb{Q}_2 \left(g + \frac{1}{2} \text{tr}(A^\top \Sigma \Lambda^\top); \mu_t, \Lambda \Sigma, A^\top \left(\mathbf{I}_n - \frac{1}{2} \Sigma A \right) \right)$$

We consider the example with the same parameters for all assets. The asset volatility is equal to 30%, the Sharpe ratio is equal to s_t and the average duration of the moving average is equal to three months¹⁷. We also assume that the correlation matrix \mathcal{C} corresponds to a uniform correlation matrix $\mathcal{C}_n(\rho)$. Since we have $\Lambda = \lambda \mathbf{I}_n$, we deduce that $\Gamma = \Lambda^\top \Sigma \Lambda = \lambda^2 \Sigma$ and $\Upsilon_\infty = \Lambda \Sigma = \lambda \Sigma$. Therefore, the correlation matrices of Γ and Υ_∞ are exactly equal to $\mathcal{C}_n(\rho)$. The results are given in Figures 17, 18, 19 and 20. The first figure shows the impact of the uniform correlation ρ when the Sharpe ratio of the assets is equal to zero. We notice that a positive correlation has the same effect as a negative correlation. Here we obtain an interesting result: the best case for diversification is reached when the correlation ρ is equal to zero.

¹³These are described on page 77.

¹⁴We will discuss this result later in Section 2.2.4 on page 25.

¹⁵If $A = \alpha \mathbf{I}_n$ and $\Lambda = \text{diag}(\lambda, \dots, \lambda)$, we obtain a simple expression:

$$\ln \frac{V_T}{V_0} = \frac{\alpha}{2\lambda} (\hat{\mu}_T^\top \hat{\mu}_T - \hat{\mu}_0^\top \hat{\mu}_0) + \alpha \int_0^T \left(\hat{\mu}_t^\top \left(\mathbf{I}_n - \frac{1}{2} \alpha \Sigma \right) \hat{\mu}_t - \frac{\lambda}{2} \text{tr}(\Sigma) \right) dt$$

We see the previous result obtained in the one-dimensional case:

$$\ln \frac{V_T}{V_0} = \frac{\alpha}{2\lambda} (\hat{\mu}_T^2 - \hat{\mu}_0^2) + \alpha \int_0^T \left(\hat{\mu}_t^2 \left(1 - \frac{\alpha \sigma^2}{2} \right) - \frac{\lambda \sigma^2}{2} \right) dt$$

¹⁶See Appendix A.5.4 on page 77.

¹⁷We have $\lambda = 4$.

Figure 17: Impact of the correlation on $\Pr \{g_t \leq g\} (|s_t| = 0)$

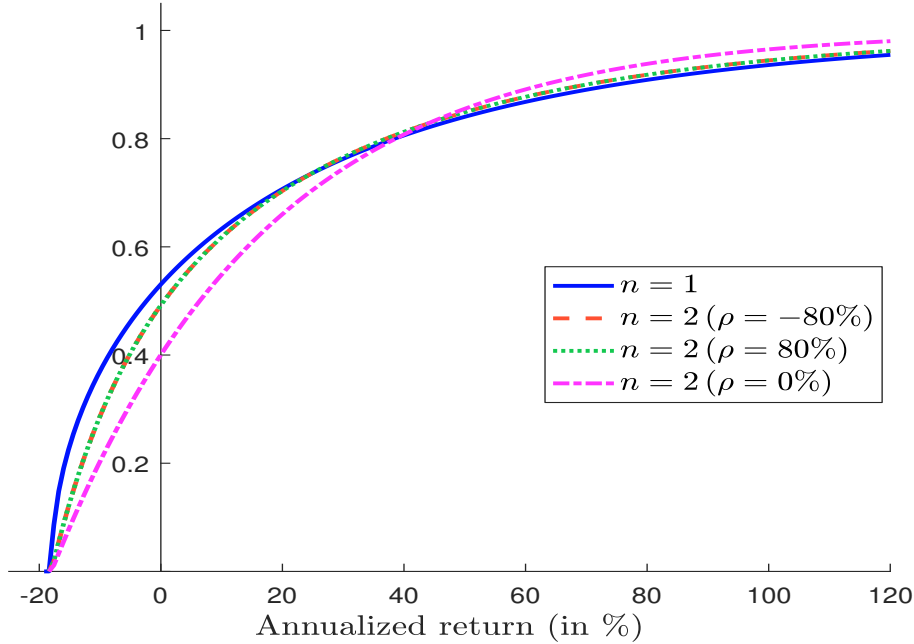


Figure 18: Impact of the correlation on $\Pr \{g_t \leq g\} (s_t = 2)$

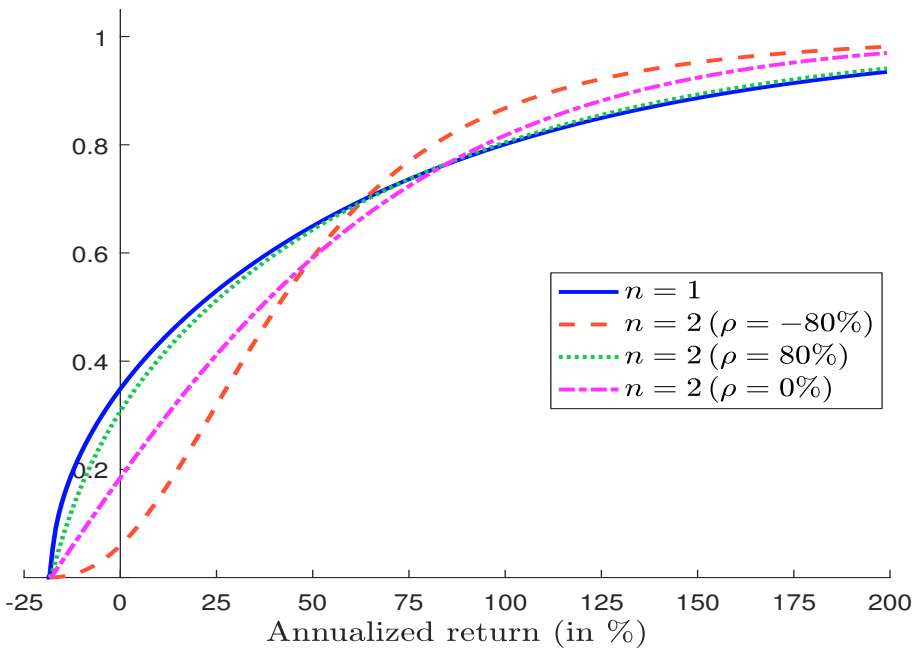


Figure 19: Impact of the number of assets on $\Pr \{g_t \leq g\}$ ($|s_t| = 0$, $\rho = 80\%$)

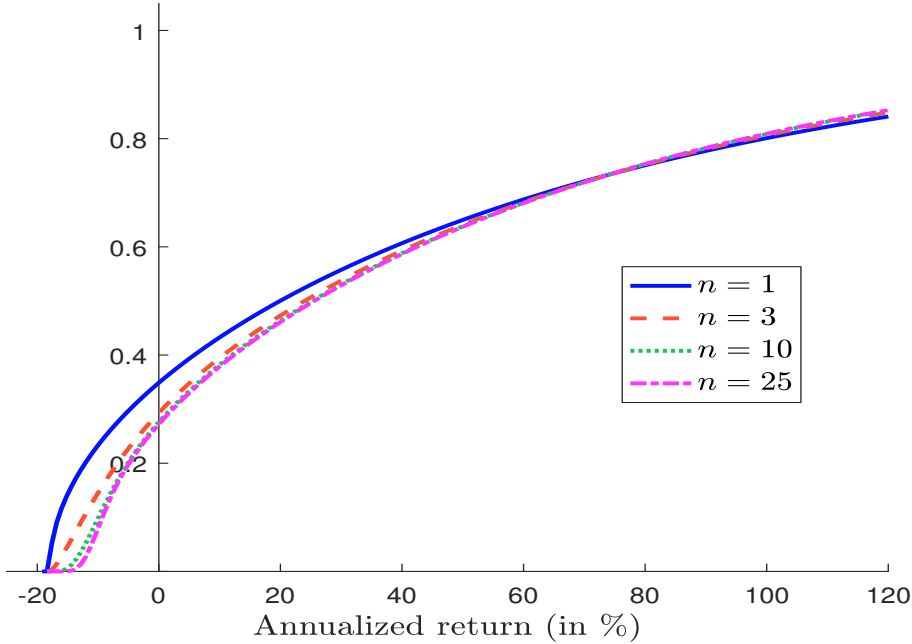
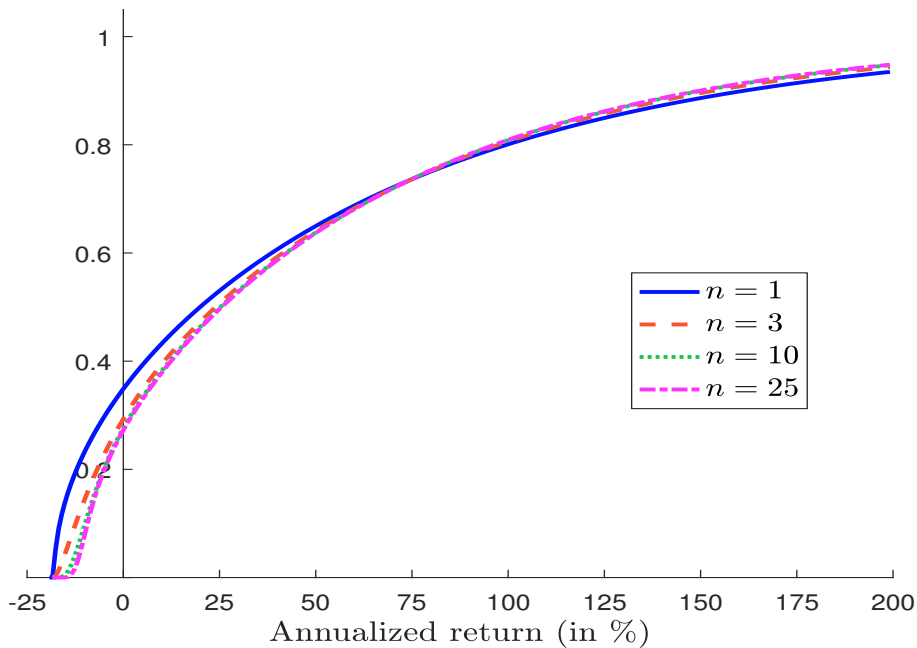


Figure 20: Impact of the number of assets on $\Pr \{g_t \leq g\}$ ($s_t = 2$, $\rho = 80\%$)



Remark 5 Let us consider a portfolio (α_1, α_2) composed of two assets. The corresponding volatility is equal to:

$$\sigma(\rho) = \sqrt{\alpha_1^2 \sigma_1^2 + 2\rho\alpha_1\alpha_2\sigma_1\sigma_2 + \alpha_2^2 \sigma_2^2}$$

In the case of a long-only portfolio, the best case for diversification is reached when the correlation is equal to -1 :

$$\sigma(-1) = |\alpha_1\sigma_1 - \alpha_2\sigma_2|$$

whereas the worst case for diversification is reached when the two assets are perfectly correlated. We have:

$$|\alpha_1\sigma_1 - \alpha_2\sigma_2| = \sigma(-1) \leq \sigma(\rho) \leq \sigma(1) = \alpha_1\sigma_1 + \alpha_2\sigma_2$$

We notice that this result does not hold in the long-short case. Let us assume that $\alpha_1 > 0$ and $\alpha_2 < 0$. We have: $\sigma(1) \leq \sigma(\rho) \leq \sigma(-1)$. However, this property is not realistic. Indeed, it is more relevant to assume that $\text{sgn}(\alpha_1\alpha_2) = \text{sgn}(\rho)$. Therefore, the best case for diversification is reached when the correlation is equal to zero:

$$\sigma(0) \leq \sigma(\rho)$$

In particular, a correlation of -1 is equivalent to a correlation of $+1$ in the long-short case. Indeed, when the correlation is equal to -1 , the investor will certainly be long on one asset and short on the other asset, implying that this is the same bet, exactly when the two assets are perfectly correlated in the long-only case.

This symmetry between positive and negative correlations is not verified when the Sharpe ratio of the assets is not equal to zero. For instance, it is better to have a negative correlation than a positive correlation when the Sharpe ratios are all positive (see Figure 18). Another interesting result is that the number of assets has a small impact on the trading impact when the correlation parameter is high (Figures 19 and 20).

2.2.3 Impact of the correlation in the two-asset case

We assume that $\Lambda = \lambda\mathbf{I}_2$ and $A = \text{diag}\left(\frac{1}{2}, \frac{1}{2}\right)$. The expression of the hit ratio is equal to:

$$\mathcal{H} = 1 - \mathbb{Q}_2\left(\frac{\lambda\sigma_1^2 + \lambda\sigma_2^2}{4}; \mu_t, \lambda\Sigma, \frac{4\mathbf{I}_2 - \Sigma}{8}\right)$$

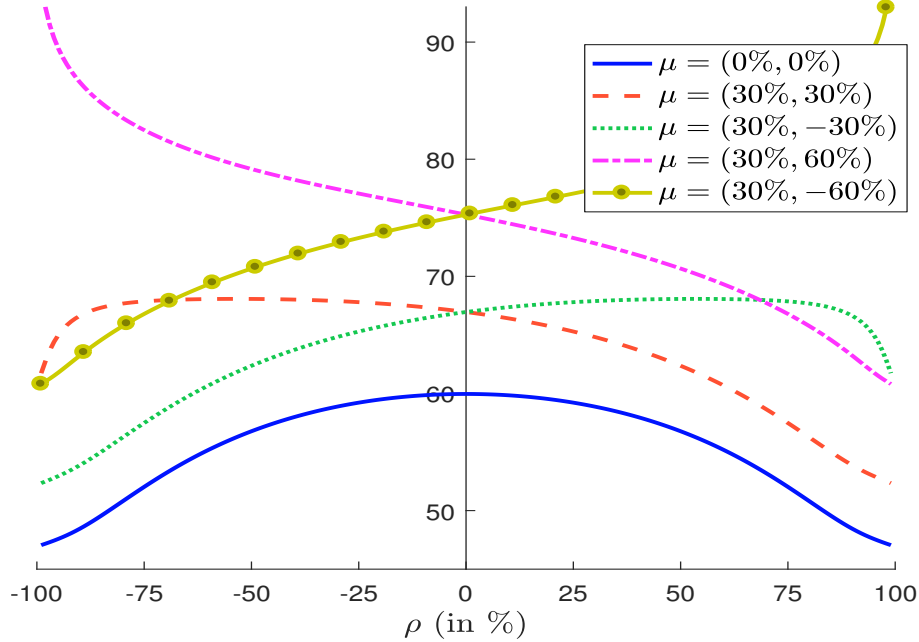
Figure 21 shows the evolution of the hit ratio with respect to the correlation parameter¹⁸. We notice that the optimal parameter ρ^* that maximizes the hit ratio satisfies the following conditions:

$$\rho^* = \begin{cases} < 0 & \text{if } \text{sgn}(\mu_1\mu_2) > 0 \\ = 0 & \text{if } \mu_1\mu_2 = 0 \\ > 0 & \text{if } \text{sgn}(\mu_1\mu_2) < 0 \end{cases}$$

Indeed, we have:

$$\begin{aligned} g_t &= \frac{1}{2} \left(1 - \frac{\sigma_1^2}{4}\right) \hat{\mu}_{t,1}^2 + \frac{1}{2} \left(1 - \frac{\sigma_2^2}{4}\right) \hat{\mu}_{t,2}^2 - \\ &\quad \frac{\rho\sigma_1\sigma_2}{4} \hat{\mu}_{t,1} \hat{\mu}_{t,2} - \frac{\lambda}{4} (\sigma_1^2 + \sigma_2^2) \end{aligned}$$

We notice that the correlation parameter ρ only impacts the term $\hat{\mu}_{t,1}\hat{\mu}_{t,2}$. Maximizing the hit ratio with respect to the correlation ρ is then equivalent to minimizing the term

Figure 21: Hit ratio (in %) with respect to the asset correlation ρ


$\rho\sigma_1\sigma_2\hat{\mu}_{t,1}\hat{\mu}_{t,2}$. Since we have $\mathbb{E}[\hat{\mu}_{t,1}\hat{\mu}_{t,2}] = \mu_1\mu_2 + \lambda\rho\sigma_1\sigma_2$, it is therefore natural that ρ^* is a function of $-\text{sgn}(\mu_1\mu_2)$.

We have reported the statistical moments of g_t in Figure 22. We notice that the impact of the correlation is rather small on the expected return¹⁸, but large on volatility, skewness and kurtosis. Moreover, we observe that the risk is minimized when the correlation is close to zero. All these results confirm the special nature of the correlation in momentum strategies: the best case for diversification is obtained when the correlation is close to zero.

¹⁸We have $\sigma_1 = \sigma_2 = 30\%$ and $\lambda = 4$.

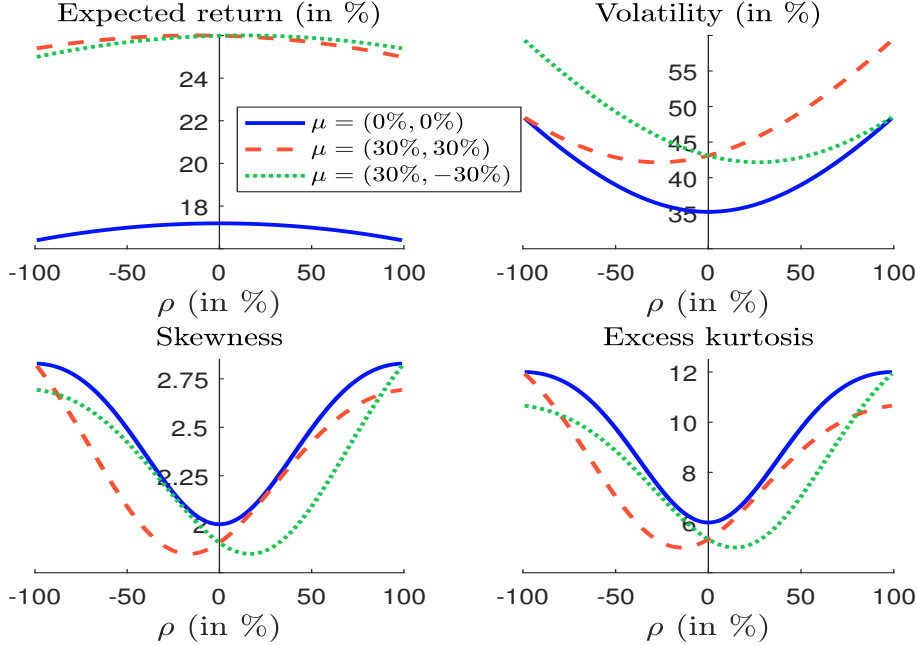
¹⁹We now assume that $A = \text{diag}(\alpha_1, \alpha_2)$. Using Appendix A.5.6 on page 78, we deduce that the first moment is equal to:

$$\begin{aligned} \mu(g_t) &= \left(\alpha_1 - \frac{1}{2}\alpha_1^2\sigma_1^2\right)(\mu_{1,t}^2 + \lambda\sigma_1^2) + \left(\alpha_2 - \frac{1}{2}\alpha_2^2\sigma_2^2\right)(\mu_{2,t}^2 + \lambda\sigma_2^2) + \\ &\quad - \alpha_1\alpha_2\rho\sigma_1\sigma_2(\mu_{1,t}\mu_{2,t} + \lambda\rho\sigma_1\sigma_2) - \\ &\quad \frac{\lambda}{2}(\alpha_1\sigma_1^2 + \alpha_2\sigma_2^2) \end{aligned}$$

It follows that:

$$\begin{aligned} \rho^* &= \arg \max \mu(g_t) \\ &= -\frac{\mu_{1,t}\mu_{2,t}}{2\lambda\sigma_{1,t}\sigma_{2,t}} \\ &= -\frac{1}{2\lambda}s_{1,t}s_{2,t} \end{aligned}$$

This result confirms the intuition about the optimal correlation for the hit ratio.

Figure 22: Statistical moments of g_t with respect to the asset correlation ρ


2.2.4 Impact of the EWMA estimator

Market practice We recall that Λ is related to the covariance matrices Σ , Γ and Υ_∞ :

$$\begin{cases} \Lambda = \Upsilon_\infty \Sigma^{-1} \\ \Gamma = \Lambda \Sigma \Lambda^\top \end{cases}$$

Until now, we have assumed that $\Lambda = \lambda \mathbf{I}_n$, meaning that $\Gamma = \lambda^2 \Sigma$ and $\Upsilon_\infty = \lambda \Sigma$. We deduce that asset and trend correlation matrices are the same – $\mathcal{C} = \mathcal{C}^*$ – while asset and trend volatilities are proportional. Therefore, the parametrization (Σ, Λ) is equivalent to imposing the covariance matrix Γ of trends. We have used this parametrization because it is the practice used in the market. Indeed, fund managers consider Λ as an exogenous parameter and most of them assume that $\Lambda = \lambda \mathbf{I}_n$. Sometimes, the fund manager will use different moving average estimators in order to reduce the model misspecification and improve the robustness. If we assume that $A = \alpha \mathbf{I}_n$, we obtain:

$$\begin{aligned} \ln \frac{V_T}{V_0} &= \frac{1}{m} \sum_{j=1}^m \frac{\alpha}{2\lambda_j} \left(\hat{\mu}_T^{(j)\top} \hat{\mu}_T^{(j)} - \hat{\mu}_0^{(j)\top} \hat{\mu}_0^{(j)} \right) + \\ &\quad \frac{\alpha}{m} \int_0^T \sum_{j=1}^m \left(\hat{\mu}_t^{(j)\top} \left(\mathbf{I}_n - \frac{1}{2}\alpha\Sigma \right) \hat{\mu}_t^{(j)} - \frac{\lambda_j}{2} \text{tr}(\Sigma) \right) dt \end{aligned}$$

when we consider m moving averages and an equally-weighted allocation between the m trend-following strategies. We show the impact on the option profile in Figure 49 on page 89 when the parameters are the following: $\alpha = 25$ and $\hat{\mu}_{i,0}^{(j)} = 30\%$. For the payoff, we notice that combining different moving averages is equivalent to considering one exponential weighted moving average, whose parameter λ is the harmonic mean of the individual EWMA

parameters:

$$\lambda = m \left(\sum_{j=1}^m \lambda_j^{-1} \right)^{-1}$$

In Figure 49 on page 89, we have $\lambda_1 = 1$, $\lambda_2 = 4$ and $\lambda = 1.6$. Therefore, combining one-year and three-month moving averages is equivalent to having a 7.5-month moving average²⁰. However, the previous analysis does not take into account the fact that $\hat{\mu}_T^{(j)} \neq \hat{\mu}_T^{(k)}$, meaning that the estimators are not the same. The problem is even trickier when we consider the trading impact:

$$g_t = \frac{\alpha}{m} \sum_{j=1}^m \hat{\mu}_t^{(j)\top} \left(\mathbf{I}_n - \frac{1}{2} \alpha \Sigma \right) \hat{\mu}_t^{(j)} - \frac{\bar{\lambda}}{2} \alpha \text{tr}(\Sigma)$$

where $\bar{\lambda} = m^{-1} \sum_{j=1}^m \lambda_j$. Indeed, g_t depends on the joint distribution of $(\hat{\mu}_t^{(1)}, \dots, \hat{\mu}_t^{(m)})$ and in particular the covariance matrix between $\hat{\mu}_t^{(j)}$ and $\hat{\mu}_t^{(k)}$. The fund manager's underlying idea is to reduce the variance of the quadratic term without decreasing the expected return of the strategy. To go further, we have to investigate what impact a misclassification of the matrix Λ has on the trend-following strategy.

Univariate versus multivariate filtering We recall that the natural parametrization of our model is (Σ, Γ) , and not (Σ, Λ) . Therefore, Λ is an endogenous parameter, and its computation requires a two-step approach:

1. we solve the algebraic Riccati equation: $\Upsilon_\infty \Sigma^{-1} \Upsilon_\infty = \Gamma$;
2. we set $\Lambda = \Upsilon_\infty \Sigma^{-1}$.

Let us assume that $\sigma = (20\%, 20\%, 20\%)$, $\sigma^* = (10\%, 20\%, 30\%)$, and $\mathcal{C} = \mathcal{C}^* = \mathcal{C}_3(\rho)$, implying that the covariance matrices Σ and Γ only differ by the volatilities. When the uniform correlation ρ is equal to 30%, we obtain:

$$\Lambda = \begin{pmatrix} 0.4600 & 0.0346 & 0.0745 \\ -0.1325 & 1.0045 & 0.0872 \\ -0.2314 & -0.0516 & 1.5661 \end{pmatrix}$$

The diagonal terms $\Lambda_{i,i}$ are approximately equal to the volatility ratio σ_i^*/σ_i . Therefore, when ρ is close to zero, Λ may be approximated by a diagonal matrix, whose elements are equal to $\Lambda_{i,i} = \sigma_i^*/\sigma_i$. Suppose now that ρ is equal to 90%. The matrix Λ becomes:

$$\Lambda = \begin{pmatrix} -0.4572 & 0.1145 & 0.7745 \\ -1.7999 & 1.0921 & 1.3524 \\ -2.4824 & 0.0099 & 3.2662 \end{pmatrix}$$

In this case, Λ can no longer be approximated by a diagonal matrix²¹.

²⁰We notice that the global duration τ is the mean of individual durations $\tau_j = \lambda_j^{-1}$:

$$\tau = \frac{1}{m} \sum_{j=1}^m \tau_j$$

²¹In Tables 4 and 5 on page 87, we have reported the values of Υ_∞ and Λ calculated using the naive and Riccati approaches. We notice that the solution $\Upsilon_\infty = \Gamma^{1/2} \Sigma^{1/2}$ is not valid when the matrices Σ and Γ are not proportional.

If we neglect the initial trend $\hat{\mu}_0$ or if t is sufficiently large, we have:

$$\hat{\mu}_t \simeq \int_0^t \omega(s) dy_{t-s}$$

where $\omega(s) = e^{-\Lambda s} \Lambda$. If we assume that all the eigenvalues of Λ are positive, $\hat{\mu}_t$ is stationary, $\omega(0) = \Lambda$ and $\lim_{s \rightarrow \infty} \omega(s) = \mathbf{0}$. Moreover, $\omega(s)$ is a diagonal matrix only if $\mathcal{C} = \mathcal{C}^* = \mathbf{I}_n$, and we have:

$$\begin{aligned}\hat{\mu}_{i,t} &= \int_0^t \sum_{j=1}^n \omega_{i,j}(s) dy_{j,t-s} \\ &\neq \int_0^t \omega_{i,i}(s) dy_{i,t-s}\end{aligned}$$

Therefore, we notice that correlations between assets or trends can be used in order to improve the estimation of trends. Let us consider the case:

$$\mathcal{C} = \mathcal{C}^* = \begin{pmatrix} 1.00 & 0.90 & 0 \\ 0.90 & 1.00 & 0 \\ 0 & 0 & 1.00 \end{pmatrix}$$

We obtain²²:

$$\Lambda = \begin{pmatrix} -0.1734 & 0.6503 & 0 \\ -1.3007 & 1.9944 & 0 \\ 0 & 0 & 1.5 \end{pmatrix}$$

In Figure 50 on page 90, we have reported the dynamics of non-zero components $\omega_{i,j}(s)$. We notice that the trend of the first and second assets is estimated using a long/short approach, which is not the case for the third asset. We recall that the naive estimator is equal to:

$$\Lambda = \begin{pmatrix} 0.5 & 0.0 & 0.0 \\ 0.0 & 1.0 & 0.0 \\ 0.0 & 0.0 & 1.5 \end{pmatrix}$$

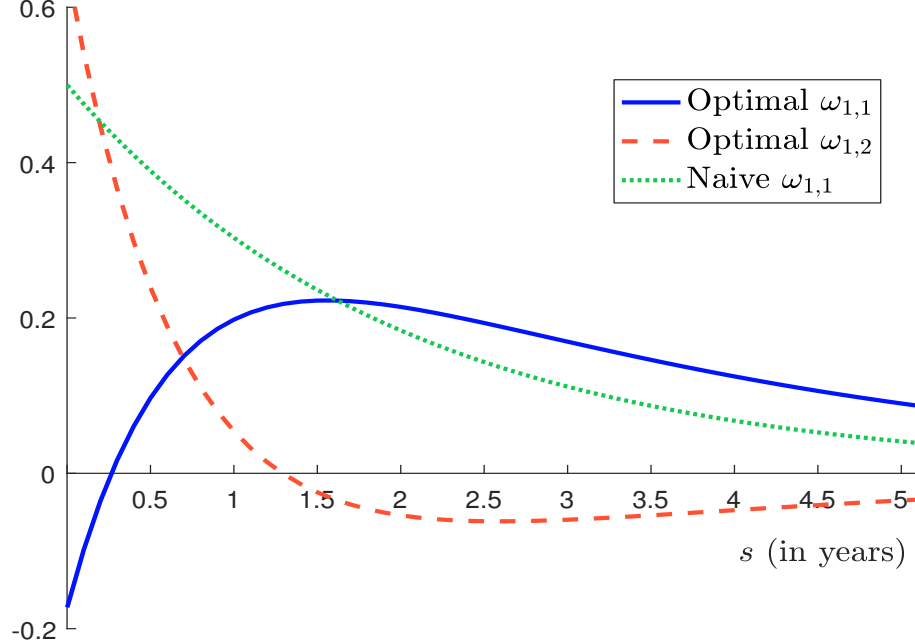
The results are given in Figure 51 on page 90. The naive estimator corresponds exactly to the univariate case. If we consider the first asset, Figure 23 presents the comparison of the two estimators. Since the (asset and trend) correlation between the first and second assets is very high, in the short run the optimal estimator uses the returns of the second asset, because the average duration of the second trend is lower than that of the first trend. When s is larger than 0.7 year, the optimal estimator put more weight on the first asset than on the second asset, because the returns of the first asset become more pertinent for estimating a trend with a two-year average duration.

Misspecification of the EWMA estimator We may wonder what is the consequence of choosing a biased EWMA estimator. The first impact concerns the covariance matrix Υ_∞ . When we use the optimal estimator Λ , we deduce its value from the optimal covariance matrix Υ_∞ that satisfies the algebraic Riccati equation: $\Gamma - \Upsilon_\infty \Sigma^{-1} \Upsilon_\infty = \mathbf{0}$. Then, we have $\Lambda = \Upsilon_\infty \Sigma^{-1}$. When the EWMA matrix is given by the portfolio manager and is equal to $\tilde{\Lambda}$, the corresponding covariance matrix $\tilde{\Upsilon}_\infty$ does not satisfy the algebraic Riccati equation, but the Lyapunov equation²³:

$$-\tilde{\Lambda} \tilde{\Upsilon}_\infty - \tilde{\Upsilon}_\infty \tilde{\Lambda}^\top + \Gamma + \tilde{\Lambda} \Sigma \tilde{\Lambda}^\top = \mathbf{0}$$

²²The results are given in Table 6 on page 87.

²³Proof is given in Appendix A.5.7 on page 78.

Figure 23: Comparison of optimal and naive estimators $\omega(s)$ for the first asset


Let us consider the examples of the previous paragraph. In Tables 7–9 in page 88, we have reported the matrices Υ_∞ and $\tilde{\Upsilon}_\infty$ when we consider three specifications of $\tilde{\Lambda}$:

- We first assume that we have optimal univariate filters:

$$\tilde{\Lambda}_1 = \text{diag}(0.5, 1.0, 1.5)$$

- Then, we consider a three-month moving average:

$$\tilde{\Lambda}_2 = \text{diag}(0.25, 0.25, 0.25)$$

- Finally, we use the average of univariate moving averages²⁴:

$$\tilde{\Lambda}_3 = \text{diag}(1.0, 1.0, 1.0)$$

We verify that any specification of $\tilde{\Lambda}$ produces a covariance matrix $\tilde{\Upsilon}_\infty$ that is larger than the optimal covariance matrix Υ_∞ in the sense of Loewner ordering:

$$x^\top \tilde{\Upsilon}_\infty x \geq x^\top \Upsilon_\infty x$$

for any $x \in \mathbb{R}^n$.

The second impact concerns the expected value of $\hat{\mu}_t$. Indeed, the Kalman-Bucy filter ensures that:

$$\hat{\mu}_t \sim \mathcal{N}(\mu_t, \Upsilon_\infty)$$

²⁴The duration of univariate moving averages is respectively equal to six months, one year and eighteen months.

When we specify a given matrix $\tilde{\Lambda}$, we obtain:

$$\hat{\mu}_t \sim \mathcal{N}(\tilde{\mu}_t, \tilde{\Upsilon}_\infty)$$

where $\tilde{\mu}_t \neq \mu_t$. Since we have²⁵:

$$d(\hat{\mu}_t - \mu_t) = -\tilde{\Lambda}(\hat{\mu}_t - \mu_t) dt + \tilde{\Lambda}\Sigma^{1/2} dZ_t - \Gamma^{1/2} dZ_t^*$$

it follows that:

$$\mathbb{E}[d(\hat{\mu}_t - \mu_t)] = -\tilde{\Lambda}\mathbb{E}[\hat{\mu}_t - \mu_t] dt$$

If all the eigenvalues of $\tilde{\Lambda}$ are positive, we notice that $\tilde{\mu}_t = \mathbb{E}[\hat{\mu}_t] \rightarrow \mu_t$ when $t \rightarrow \infty$. Therefore, the bias $\tilde{\mu}_t - \mu_t$ decreases over time. Nevertheless, this result may be misunderstood because we may feel that we could obtain an unbiased estimator and the choice of $\tilde{\Lambda}$ is not important. Let us consider the market practice $\tilde{\Lambda} = \lambda I_n$. We have:

$$d(\hat{\mu}_t - \mu_t) = -\lambda(\hat{\mu}_t - \mu_t) dt + \tilde{\Lambda}\Sigma^{1/2} dZ_t - \Gamma^{1/2} dZ_t^*$$

The Lyapunov equation becomes:

$$-\lambda\tilde{\Upsilon}_t - \lambda\tilde{\Upsilon}_t + \Gamma + \lambda^2\Sigma = \mathbf{0}$$

We deduce the following solution:

$$\tilde{\Upsilon}_t = \frac{\lambda^{-1}\Gamma + \lambda\Sigma}{2}$$

We notice that:

$$\lim_{\lambda \rightarrow \infty} \tilde{\Upsilon}_t = \lim_{\lambda \rightarrow 0} \tilde{\Upsilon}_t = \Xi$$

where Ξ is an infinite matrix. We conclude that the arbitrary choice of $\tilde{\Lambda}$ leads to a trade-off between the bias $\mathbb{E}[\hat{\mu}_t - \mu_t]$ of the estimator and the error magnitude $\tilde{\Upsilon}_\infty - \Upsilon_\infty$ of the covariance.

Remark 6 In the univariate case, we verify that the lowest variance \tilde{v}_t of the trend estimator is obtained²⁶ when $\lambda^* = \gamma\sigma^{-1}$. Figure 24 illustrates the behavior of \tilde{v}_t with respect to the frequency λ for different values of σ and γ . We check that the variance is infinite at the extremes. However, if the choice of λ is not so far from the optimal value, the efficiency loss is limited, because the variance \tilde{v}_t is almost flat around λ^* .

2.2.5 Time-series versus cross-section momentum

Asset managers distinguish two trend-following strategies: time-series momentum and cross-section momentum. The first strategy, also called trend continuation, assumes that the past trend is a good estimate of the future trend (Moskowitz *et al.*, 2012). In this case, we have:

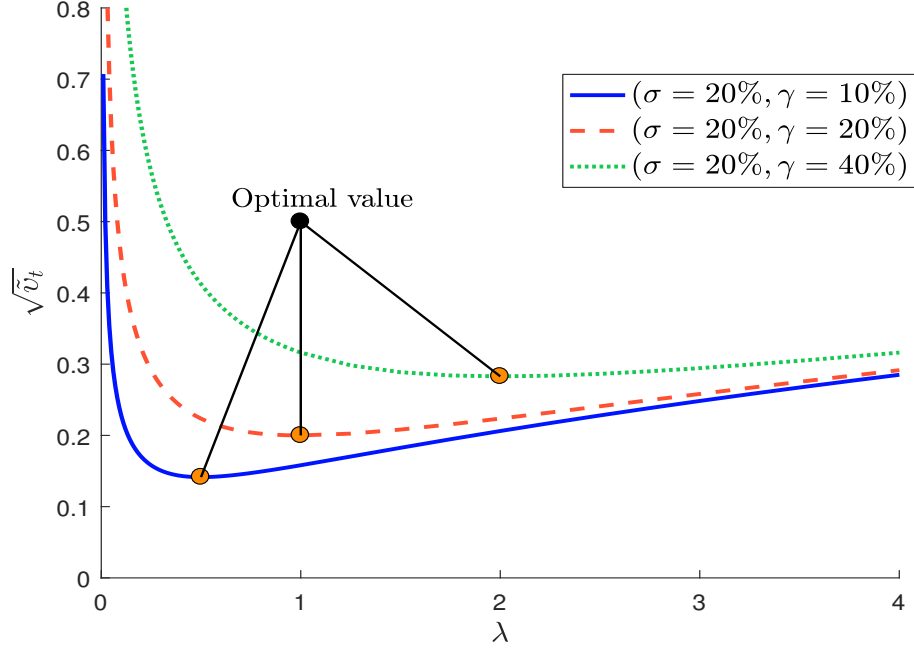
$$\begin{cases} \hat{\mu}_{i,t} \geq 0 \Rightarrow e_{i,t} \geq 0 \\ \hat{\mu}_{i,t} < 0 \Rightarrow e_{i,t} < 0 \end{cases}$$

²⁵See Appendix A.5.7 on page 78.

²⁶Let $\Gamma = \gamma^2$ and $\Sigma = \sigma^2$. The first-order condition is:

$$\frac{\partial \tilde{v}_t}{\partial \lambda} = \frac{1}{2} \left(-\frac{\gamma^2}{\lambda^2} + \sigma^2 \right) = 0$$

We deduce that $\lambda^* = \gamma\sigma^{-1}$ and $\tilde{v}_t = \gamma\sigma$.

Figure 24: Evolution of the volatility $\sqrt{\tilde{v}_t}$ with respect to the frequency λ


This implies that the exposure on Asset i depends on the sign of the trend. For instance, the specification $A = \text{diag}(\alpha_1, \dots, \alpha_n)$ where $\alpha_i > 0$ corresponds to a time-series momentum strategy since we have:

$$e_{i,t} = \alpha_i \hat{\mu}_{i,t}$$

The consequence is that the portfolio is long (resp. short) on all assets if they all have a positive (resp. negative) trend. The second strategy consists in being long on past best performing assets and short on past worst performing assets (Jegadeesh and Titman, 1993; Carhart, 1997). A typical cross-section momentum approach consists of selecting assets within the top and bottom quantiles, for example the top 20% and bottom 20%. If we use the mean as the selection threshold, we obtain:

$$\begin{cases} \hat{\mu}_{i,t} \geq \bar{\mu}_t \Rightarrow e_{i,t} \geq 0 \\ \hat{\mu}_{i,t} < \bar{\mu}_t \Rightarrow e_{i,t} < 0 \end{cases}$$

where:

$$\bar{\mu}_t = \frac{1}{n} \sum_{j=1}^n \hat{\mu}_{j,t}$$

Remark 7 This ranking system is very popular with asset managers and hedge funds. For instance, it is much used in statistical arbitrage or relative value. However, the allocation rule $e_{i,t} = \alpha_i \hat{\mu}_{i,t}$ is naive and may be not realistic. Fund managers prefer to use an equally-weighted or an equal risk contribution portfolio on the selected assets in order to have a diversified portfolio of active bets. Another approach consists in using Markowitz optimization. The goal is then to eliminate common risk factors and to keep only specific risk factors.

Let $\alpha = (\alpha_1, \dots, \alpha_n)$ be the vector of weights. The cross-section momentum strategy can be studied in our framework by setting:

$$\begin{aligned} e_{i,t} &= \alpha_i \left(\hat{\mu}_{i,t} - \frac{1}{n} \sum_{j=1}^n \hat{\mu}_{j,t} \right) \\ &= \alpha_i \left(1 - \frac{1}{n} \right) \hat{\mu}_{i,t} - \frac{\alpha_i}{n} \sum_{j \neq i} \hat{\mu}_{j,t} \end{aligned}$$

We deduce that:

$$\begin{aligned} A &= \begin{pmatrix} \alpha_1 (1 - n^{-1}) & -\alpha_1 n^{-1} & -\alpha_1 n^{-1} \\ -\alpha_2 n^{-1} & \alpha_2 (1 - n^{-1}) & -\alpha_2 n^{-1} \\ & \ddots & \\ -\alpha_n n^{-1} & -\alpha_n n^{-1} & \alpha_n (1 - n^{-1}) \end{pmatrix} \\ &= \text{diag}(\alpha) - \frac{1}{n} \alpha \otimes \mathbf{1}_n^\top \end{aligned}$$

Remark 8 There are two issues concerning the determination of the probability distribution of trading impact. First, we are not sure that $A^\top \Lambda^{-1}$ is a symmetric matrix²⁷. This means that the formulas of $G_{0,T}$ and g_t are only approximations of the ‘true’ payoff and trading impact. Second, $Q = A^\top (\mathbf{I}_n - \frac{1}{2} \Sigma A)$ may be not a symmetric positive definite matrix. This implies that the trading impact is not necessarily a definite quadratic form. If we assume that $\alpha_i = \alpha_j = \alpha$ and Λ is a diagonal matrix, the first issue is solved. We also deduce that Q is symmetric²⁸.

Let us consider the two-asset case. We assume that $\alpha_1 = \alpha_2 = \alpha$ and $\Lambda = \lambda \mathbf{I}_2$. In this case, the option profile is equal to:

$$G_{0,T} = \frac{\alpha}{4\lambda} \left((\hat{\mu}_{1,T} - \hat{\mu}_{2,T})^2 - (\hat{\mu}_{1,0} - \hat{\mu}_{2,0})^2 \right)$$

Figure 25 shows the option profile when the parameters are $\alpha = 1$, $\lambda = 1$ and $\hat{\mu}_{1,0} = \hat{\mu}_{2,0}$. The option profile is a convex function and is maximum when $|\hat{\mu}_{1,T} - \hat{\mu}_{2,T}|$ is maximum. While time-series momentum is based on absolute trends, cross-section momentum is sensitive to relative trends, and its performance depends on the dispersion of trends. However, it is certainly not realistic for a cross-momentum strategy to be based on two opposite trends. Indeed, this generally means that the two assets are anti-correlated. Therefore, this case is equivalent to a time-series momentum strategy. It is more realistic to focus on the region around the line $\hat{\mu}_{1,T} = \hat{\mu}_{2,T}$. Here, the rationale of the cross-section momentum is to benefit from the dispersion of realized trends when the assets are (highly) correlated.

If we consider the trading impact, we obtain:

$$\begin{aligned} g_t &= \frac{\alpha}{2} \left(1 - \frac{\alpha}{4} (\sigma_1^2 + \sigma_2^2) \right) (\hat{\mu}_{1,t} - \hat{\mu}_{2,t})^2 - \frac{\alpha\lambda}{4} (\sigma_1^2 + \sigma_2^2) + \\ &\quad \frac{\alpha}{2} \rho \sigma_1 \sigma_2 \left(\frac{\alpha}{2} (\hat{\mu}_{1,t} - \hat{\mu}_{2,t})^2 + \lambda \right) \end{aligned}$$

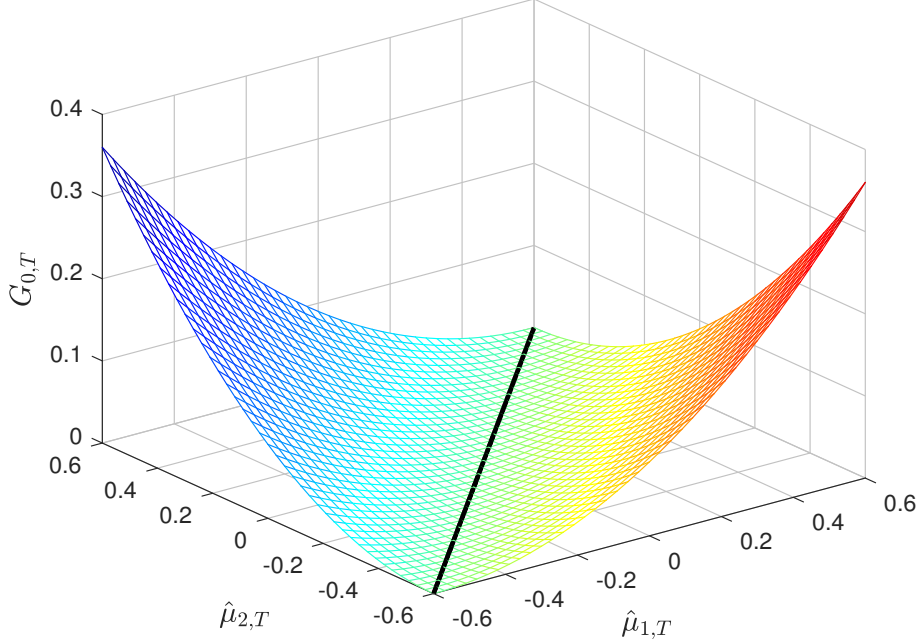
In Figure 53 (Appendix C on page 91), we have reported the distribution²⁹ of g_t for different correlation values ρ . Contrary to the time-series strategy, the sign of the correlation has

²⁷See Footnote 71 on page 75.

²⁸Because A is symmetric.

²⁹We use the following parameters: $\alpha = 1$, $\lambda = 1$, $\mu_{1,t} = 30\%$, $\mu_{2,t} = 10\%$ and $\sigma_{1,t} = \sigma_{2,t} = 30\%$.

Figure 25: Option profile of the cross-section momentum



an impact on the trading impact. This is confirmed by the statistical moments of g_t given in Figure 26. The expected return is a decreasing function of the correlation ρ . However, the risk of the strategy is maximal when ρ is equal to -1 whatever the risk measure we use (volatility, skewness and kurtosis). Contrary to a long-only portfolio, the diversification of cross-section momentum is not improved when we have negative correlations. Finally, we notice that the best Sharpe ratio is obtained when the correlation is positive and high (see Figure 54 on page 92). This result can be readily understood as the cross-section strategy is a relative strategy between trends. Therefore, we would like the assets to be correlated in order to capture spread risk between trends, and not the directional risk of trends.

Remark 9 In Appendix C on page 92, we have reported the probability distribution, the statistical moments and the Sharpe ratio of g_t in a four-asset case (Figures 55, 56 and 57). The results are similar to those obtained in the two-asset case. In particular, the best case for reducing risk and increasing the Sharpe ratio is to consider assets that are highly correlated.

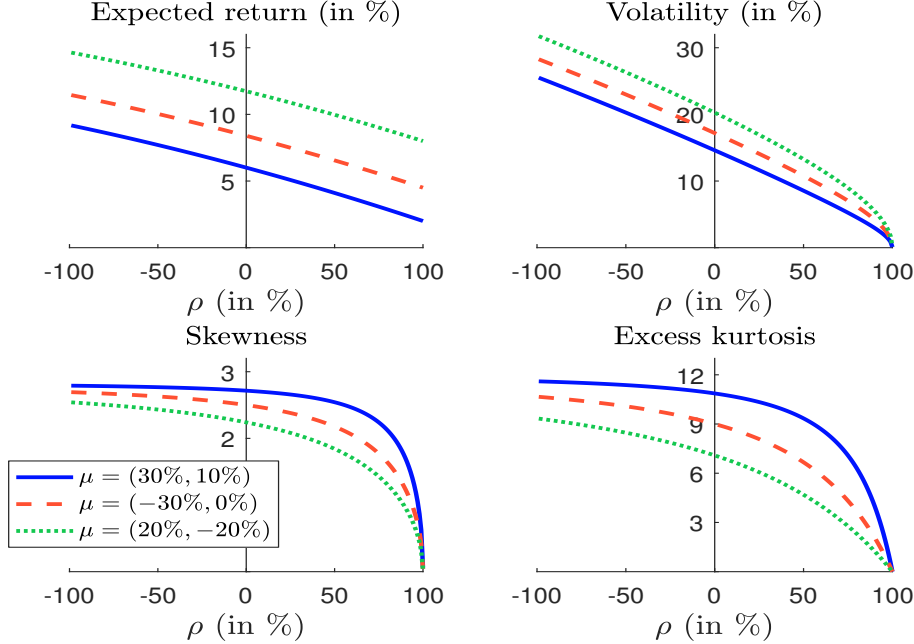
3 Empirical properties of trend-following strategies

3.1 P&L decomposition into low- and high-frequency components

Our model has been developed in continuous-time in order to obtain analytical formulas. For the implementation, we now consider the discrete-time version. We assume that we rebalance the portfolio at a series of pre-fixed dates $\{t_0, t_1, t_2, \dots\}$. We recall that the trend-following strategy is defined by the following exposure at time³⁰ t_k :

$$e_k = \alpha \hat{\mu}_k$$

³⁰We use the notation \square_k instead of \square_{t_k} in order to simplify the equations.

Figure 26: Statistical moments of g_t with respect to the correlation ρ (cross-section, $n = 2$)


where³¹:

$$\hat{\mu}_k = (1 - \lambda \cdot (t_k - t_{k-1})) \cdot \hat{\mu}_{k-1} + \lambda \cdot R_k^S$$

where λ is the frequency of the exponentially weighted moving average and R_k^S is the return of the underlying asset $S(t)$ between t_{k-1} and t_k . Therefore, the empirical return of the trend-following strategy $V(t)$ at time t_k is equal to:

$$R_k^V = e_{k-1} \cdot R_k^S$$

According to our model, we can calculate the theoretical return as follows:

$$\tilde{R}_k^V = \tilde{R}_k^G + \tilde{R}_k^g$$

where:

$$\tilde{R}_k^G = \frac{\alpha}{2\lambda} (\hat{\mu}_k^2 - \hat{\mu}_{k-1}^2)$$

and³²:

$$\tilde{R}_k^g = \alpha \sigma^2 \left(\frac{\hat{\mu}_{k-1}^2}{\sigma^2} \left(1 - \frac{\alpha \sigma^2}{2} \right) - \frac{\lambda}{2} \right) (t_k - t_{k-1})$$

\tilde{R}_k^G corresponds to the option profile component whereas \tilde{R}_k^g is the part of the performance due to the trading impact. By construction, the empirical return converges to the empirical

³¹The true formula is:

$$\hat{\mu}_k = (1 - \lambda \cdot (t_k - t_{k-1})) \cdot \hat{\mu}_{k-1} + (\lambda \cdot (t_k - t_{k-1})) \cdot \frac{R_k^S}{(t_k - t_{k-1})}$$

Indeed, we have to scale the return in order to obtain a yearly estimate of the trend.

³²In practice, we do not know the true volatility σ so we replaced it by an estimate $\hat{\sigma}_{k-1}$. In what follows, $\hat{\sigma}_{k-1}$ is calculated using a one-year exponentially weighted average.

return of the trend-following strategy when the rebalancing period tends to zero:

$$\lim_{t_k - t_{k-1} \rightarrow 0^+} \tilde{R}_k^V = R_k^V$$

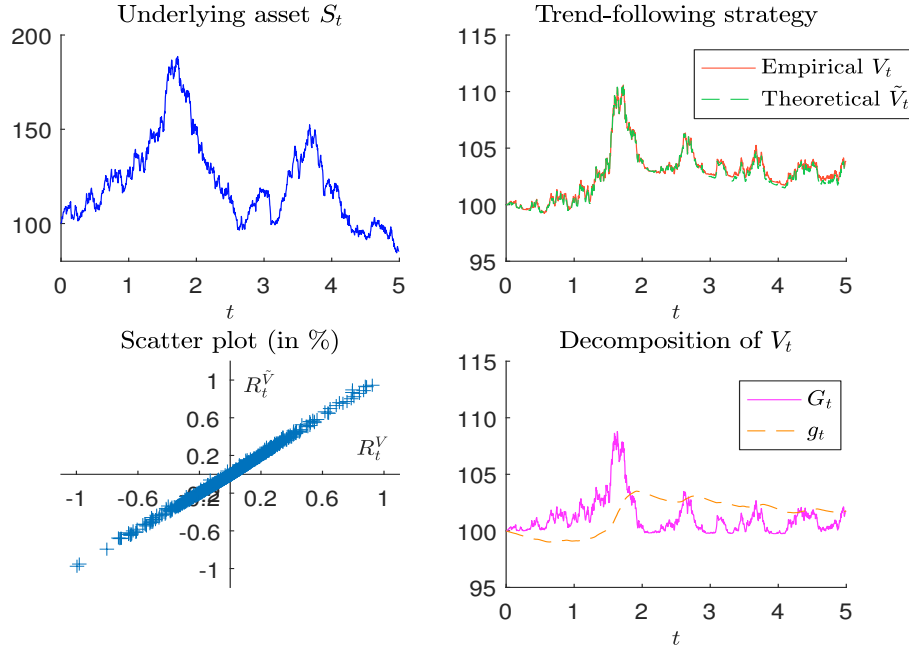
In this paper, we consider daily rebalancing, implying that $\tilde{R}_k^V \approx R_k^V$.

Let us illustrate the decomposition $R_k^V \approx \tilde{R}_k^G + \tilde{R}_k^g$. To do this, we simulate a geometric Brownian motion and we backtest the trend-following strategy with $\alpha = 1$ and $\lambda = 2$. In Figure 27, we have reported the underlying asset S_t in the first panel, and the cumulative performance³³ of the trend-following strategy in the second panel³⁴. We notice that \tilde{V}_t is very close to V_t . The accuracy of the model is also verified with the scatter plot between \tilde{R}_t^V and R_t^V (third panel). Therefore, we can decompose the cumulative performance of V_t by two components:

- a low-frequency component, which corresponds to the trading impact g_t ;
- a high-frequency component, which corresponds to the option profile G_t ;

Contrary to the widely-held belief, the long-term dynamics of V_t are explained by the trading impact whereas the short-term dynamics of V_t are explained by the option profile.

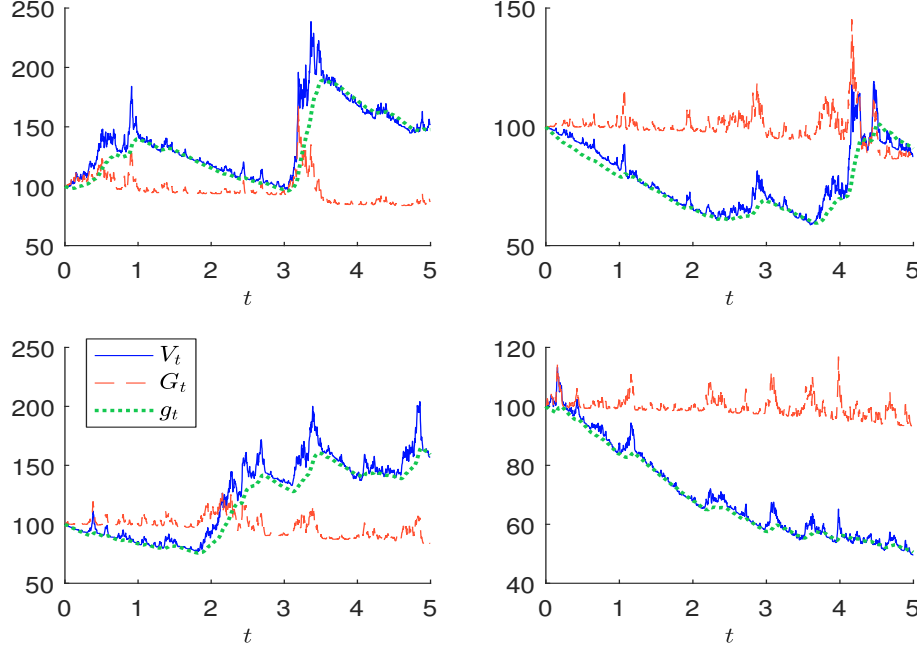
Figure 27: Comparison of the strategy performance V_t and the model performance \tilde{V}_t when the underlying asset is a simulated geometric Brownian motion



We now apply the previous decomposition to some financial assets. In Figure 29, we report the cumulative performance of V_t , G_t and g_t in the case of the Eurostoxx 50 Index. For this, we follow Bruder and Gaussel (2011) who prefer to perform the trend-following

³³All cumulative performances are calculated using the recursive formula: $X_k = (1 + R_k^X) X_{k-1}$ where $X_0 = 100$ and X_t stands for V_t , \tilde{V}_t , G_t and g_t .

³⁴Two other simulations are reported in Appendix C on page 94 (Figures 58 and 59).

Figure 28: The low- and high-frequency components of V_t


strategy on the volatility targeted index rather than on the index itself. We consider a 20% volatility target strategy and we assume that the parameter λ is equal to 2, meaning that the average momentum duration is six months, whereas the leverage α is set to 1. Again, we obtain the decomposition between the option profile and the trading impact. We also confirm that most of the performance of the momentum strategies comes from the trading impact, while the contribution of the option profile is not significant. In Figure 30, we have represented the relationship between the returns of the underlying asset and the returns of the trend-following strategy³⁵. We verify that:

1. the momentum strategy exhibits a convex option profile³⁶ (first panel in Figure 30);
2. the large losses are due to the option profile G_t ;
3. the performance of the option profile is close to zero;
4. the trading impact is not necessarily a convex function of the asset return³⁷ (second panel in Figure 30);
5. the losses of the trading impact are limited;
6. the expected return of the trading impact is positive.

If we consider other assets, we obtain similar results (see Appendix C on Page 95 for the results with S&P 500 and Nikkei 225 indices).

³⁵The returns correspond to the annualized 4-month rolling performance.

³⁶The solid black line corresponds to the quartic polynomial fit between R_k^S and R_k^G .

³⁷The solid black line corresponds to the quartic polynomial fit between R_k^S and R_k^g .

Figure 29: Decomposition of the trend-following strategy (Eurostoxx 50)

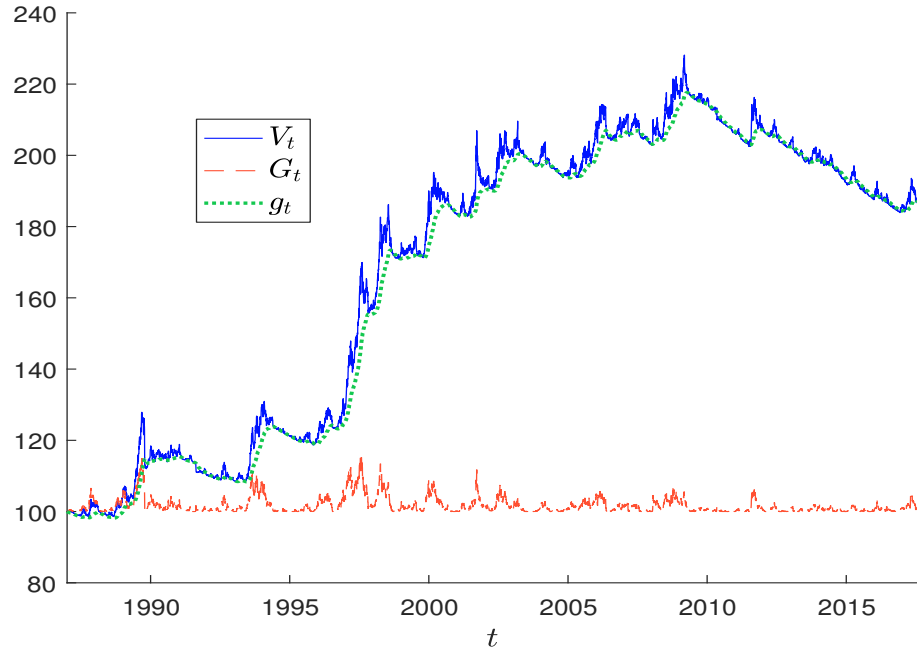
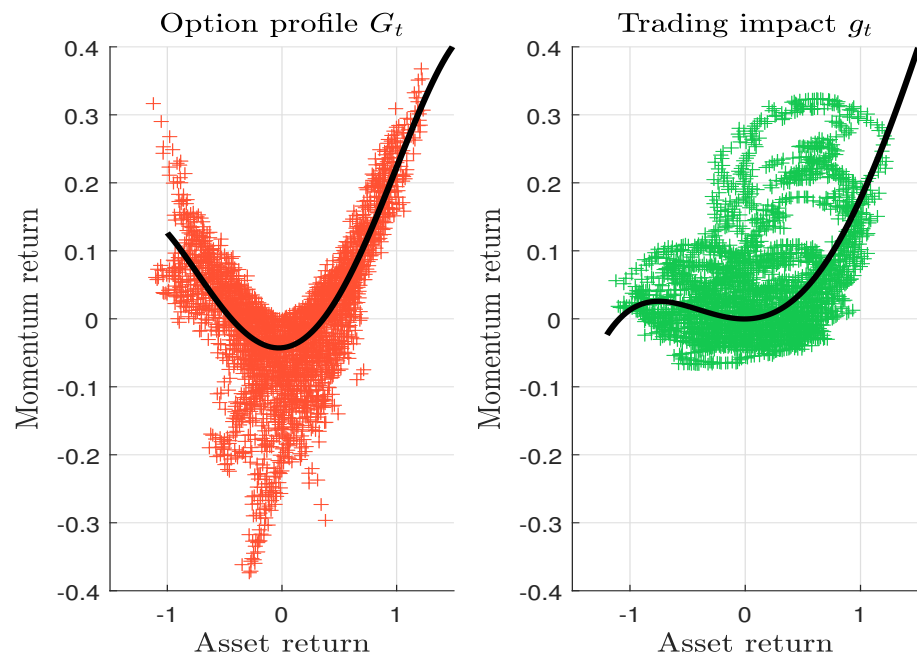


Figure 30: Scatterplot between asset returns and momentum returns (Eurostoxx 50)



3.2 Optimal estimation of the trend frequency

We recall that:

$$\begin{cases} dy_t = \mu_t dt + \sigma dW_t \\ d\mu_t = \gamma dW_t^* \end{cases}$$

where $dy_t = dS_t/S_t$. The corresponding discrete-time state space model is:

$$\begin{cases} R_k^S = (t_k - t_{k-1}) \mu_k + \sigma \sqrt{t_k - t_{k-1}} \epsilon_k \\ \mu_k = \mu_{k-1} + \gamma \sqrt{t_k - t_{k-1}} \epsilon_k^* \end{cases}$$

where $\epsilon_k \sim \mathcal{N}(0, 1)$ and $\epsilon_k^* \sim \mathcal{N}(0, 1)$ are two independent Gaussian processes. The log-likelihood function for the sample³⁸ is equal to³⁹:

$$\ell(\theta) = -\frac{T}{2} \ln 2\pi - \frac{1}{2} \sum_{k=1}^T \ln F_k - \frac{1}{2} \sum_{k=1}^T \frac{v_k^2}{F_k}$$

where v_k and F_k are the innovation process and its variance for the observation t_k . These two quantities are easily calculated using the Kalman filter. Therefore, we can estimate the parameters $\theta = (\sigma, \gamma)$ by maximizing the log-likelihood function $\ell(\theta)$. This approach is called the time-domain maximum likelihood method.

Another approach is to consider the frequency-domain maximum likelihood method. We assume that $t_k - t_{k-1}$ is a constant δ . It follows that:

$$\begin{aligned} R_k^S - R_{k-1}^S &= \delta(\mu_k - \mu_{k-1}) + \sigma \delta^{1/2} (\epsilon_k - \epsilon_{k-1}) \\ &= \gamma \delta^{3/2} \epsilon_k^* + \sigma \delta^{1/2} (1 - L) \epsilon_k \end{aligned}$$

We deduce that the stationary form of R^S is $\mathcal{S}(R^S) = R_k^S - R_{k-1}^S$ and the spectral density of $\mathcal{S}(R^S)$ is equal to:

$$f_{\mathcal{S}(R^S)}(\vartheta) = \frac{\gamma^2 \delta^3}{2\pi} + 2(1 - \cos \vartheta) \frac{\sigma^2 \delta}{2\pi}$$

where $\vartheta \in [0, 2\pi]$. Let $I_{\mathcal{S}(R^S)}(\vartheta)$ be the periodogram of $\mathcal{S}(R^S)$. Whittle (1953) shows that the log-likelihood function is given by:

$$\ell(\theta) = -\frac{T}{2} \ln 2\pi - \frac{1}{2} \sum_{j=0}^{T-1} \ln f_{\mathcal{S}(R^S)}(\vartheta_j) - \frac{1}{2} \sum_{j=0}^{T-1} \frac{I_{\mathcal{S}(R^S)}(\vartheta_j)}{f_{\mathcal{S}(R^S)}(\vartheta_j)}$$

where $\vartheta_j = 2\pi j/T$.

Using the (time-domain or frequency-domain) maximum likelihood method, we estimate the parameters $\theta = (\sigma, \gamma)$. We deduce that the ML estimate of the trend frequency λ is equal to:

$$\hat{\lambda} = \frac{\hat{\gamma}}{\hat{\sigma}}$$

We can also calculate the variance⁴⁰ of $\hat{\lambda}$:

$$\text{var}(\hat{\lambda}) = \frac{1}{\hat{\sigma}^2} (\hat{\lambda}^2 \text{var}(\hat{\sigma}) + \text{var}(\hat{\gamma}) - 2\hat{\lambda} \text{cov}(\hat{\sigma}, \hat{\gamma}))$$

We consider the universe of indices (equities, bonds, currencies and commodities) studied by Dao *et al.* (2016):

³⁸ T is the number of observations in the sample.

³⁹We apply the results given in Appendix A.1.2 on page 62.

⁴⁰The covariance matrix of $\hat{\theta} = (\hat{\sigma}, \hat{\gamma})$ is estimated by $(-\mathcal{H}(\hat{\theta}))^{-1}$ where $\mathcal{H}(\hat{\theta}) = \partial_{\theta}^2 \ell(\hat{\theta})$.

Table 2: Results of the frequency-domain maximum likelihood method

Index	$\hat{\sigma}$ (in %)	$\hat{\gamma}$ (in %)	$\hat{\lambda}$	$\sigma(\hat{\lambda})$	sign.	(in days)	$\hat{\tau}$ (in months)
Euribor	0.40	4.51	11.27	0.76	***	23	1M
Eurodollar	0.69	1.37	1.97	0.35	***	132	6M
Short Sterling	0.57	7.85	13.72	0.65	***	19	1M
UST	6.16	42.90	6.97	0.37	***	37	2M
Bund	5.44	8.26	1.52	0.24	***	171	8M
Gilts	6.09	78.87	12.95	0.49	***	20	1M
JGB	3.20	36.38	11.38	0.42	***	23	1M
SPX	19.62	200.21	10.20	0.31	***	25	1M
SX5E	24.72	288.88	11.68	0.38	***	22	1M
FTSE 100	19.08	236.26	12.38	0.37	***	21	1M
Nikkei 225	24.91	74.09	2.97	0.25	***	87	4M
EUR/USD	10.16	94.23	9.28	0.43	***	28	1M
JPY/USD	10.33	69.77	6.76	0.33	***	38	2M
GBP/USD	9.36	50.26	5.37	0.38	***	48	2M
AUD/USD	13.15	12.26	0.93	0.19	***	279	1Y
CHF/USD	11.75	63.46	5.40	0.25	***	48	2M
Crude Oil	37.05	104.29	2.82	0.31	***	92	4M
Gold	18.11	67.01	3.70	0.18	***	70	3M
Copper	27.57	127.43	4.62	0.42	***	56	3M
Soybean	23.98	125.57	5.24	0.42	***	50	2M

- Short term interest rates: Euribor, Eurodollar and Short Sterling;
- Government bonds: 10Y US Treasury Note, Bund, Gilts and JGB;
- Stock indices: S&P 500, EuroStoxx 50, FTSE 100 and Nikkei 225;
- Foreign exchange rates: EUR/USD, JPY/USD, GBP/USD, AUD/USD and CHF/USD;
- Commodities: WTI Crude Oil, Gold, Copper and Soybean.

The study period is from January 2000 to July 2017. We estimate the optimal value of λ by the maximum likelihood in the frequency domain. The idea is to determine which assets have a long trend or a short trend. The results⁴¹ are given in Table 2. We notice that the optimal moving average is generally short, between one and four months. We also find that commodities have a longer trend than equities. Results concerning Eurodollar, Bund, Nikkei 225 and AUD/USD are surprising and are not in line with those obtained for the other assets of the same asset class. The cases of Nikkei 225 and AUD/USD may be explained by the fact that the Japanese equity market is very singular and because the Australian dollar is considered as a commodity currency that mainly depends upon exports such as minerals and agricultural products. However, these results should be taken with some caution, because they are very sensitive to the study period. For instance, if we consider the last five years, equities present more longer trends with a 4-month average duration. If we focus on the last 10 years, government bonds have an average duration of one year, whereas the average duration of short term interest rates is three months.

⁴¹ ***, **, and * indicate significance at the 1%, 5%, and 10% levels, respectively.

3.3 Trends versus risk premia

For some assets, we notice that the exposure is mainly positive except for some short periods. It follows that the momentum risk premium can then benefit from two main patterns: trends and risk premia. In the first case, the asset must exhibit strong trends in order to obtain good performance. This is less relevant in the second case, since the momentum risk premium comes from the capacity to leverage or deleverage traditional risk premia. Therefore, the timing risk of the risk premium can be reduced by considering positive high Sharpe ratio assets.

Table 3: Exposure of the trend-following strategy (in %)

Index	Average \bar{e}	Absolute $ \bar{e} $	Negative \bar{e}_-	Positive \bar{e}_+	Frequency f_+
Euribor	56.5	153.3	-117.8	178.1	58.9
Eurodollar	157.6	250.7	-227.1	256.8	79.5
Short Sterling	59.3	157.8	-124.0	180.1	60.2
UST	48.8	108.2	-102.8	110.4	71.1
Bund	76.4	107.6	-107.4	107.6	85.5
Gilts	22.6	107.0	-105.8	107.8	60.1
JGB	82.8	135.5	-82.3	160.7	67.9
SPX	63.9	138.4	-91.2	171.1	59.1
SX5E	54.2	127.0	-83.4	160.7	56.4
FTSE 100	43.7	124.8	-92.9	149.6	56.3
Nikkei 225	47.5	124.5	-84.0	158.9	54.1
EUR/USD	22.2	108.8	-95.0	120.6	54.3
JPY/USD	-9.9	103.8	-114.2	93.5	50.2
GBP/USD	16.7	106.7	-91.2	121.9	50.6
AUD/USD	28.4	116.4	-101.2	128.1	56.5
CHF/USD	32.4	112.3	-114.0	111.4	65.0
Crude Oil	34.9	113.3	-98.8	122.8	60.3
Gold	28.7	105.3	-101.3	107.9	62.1
Copper	10.9	114.9	-115.5	114.5	55.0
Soybean	16.9	109.3	-115.7	105.1	60.1

Let us illustrate the relationship between momentum and risk premia with the previous asset universe. We backtest the EWMA trend-following strategy for each asset class⁴² and analyze the time-varying exposure for each asset. We then calculate the empirical values of the average exposure $\bar{e} = \mathbb{E}[e_t]$, the average absolute exposure $|\bar{e}| = \mathbb{E}[|e_t|]$, the average negative exposure $\bar{e}_- = \mathbb{E}[e_t | e_t < 0]$, the average positive exposure $\bar{e}_+ = \mathbb{E}[e_t | e_t > 0]$ and the frequency of positive exposure $f_+ = \Pr\{e_t > 0\}$. The results are given in Table 3. Except for the JPY/USD exchange rate, the average exposure \bar{e} is systematically positive. On average, it is equal to 10% for currencies, 23% for commodities, 52% for equities, 58% for bonds and more for interest rates instruments. It is generally accepted that currencies and commodities do not exhibit risk premia. This explains that their average momentum exposure is low. On the contrary, equities and bonds have risk premia and their momentum exposure is high. In the case of these two asset classes, we can then assume that the momentum strategy benefits from their risk premium. If we consider the average absolute

⁴² α is calibrated for each asset class such that the realized volatility of the trend-following strategy is equal to the realized volatility of the buy-and-hold strategy.

exposure $|\bar{e}|$, it is generally close to 100%, meaning that the gross exposure is comparable to that of the buy-and-hold strategy. An interesting point is the symmetry between \bar{e}_- and \bar{e}_+ . Indeed, the average positive exposure is similar to the average negative exposure for all asset classes, except for equities. In this last case, the value of long exposures is generally two times the value of short exposures. This result confirms the specific nature of equities and the associated risk premium. Another interesting point is the high level of the positive exposure frequency f_+ in the case of bonds. Positive trends are more frequent than negative trends with the same magnitude, but their strengths are similar.

3.4 Replication of trend-following strategies

In Section 3.1 on page 32, we have built trend-following strategies for some assets. We now consider the following exercise: Given a well-known trend-following strategy, is it possible to replicate its performance using our theoretical framework? This question is related to the subject of hedge fund replication that emerged in the mid-2000s. Hasanhodzic and Lo (2007) show that we can replicate the performance of a hedge fund portfolio using a linear factor model with traditional asset classes. This portfolio replication is based on the linear factor model:

$$R_t^{(\text{HF})} = r_t + \sum_{j=1}^{n_{\mathcal{F}}} \beta_{j,t} \mathcal{F}_{j,t} + \varepsilon_t$$

where $R_t^{(\text{HF})}$ is the hedge fund portfolio's return, r_t is the risk-free rate, $\mathcal{F}_{j,t}$ is the excess return of factor j , $\beta_{j,t}$ is the exposure of the hedge fund portfolio to factor j and ε_t is a white noise process. Contrary to traditional factor models where $\beta_{j,t}$ is assumed to be constant, the idea of Hasanhodzic and Lo (2007) is to assume that the exposure $\beta_{j,t}$ is time-varying:

$$\beta_{j,t} = \beta_{j,t-1} + \eta_{j,t}$$

where $\eta_{j,t}$ is a white noise process independent of ε_t . When we apply this framework to a well-diversified hedge fund portfolio, the R -squared coefficient of this dynamic model is generally larger than 80%. The reason is that a large part of the hedge fund's performance is linked to alternative betas (Roncalli and Teiletche, 2007). However, the replication of a specific hedge fund strategy and not a diversified portfolio of hedge fund strategies is more problematic (Roncalli and Weisang, 2011). This is the case of CTA or managed futures strategies (Hamdan *et al.*, 2016). Even if we use a sophisticated approach for estimating the time-varying exposure (like the Kalman filter), the R -squared coefficient of the factor model is generally lower than 20%.

Dao *et al.* (2016) suggest that the issue with CTA replication does not come from the estimates of the exposures $\beta_{j,t}$, but from the poor specification of the risk factors $\mathcal{F}_{j,t}$. Indeed, using an equally-weighted portfolio of basic trend-following strategies, they are able to replicate the SG CTA Index with a correlation of 80%. To align with the work of Dao *et al.* (2016), we implement the trend-following strategy on each asset in the previous universe⁴³ with a volatility target of 20%. Then, we consider an equally-weighted portfolio of the 20 trend-following strategies⁴⁴. In Figure 31, we report the daily correlation between this naive trend-following strategy and the SG CTA Index with respect to the frequency parameter λ . We notice that the daily correlation is larger than 70% when $\lambda \geq 1$. We find that the optimal value of λ is equal to 2.3, meaning that the optimal average duration is close to five months⁴⁵. In this case, the daily correlation is equal to 78%. In Figure 32, we have

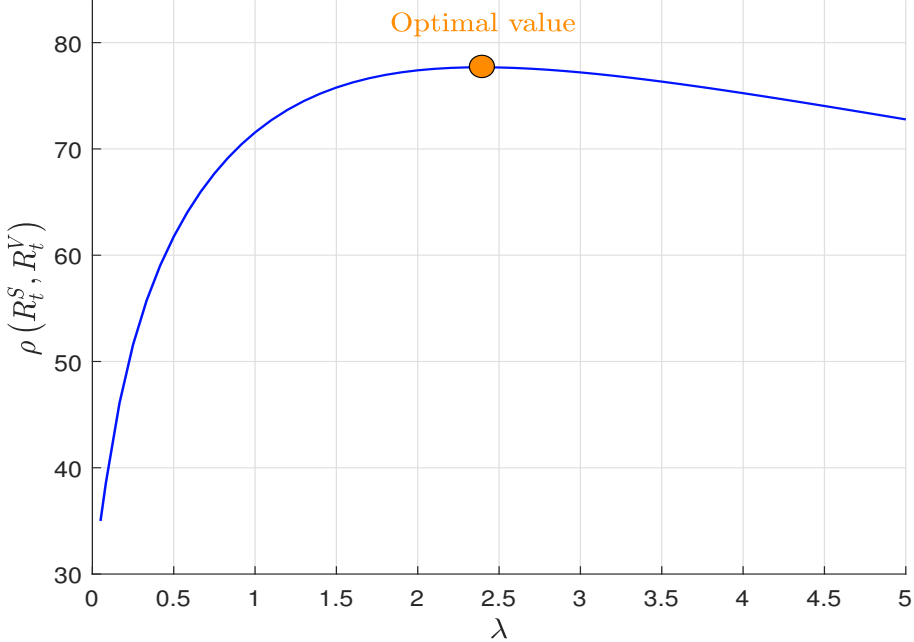
⁴³Described on page 37 (see also Table 2).

⁴⁴The exposure α is calibrated in order to obtain the volatility of the SG CTA Index.

⁴⁵This figure should be compared with the 6-month optimal moving average found by Dao *et al.* (2016).

reported the cumulative performance of the naive strategy and its decomposition between low- and high-frequency components. This result revisits the findings of Fung and Hsieh (2001), since it shows that the most important component is the trading impact and not the straddle option profile.

Figure 31: Correlation between the naive replication strategy and the SG CTA Index



We may wonder what contribution is made by each asset class. To see this, we perform the same replication exercise asset class by asset class. The results⁴⁶ are given in Figures 33 and 34. First, we notice that the daily correlation decreases and is generally below 50%. Second, the cumulative performance of the replicated strategies cannot be compared to the cumulative performance of the SG CTA Index. We conclude that diversification is a key parameter for understanding the performance of CTA strategies⁴⁷.

Remark 10 *We notice that the optimal value of λ obtained by the replication method is far from the optimal value estimated by the method of Whittle. Therefore, hedge funds prefer to use longer moving averages. Turnover and transaction costs may explain such choice.*

4 Tail risk management

Tail risk management is generally associated with portfolio insurance, which can be implemented using the CPPI method (Black and Perold, 1992; Perold and Sharpe 1995) or the OPBI approach (Leland, 1980; Rubinstein and Leland; 1981). The constant proportion portfolio insurance (CPPI) method is a dynamic trading strategy that allocates investments between the underlying asset and the reserve (or risk-free) asset. The option-based portfolio insurance (OBPI) method considers a portfolio that is invested in the underlying asset

⁴⁶We do not report those obtained with short rate instruments, because the daily correlation is very low about 30%.

⁴⁷See page 97 for more results concerning the combination of asset classes.

Figure 32: Comparison between the cumulative performance of the naive replication strategy and the SG CTA Index ($\lambda = 2.3$)

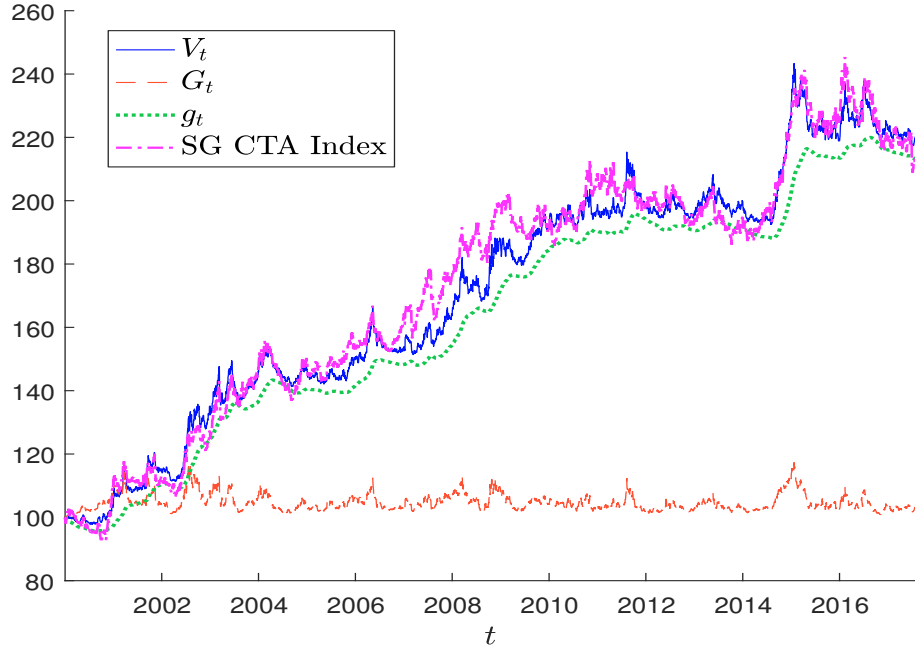


Figure 33: Correlation between the asset class trend-following strategy and the SG CTA Index

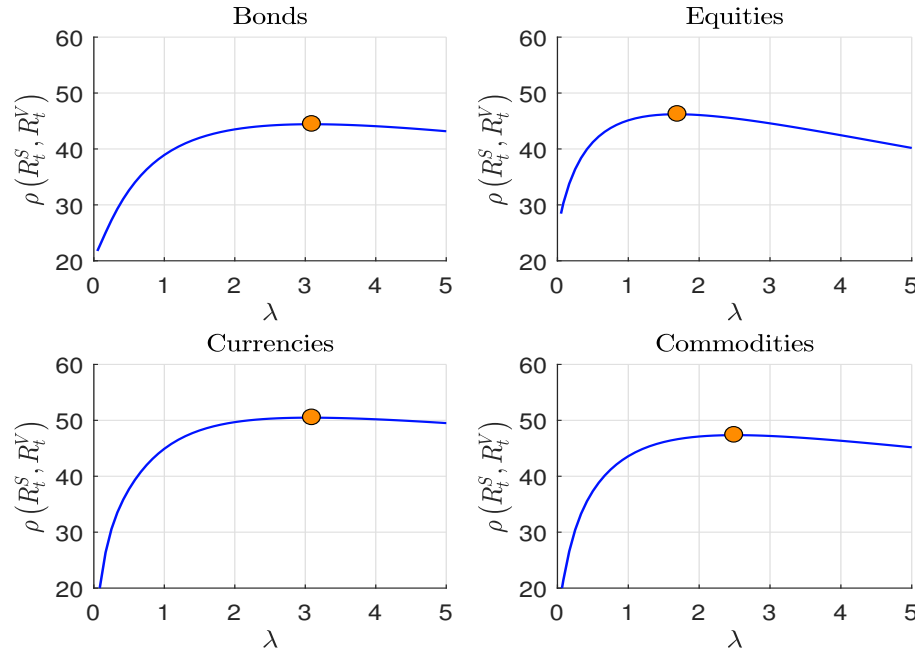
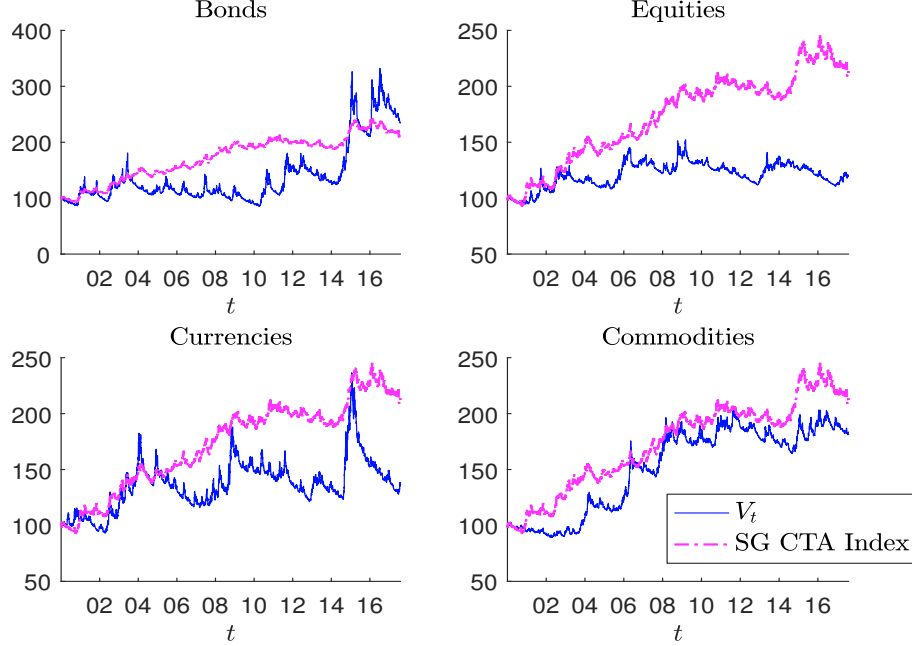


Figure 34: Comparison between the cumulative performance of the asset class trend-following strategy and the SG CTA Index



and a protective put option. In this case, the allocation between the two assets may be dynamically rebalanced. CPPI and OPBI methods have evolved significantly since the end of 1990s. For instance, CPPI may now be implemented using adjusted floors⁴⁸ (Estep and Kritzman, 1988), managed drawdowns (Grossman and Zhou, 1993), conditional multiples (Hamidi *et al.*, 2014) and adaptive protection (Soupé *et al.*, 2016), whereas OBPI strategies may use put spreads, calendar collars, etc. Today, asset managers and banks also propose a new spectrum of other methodologies, in particular managed volatility strategies (Hocquard *et al.*, 2013) and volatility overlay methods (Whaley, 2013).

At first sight, all these methods seem to be very different. However, they have at least two points in common:

- they are dynamic trading strategies;
- they exchange short-term volatility for long-term volatility.

The first point is related to the difference between passive and dynamic asset allocation. Even if the strategic asset allocation (SAA) is very well-diversified, investors must be active if they want to control their tail risk⁴⁹. This is particularly true given that many institutional investors implement a constant-mix strategy for their SAA portfolio. Such a strategy is clearly contrarian and may increase the tail risk because of its concave option profile⁵⁰. Only a strategy that presents a convex option profile may then reduce the drawdown risk. The second point is related to the price of hedging strategies. By exchanging short-term

⁴⁸This method is called time-invariant portfolio protection (TIPP).

⁴⁹This is why buy-and-hold strategies are not really efficient.

⁵⁰An alternative approach is to consider a risk parity strategy, which helps, but is not sufficient (Roncalli, 2013).

volatility for long-term volatility, managing tail risk necessarily induces a positive cost and raises the issue of profitability.

Since trend-following strategies have a convex option profile, they are good candidates for hedging tail risk. The empirical works of Fung and Hsieh (2001) and the 2008 Global Financial Crisis (GFC) have pushed asset owners and managers to use CTAs as a tail protection. For instance, the SGA CTA Index posted a performance of +13% in 2008, whereas the return of many long-term CTAs was higher than 20% during the same period. Moreover, we know that the delta hedging of options is highly related to momentum trading strategies. For example, a call option can be seen as a long-only trend-following strategy where the trend estimate corresponds to the delta of the option. In this section, we therefore consider all these elements for analyzing the momentum risk premium from a tail protection perspective.

4.1 The single-asset case

4.1.1 Theoretical results

We again consider the Bruder-Gaussel model, but the portfolio now consists in a 100% long position on the asset and an unfunded trend-following strategy on the same asset. Thus, the exposure becomes:

$$e_t = 1 + \alpha \hat{\mu}_t$$

In Appendix A.6 on page 80, we show that the portfolio's P&L may be decomposed into an option profile $\tilde{G}_{0,T}$ and a trading impact \tilde{g}_t :

$$\ln \frac{V_T}{V_0} = \tilde{G}_{0,T} + \int_0^T \tilde{g}_t dt$$

where:

$$\tilde{G}_{0,T} = \frac{\alpha}{2\lambda} (\hat{\mu}_T^2 - \hat{\mu}_0^2) + \frac{1}{\lambda} (\hat{\mu}_T - \hat{\mu}_0)$$

and:

$$\tilde{g}_t = \alpha \left(1 - \frac{\alpha \sigma^2}{2} \right) \left(\hat{\mu}_t - \frac{\alpha \sigma^2 - 1}{\alpha (2 - \alpha \sigma^2)} \right)^2 - \left(\frac{(1 - \alpha \sigma^2)^2}{\alpha (4 - 2\alpha \sigma^2)} + \frac{1}{2} (1 + \alpha \lambda) \sigma^2 \right)$$

We notice that the hedged portfolio's option profile is the sum of the asset's option profile and the option profile of the momentum strategy. In Figure 35, we report the different option profiles when the average duration τ is equal to six months. We verify that the convexity of the long-only strategy is improved. In particular, the return is larger when the asset's performance is negative. We can increase the convexity by using a higher leverage for the momentum strategy (see Figure 36). However, these results create the illusion that the option profile is always improved for any state of the asset. This is due to the initial trend, which is equal to zero. When $\hat{\mu}_0 \neq 0$, the option profile of the hedged portfolio may be lower than the option profile of the asset in some scenarios (see Figures 66 and 67 on page 98). In this case, we must have a very strong negative trend in order to be sure to improve the option profile of the hedged portfolio. This means that there are many situations where hedging the asset with a trend-following strategy induces a cost. This is particularly true when we observe a reversal of the trend, for instance when the past trend is strongly negative and the current trend is medium.

Let us now see the behavior of the trading impact. In Figures 37 and 38, we assume that $\alpha = 1$, $\mu_t = -20\%$, $\sigma = 20\%$ and $\lambda = 1$. The expected Sharpe ratio s_t is then equal

Figure 35: Option profile of the hedged strategy ($\alpha = 1, \hat{\mu}_0 = 0\%$)

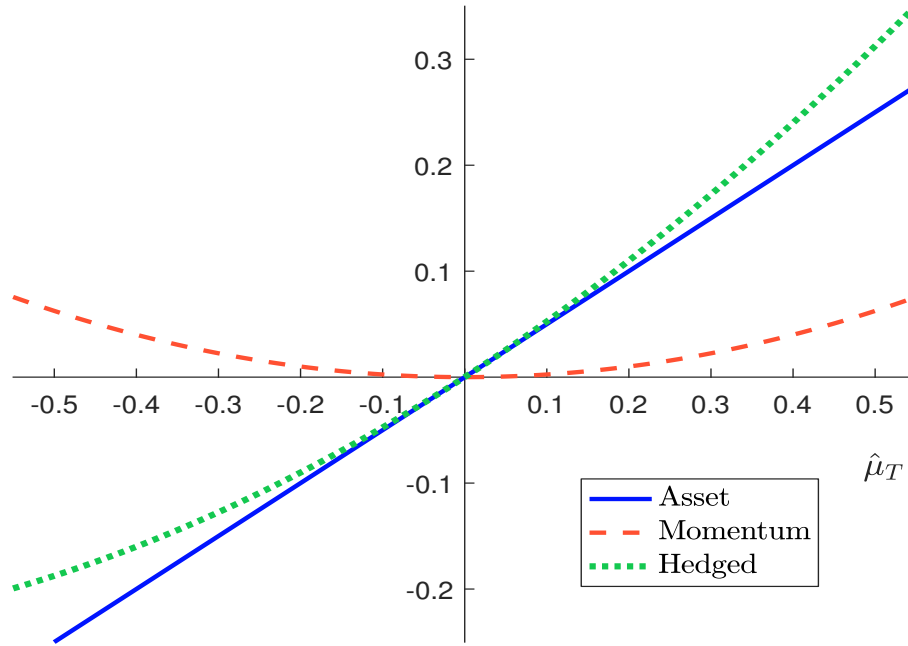
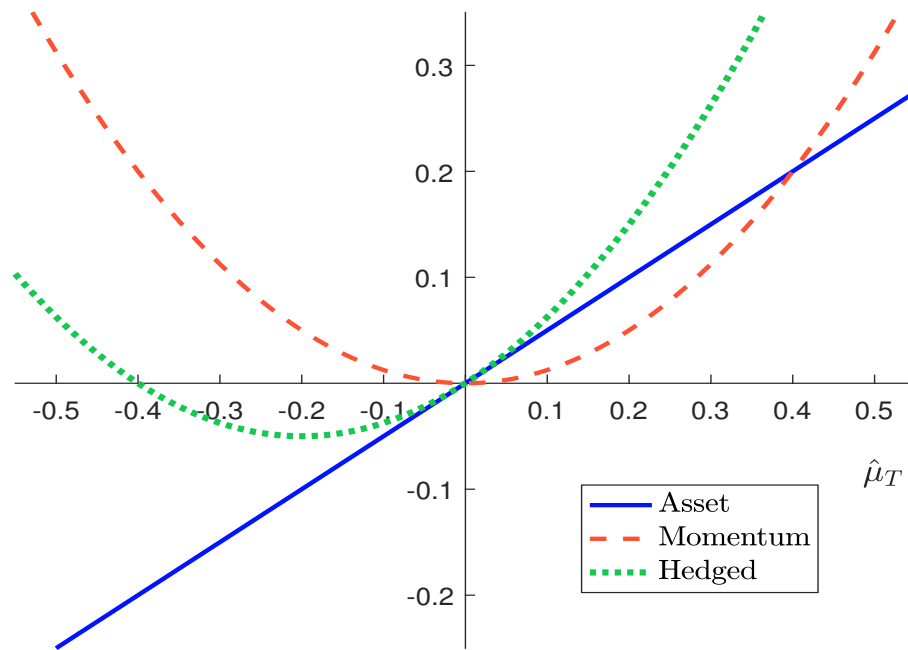
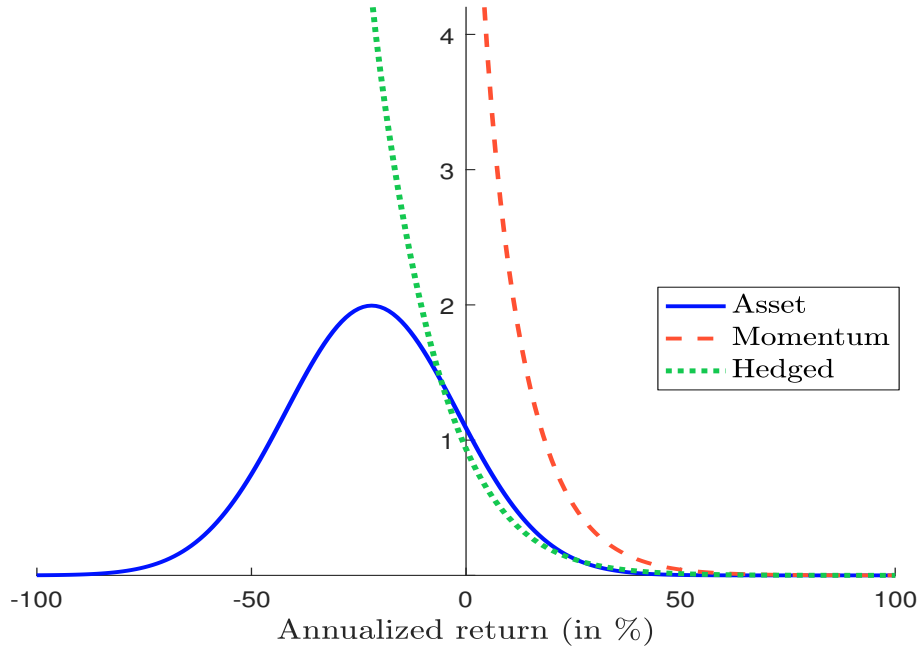


Figure 36: Option profile of the hedged strategy ($\alpha = 5, \hat{\mu}_0 = 0\%$)



to -1 . In our model, the asset has a Gaussian distribution and the momentum strategy has a noncentral chi-square distribution. The mix of the two strategies gives a noncentral chi-square distribution. This is why introducing the trend-following strategy reduces the magnitude of the largest loss (Figure 38). However, the loss reduction depends on the quantity α . For instance, we obtain Figures 68 and 69 on page 99 when α is set to 50%. The reduction is smaller⁵¹. The shape of the distribution is then highly dependent on the value of α . In Appendix A.6.3 on page 84, we show that α must be sufficiently large in order to change the shape of the P&L.

Figure 37: Probability density function of \tilde{g}_t ($s_t = -1$, $\alpha = 1$, $\lambda = 1$)

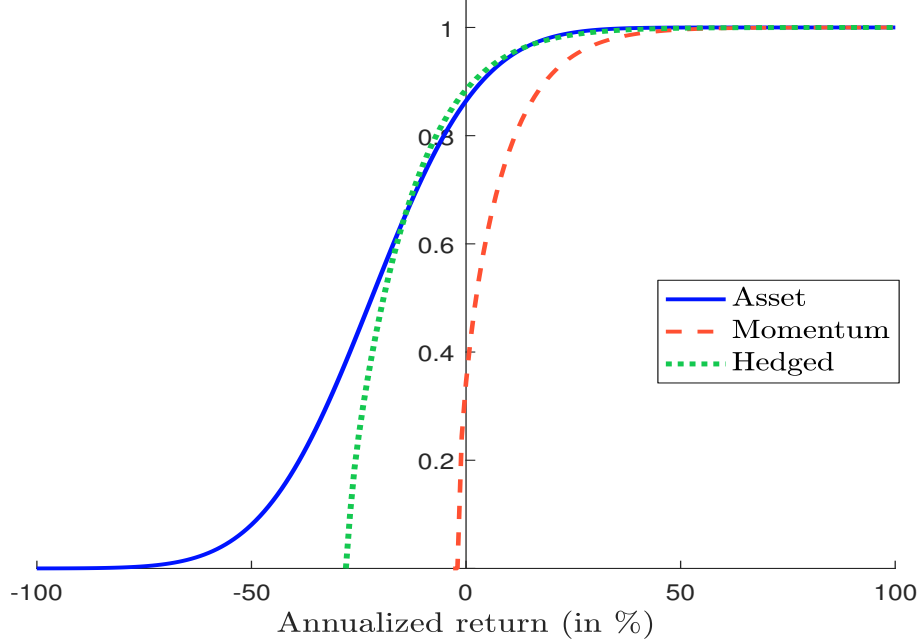


The impact of α may also be illustrated by calculating the statistical moments⁵² of \tilde{g}_t . In Figure 39, we notice that increasing alpha is equivalent to increasing the skewness and the kurtosis⁵³. This is normal since the underlying asset in our model is a Gaussian random variable. The impact on volatility is less obvious. When the Sharpe ratio is negative, introducing the trend-following strategy in the buy-and-hold portfolio first reduces the hedged portfolio's volatility risk. However, the volatility increases if the exposure on the trend-following strategy is too large, because we accumulate too much risk. The volatility reduction is related to the diversification effect of the trend-following strategy. For instance, this property disappears when the Sharpe ratio is positive, because buy-and-hold and trend-following strategies both lead to a long position on the underlying asset. We also notice that the expected return is improved, but this is due to the unfunded nature of the trend-following strategy. In order to better understand the loss reduction, we can calculate the value-at-risk

⁵¹Other illustrations are provided on pages 100 and 101 when the frequency λ is set to 2.

⁵²The formulas are given on page 82.

⁵³The parameters are $\sigma = 20\%$ and $\lambda = 2$.

Figure 38: Cumulative distribution function of \tilde{g}_t ($s_t = -1$, $\alpha = 1$, $\lambda = 1$)


of the hedged strategy:

$$\text{VaR}(\tilde{g}_t; p) = \frac{\lambda\alpha\sigma^2(2-\alpha\sigma^2)}{2}\mathbb{F}^{-1}(1-p; 1, \zeta) - \left(\frac{\beta^2(1-\alpha\sigma^2)^2}{\alpha(4-2\alpha\sigma^2)} + \frac{\beta^2\sigma^2}{2} + \frac{1}{2}\alpha\lambda\sigma^2 \right)$$

where p is the confidence level of the VaR and ζ is the noncentral chi-square coefficient:

$$\zeta = \lambda^{-1} \left(s_t - \frac{\beta(\alpha\sigma^2 - 1)}{\alpha\sigma(2 - \alpha\sigma^2)} \right)^2$$

Using the previous parameters, we obtain Figure 40. We observe that there is an optimal value of α that corresponds to the minimum value-at-risk.

4.1.2 Empirical results

We consider the asset universe described on page 37. For each asset, we calculate the simulated performance of the hedged portfolio. The hedging strategy is implemented on the 20% volatility targeted asset. In order to avoid overfitting, we consider the same parameter $\lambda = 2$ for all the assets. Moreover, the exposure α on the trend-following strategy is chosen such that the risk contribution of this strategy to the hedged portfolio's volatility is equal to δ . The results⁵⁴ are given in Figures 41 and 42 for one asset per asset class (Bund, S&P 500, AUD/USD and Crude Oil). We observe that the trend-following strategy reduces extreme losses, but it may increase medium losses. We also notice that the convexity of the hedged portfolio is more pronounced in bull markets than in bear markets. These results are disturbing, because there is clearly an asymmetry between negative and positive trends.

⁵⁴The returns correspond to the annualized 4-month rolling performance.

Figure 39: Statistical moments of \tilde{g}_t ($\lambda = 2$)

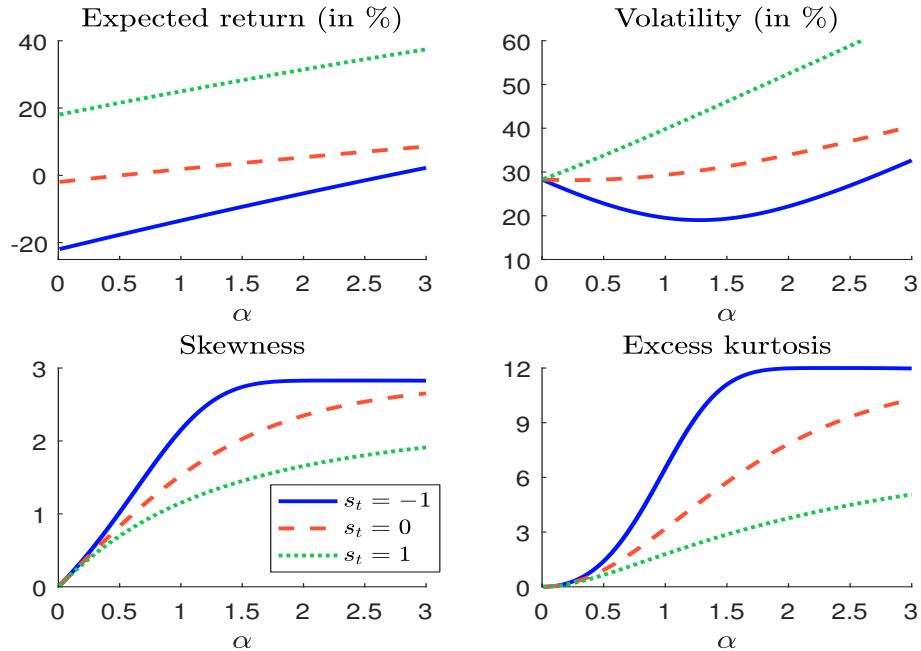


Figure 40: 95% Value-at-risk of the hedged portfolio ($\sigma = 20\%$, $\lambda = 2$)

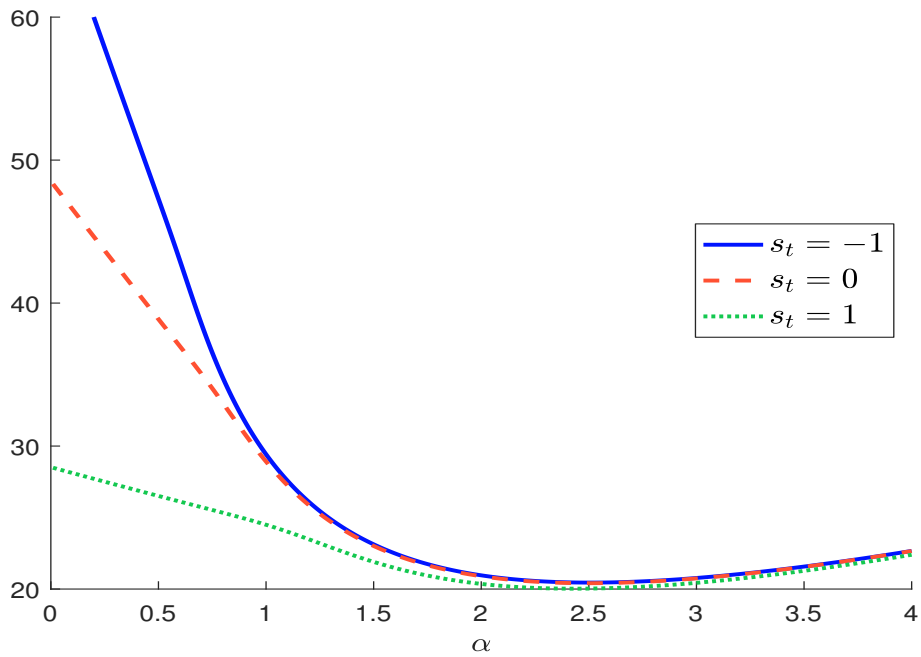


Figure 41: Scatterplot between returns of the asset and the hedged portfolio ($\delta = 20\%$)

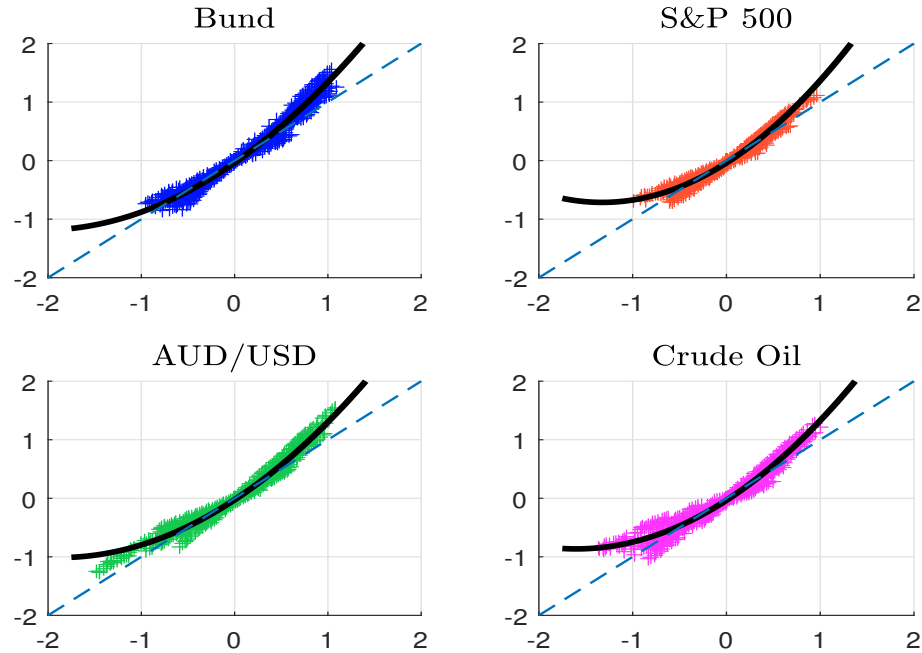
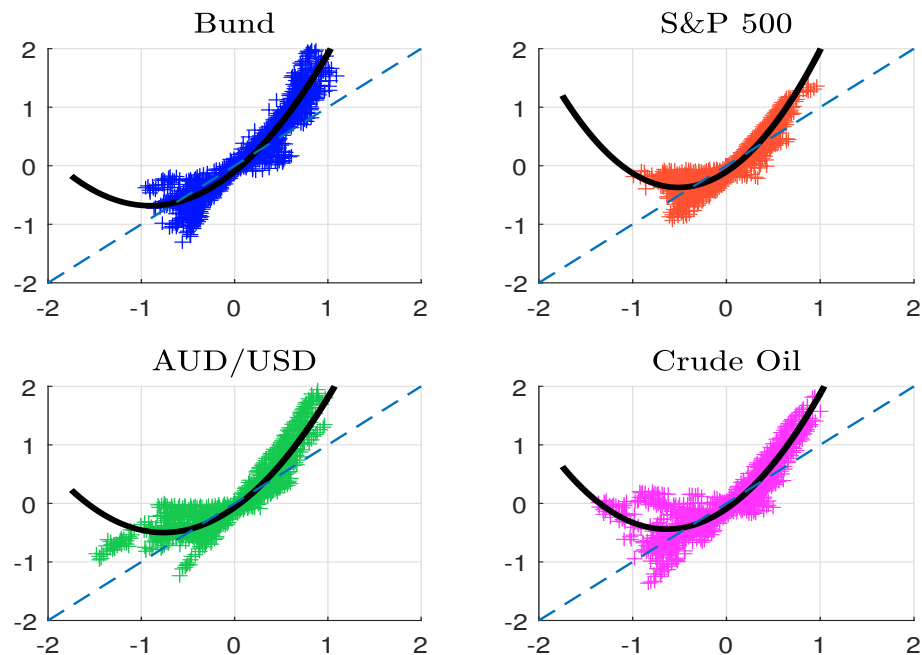


Figure 42: Scatterplot between returns of the asset and the hedged portfolio ($\delta = 40\%$)



4.2 The multi-asset case

4.2.1 Hedging a diversified portfolio

In the multivariate case, the allocation becomes:

$$\mathbf{e}_t = A\hat{\mu}_t + B$$

In Appendix A.6.2 on page 83, we show that:

$$\ln \frac{V_T}{V_0} = \tilde{G}_{0,T} + \int_0^T \tilde{g}_t dt$$

where the option profile is equal to:

$$\tilde{G}_{0,T} = \frac{1}{2} (\hat{\mu}_T^\top A^\top \Lambda^{-1} \hat{\mu}_T - \hat{\mu}_0^\top A^\top \Lambda^{-1} \hat{\mu}_0) + B^\top \Lambda^{-1} (\hat{\mu}_T - \hat{\mu}_0)$$

and the trading impact has the following expression:

$$\tilde{g}_t = \hat{\mu}_t^\top A^\top \left(\mathbf{I}_n - \frac{1}{2} \Sigma A \right) \hat{\mu}_t - \frac{1}{2} \text{tr} (A^\top \Sigma \Lambda^\top) + B^\top (I_n - \Sigma A) \hat{\mu}_t - \frac{1}{2} B^\top \Sigma B$$

Dao *et al.* (2016) show that there is a link between convexity and diversification. In particular, they notice that a diversified trend-following strategy provides a hedge for a multi-asset risk parity portfolio. In fact, our experience shows that this result depends on the portfolio construction of the diversified strategy and the trend-following strategy. It is obvious that using the same allocation scheme helps⁵⁵. More generally, the hedging gain depends on the correlation between the diversified portfolio and the equivalent long-only portfolio deduced from the trend-following strategy. In order to better understand this point, in the next paragraph we develop the case where we hedge a first asset by a second asset. The following analysis can then be applied to hedge a diversified portfolio by another (diversified) portfolio.

4.2.2 Hedging one asset with another asset

We consider a portfolio composed of a 100% long position on one asset and an unfunded trend-following strategy on another asset. This is a special case of the multi-asset model, where the allocation is given by $A = \text{diag}(0, \alpha)$ and $B = (1, 0)$. Therefore, the P&L is equal to:

$$\frac{dV_t}{V_t} = \underbrace{\frac{dS_{1,t}}{S_{1,t}}}_{\text{Asset}} + \underbrace{\alpha \hat{\mu}_{2,t} \frac{dS_{2,t}}{S_{2,t}}}_{\text{Hedging}}$$

If we assume that $\Lambda = \lambda \mathbf{I}_2$, we obtain:

$$\tilde{G}_{0,T} = \frac{\alpha}{2\lambda} (\hat{\mu}_{2,T}^2 - \hat{\mu}_{2,0}^2) + \frac{1}{\lambda} (\hat{\mu}_{1,T} - \hat{\mu}_{1,0})$$

and:

$$\begin{aligned} \tilde{g}_t &= \alpha \left(1 - \frac{\alpha \sigma_2^2}{2} \right) \hat{\mu}_{2,t}^2 - \frac{1}{2} \alpha \lambda \sigma_2^2 + \hat{\mu}_{1,t} - \alpha \rho \sigma_1 \sigma_2 \hat{\mu}_{2,t} - \frac{1}{2} \sigma_1^2 \\ &= g_{2,t} + \left(\hat{\mu}_{1,t} - \frac{1}{2} \sigma_1^2 \right) - c_t \end{aligned}$$

⁵⁵For instance, A may be a diagonal matrix that is proportional to the vector B .

where c_t is the hedging cost that depends on the correlation ρ between the two assets:

$$c_t = \alpha\rho\sigma_1\sigma_2\hat{\mu}_{2,t}$$

The previous formulas show that we can theoretically hedge the first asset by the second asset if the following conditions are met⁵⁶:

- the absolute value of the correlation is high:

$$|\rho| \simeq 1$$

- the Sharpe ratio of the second asset is larger than the Sharpe ratio of the first asset:

$$|s_{2,t}| \gg |s_{1,t}|$$

These results are obvious and are well known by overlay managers. It is sometimes more efficient to hedge one asset by a proxy, which is easier to trade because it is more liquid and for which a futures contract is available. The key point is then the basis risk, which is the tracking error between the asset and the hedge. In order to reduce this basis risk, we can choose proxies that are highly correlated to the hedged asset.

Our results highlight another important fact. Indeed, we notice that the hedging strategy may be implemented by a proxy that is negatively correlated with the asset. At first sight, we have the feeling that cases $\rho < 0$ and $\rho > 0$ are symmetric:

- $\rho < 0$

$$\hat{\mu}_{1,t} < 0 \Rightarrow \hat{\mu}_{2,t} > 0 \Rightarrow c_t < 0$$

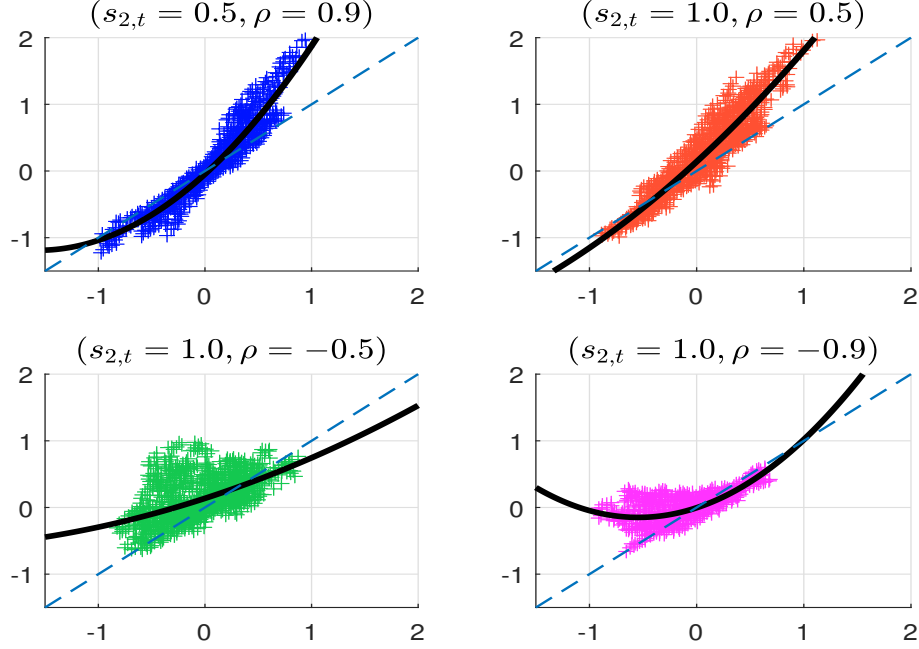
- $\rho > 0$

$$\hat{\mu}_{1,t} < 0 \Rightarrow \hat{\mu}_{2,t} < 0 \Rightarrow c_t < 0$$

This analysis ignores the impact of the correlation on the dependence between $\hat{s}_{1,t}$ and $\hat{s}_{2,t}^2$. In order to illustrate this asymmetry, we run a five-year Monte Carlo simulation. We assume that $\mu_1 = 0$, $\sigma_1 = 20\%$, $\sigma_2 = 20\%$ and $\lambda = 2\%$. As previously, the exposure α is chosen such that the risk contribution of the trend-following strategy to the hedged portfolio's volatility is equal to δ . In Figure 43, we report one run of the MC simulation for different values of $s_{2,t}$ and ρ . In the first panel, the correlation is set to 90%, we see the convexity of the hedged portfolio. In the second panel, we have increased the Sharpe ratio and decreased the correlation. It seems that the hedging strategy is less efficient. In the two last panels, the correlation is negative and the hedged portfolio presents a convex profile. If we run another simulation, we obtain different results (see Figure 75 on page 102). However, we find some common patterns between these different simulations on average. Among the four sets of parameters, it is the first set that exhibits the most important left and right convexity. This implies that the trend-following strategy generally reduces extreme losses, but also increases the best returns. This case corresponds to a high correlation between the buy-and-hold asset and the hedging asset. When the correlation is medium and positive, the hedged portfolio's option profile is more concave than convex. Therefore, the trend-following strategy may increase extreme losses. When the correlation is negative, both losses and gains

⁵⁶Another expression of the trading impact is:

$$\tilde{g}_t = \alpha\sigma_2^2 \left(\left(1 - \frac{\alpha\sigma_2^2}{2} \right) \hat{s}_{2,t}^2 - \frac{\lambda}{2} \right) + \sigma_1 \left(\hat{s}_{1,t} - \alpha\rho\sigma_2^2\hat{s}_{2,t} - \frac{1}{2}\sigma_1 \right)$$

Figure 43: Simulation of the cross-hedging strategy ($\delta = 0.40$)


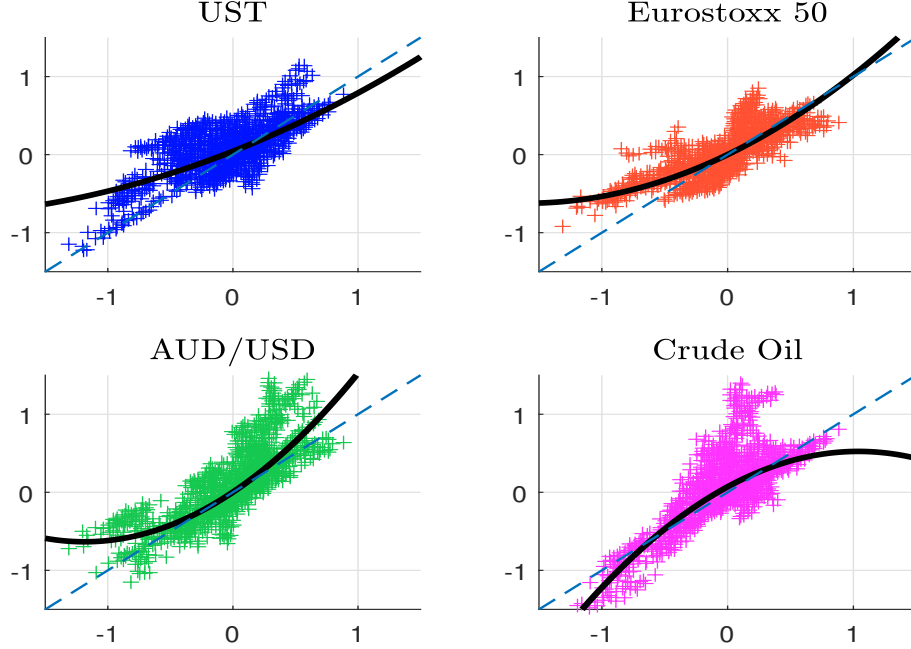
are highly reduced. In order to verify these patterns, we conduct a Monte Carlo simulation with 500 trials using the same parameters. For each simulation, we calculate the reduction in drawdown $\Delta(R^-)$ and the increase in the maximum gain $\Delta(R^+)$ of the hedged portfolio with respect to the asset. We also calculate the increase in the positive return frequency $\Delta(f^+)$ and the variation of the average return. The results are given below:

$s_{2,t}$	ρ	$s_{1,t} = 0$				$s_{1,t} = 1$			
		$\Delta(R^-)$	$\Delta(R^+)$	$\Delta(f^+)$	$\Delta(R)$	$\Delta(R^-)$	$\Delta(R^+)$	$\Delta(f^+)$	$\Delta(R)$
0.5	0.90	9.3	64.3	-6.0	2.3	7.5	56.4	-8.1	2.5
1.0	0.50	-9.1	45.0	3.2	8.5	-10.0	36.8	-1.9	8.2
1.0	-0.50	43.4	-8.2	9.1	8.7	62.1	-7.8	8.0	8.6
1.0	-0.90	84.4	-10.9	12.4	8.6	92.9	-7.4	16.3	8.3

We observe that the drawdown is reduced by 9% for the parameter set $(s_{2,t} = 0.5, \rho = 0.9)$, whereas it is increased by 9% for the parameter set $(s_{2,t} = 1.0, \rho = 0.5)$. The cross-hedging strategy significantly improves the best return for these two sets of parameters. However, it reduces the best return when the correlation is negative. On average, the hedged performance has a better return than the buy-and-hold strategy. Curiously, this improvement is lower for the first set of parameters than for the other sets of parameters.

Remark 11 We applied the cross-hedging strategy to the S&P 500 Index. Some results are given in Figure 44. We notice that some assets provide a partial hedge to a long exposure on the S&P 500. We also observe that the profile of the hedged portfolio may be concave⁵⁷. Curiously, assets that are negatively correlated with the S&P 500 do not necessarily provide a good hedge. For instance, this is the case of the Bund or the 10Y T-bond. Moreover, the

⁵⁷This is the case when we would like to hedge the S&P 500 with crude oil.

Figure 44: Cross-hedging of the S&P 500 Index ($\delta = 0.40$)


efficiency of the hedge highly depends on the period. We do not observe the same patterns during the internet bubble crisis and the subprime crisis.

4.3 The skewness risk puzzle

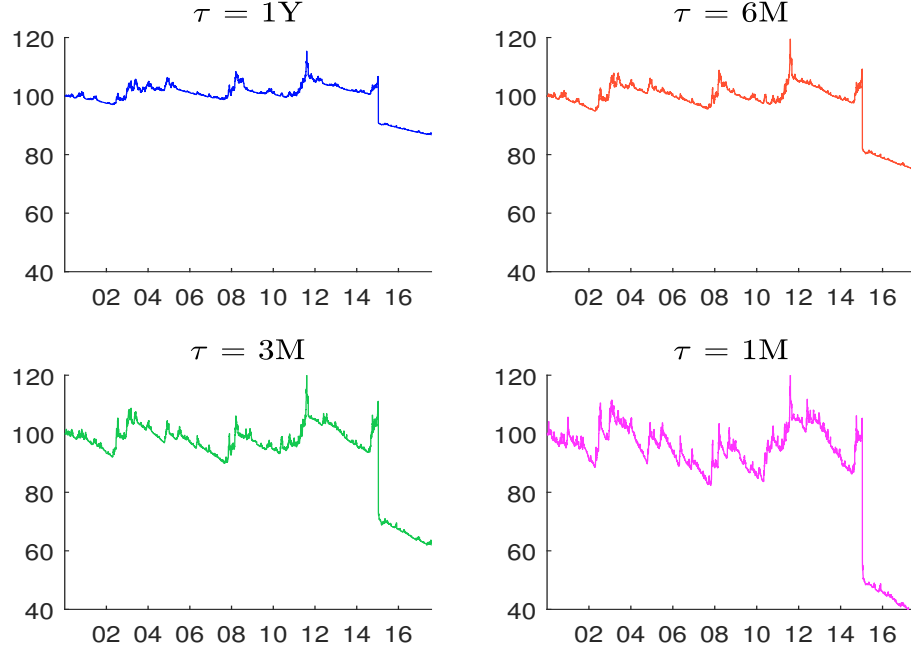
One important issue when implementing a hedge is the choice of the frequency λ of the trend-following strategy. More precisely, it is obvious that the hedging efficiency is related to this parameter and the frequency ω of the drawdown risk that we would like to hedge. The basic hedging rule suggests to use the following tip:

$$\lambda \simeq 2\omega$$

However, trend-following strategies are generally implemented by investors at medium or low frequencies. Therefore, short-term hedging is a challenge in this framework, because the time scale of skewness events is very different than the time scale of trends.

In fact, we think that there is a misconception about CTAs. Many people think that CTAs are good strategies for hedging the skewness risk of the stock market. In reality, trend-following strategies help to hedge drawdowns due to volatility risk. For instance, CTAs did a very good job in 2008, because the Global Financial Crisis is more a high volatility event than a pure event of skewness risk. However, it is not obvious that CTAs may post similar performances when facing skewness events. For instance, the performance of CTAs was disappointing during the Eurozone crisis in 2011 and the Swiss CHF chaos in January 2015. In Figure 45, we have reported the cumulative performance of the trend-following strategy applied to the CHF/USD currency. On January 15th 2015, we observe a large drawdown whatever the frequency of the moving average estimator. This illustration shows that hedging skewness events with a trend-following strategy is inefficient.

Figure 45: Cumulative performance of the trend-following strategy (CHF/USD)



5 Conclusion

The momentum risk premium has been extensively documented by academics and professionals. There is no doubt that momentum strategies have posted impressive (real or simulated) past performance. There is no doubt that asset owners and asset managers widely use momentum strategies in their portfolios. There is also no doubt that the momentum risk factor explains part of the performance of assets. With the emergence of alternative risk premia, momentum is now under the scrutiny of sophisticated institutional investors, in particular pension funds and sovereign wealth funds. Therefore, Roncalli (2017) supports the view that carry and momentum⁵⁸ are the most relevant alternative risk premia since they are present across different asset classes, and must be included in a strategic asset allocation. Nevertheless, the development of alternative risk premia has some big impacts on portfolio construction, because the relationships between these strategies are non-linear. In this case, the traditional diversification approach based on correlations must be supplemented by a payoff approach. However, most risk premia have a concave payoff. The momentum risk premium thus plays a central role as it exhibits a convex payoff, and we know that mixing concave and convex strategies is key for managing skewness risk in bad times.

Sophisticated institutional investors need to profoundly understand these new risk premia in order to allocate them in an optimal way. On the one hand, there are many academic and professional studies based on backtesting. Such an approach is interesting to understand past performance, but it is limited when we consider portfolio construction. On the other hand, there are a few research studies that have proposed analytical models, but most of them are not known by professionals (or by academics⁵⁹). The objective of our article was

⁵⁸Carry and momentum are, along with the value (or contrarian) strategy, generic trading strategies. Other trading programs can be viewed as a combination of these 3 investment styles.

⁵⁹With the exception of Fung and Hsieh (2001), which has about 1100 quotes, the other articles have very

twofold. First, this was an opportunity to review the different results obtained previously. Second, most of these results only concern the single-asset case. Hence, our objective was therefore to extend them to a multi-asset framework. It was important to consider a simple model in order to use a unified approach for treating the various questions related to the momentum risk premium. The continuous-time model was also chosen to obtain tractable formulas. The framework used by Bruder and Gausse (2011) was sufficiently flexible to develop a multivariate momentum model, which is why we adopted this framework.

In our model, asset prices follow a multi-dimensional geometric Brownian motion with a stochastic trend. It is then a variant of the standard Black and Scholes financial model. We can then deduce that the optimal estimator of the trend is an exponentially weighted moving average. We see a standard market practice. However, contrary to investors who generally use an exogenous moving average frequency, the optimal frequency is the ratio between the trend volatility and the asset volatility. A short moving average is then optimal when the short-term component of the volatility dominates the long-term component. In the multivariate case, we show that the optimal filtering of the trend depends on the correlation structure of asset returns. We also demonstrate that a multivariate moving average produces better trend estimates than a collection of univariate moving averages. However, errors due to a misspecification of the moving average are relatively low. In other words, estimating a 4-month trend with a 6-month or a 3-month moving average does not make much difference.

By assuming that the exposure of the strategy is proportional to the moving average, we demonstrate that the P&L of the trend-following strategy has two components. The first component is the option profile and the second component is the trading impact (Gausse and Bruder, 2011). This decomposition is very similar to the robustness equation of the Black-Scholes formula (El Karoui *et al.*, 1998). We establish a bridge between trend-following and delta hedging. As already found by Fung and Hsieh (2001), we obtain a convex payoff, but it is a second-order. The primary effect is the trading impact, which depends on the absolute value of the asset's Sharpe ratio and the frequency of the moving average. The trading impact is bounded below, implying that the loss of a momentum strategy is bounded, but its gain may be infinite. In the case where the absolute value of the Sharpe ratio is low, the hit ratio is smaller than 50%. We confirm the result of Potters and Bouchaud (2006), who argue that “*trend followers lose more often than they gain*”. However, this result does not hold when the Sharpe ratio is highly negative or positive. In this case, the gain frequency may be larger than the loss frequency.

Another outcome is that the expected gain is larger than the expected loss whatever the value taken by the Sharpe ratio. It is also remarkable that the probability distribution of the P&L is related to the chi-square distribution. Contrary to traditional assets, the returns of a momentum strategy cannot be approximated by a Gaussian distribution. This is why the momentum risk premium has a positive skewness contrary to traditional risk premia. This result makes the momentum very singular in the universe of risk premia, because it is certainly the only strategy that presents this property of positive skewness. However, this does not mean that it is not a risky strategy. The momentum risk premium has two main risks. The first one is obvious, and concerns trend reversals. This point has been already observed by Daniel and Moskowitz (2016), who showed that investors may face momentum crashes, especially when they use a cross-section implementation. This point is also related to the coherency between the duration of the trend and the duration of the moving average. The second risk is less obvious because it is associated with the leverage effect. At first sight, leverage may be viewed as a homogeneous scaling mechanism. In the case of CPPI products, we know that the scaling is not homogenous and that an excessively high leverage

few quotes: 19 for Potters and Bouchaud (2006), 11 for Bruder and Gausse (2011), 8 for Martin and Zou (2012), 2 for Dao *et al.* (2016), etc. (source: Google Scholar).

dramatically destroys the performance of such products. For momentum strategies, we observe a similar effect, because the gamma costs may be prohibitive when we exceed a certain level of leverage and when the asset volatility is high. As a consequence, even if the ruin probability of a momentum strategy is significantly lower than for value and contrarian strategies, investors may pay attention to the leverage risk.

As already said, to understand performance, two market parameters are important: the realized Sharpe ratio and the realized volatility. Since a trend-following strategy has a negative vega, the momentum risk premium does not like volatility to increase. This result is the opposite of that obtained with value and contrarian strategies. In contrast, the momentum risk premium likes assets with high negative or positive Sharpe ratios. However, it is essential that the temporal measure of the Sharpe ratio corresponds to the duration of the moving average. The Sharpe ratio is a relative measure of the strength of the trend. Our model shows that a strong trend with a high volatility is not necessarily better than a medium trend with a very low volatility. This is why a momentum risk premium faces a trade-off between trend and volatility. A famous example is the Global Financial Crisis in 2008. Some people think that the incredible performance of trend-following strategies in 2008 is mainly due to short exposures on the equity market. This is not true, because even though we had a very strong negative trend on stocks, the volatility of this market was also very high. Because the performance of stocks and bonds was negatively correlated during this period, trend-following strategies benefited from the positive trend on sovereign bonds, whose volatility was contained. In the end, long fixed-income exposures contributed more to the momentum risk premium in 2008 than short equity exposures.

The diversification effect is an important topic when we build a multi-asset trend-following strategy. In the case of a long-only investment portfolio, the best case for diversification is when some assets are negatively correlated to other assets. This explains why the stock/bond asset mix policy is certainly the most well-known diversified portfolio. However, the case of negative correlation is symmetric to the case of positive correlation. For instance, if we consider the two extreme cases, a correlation of +1 between two assets is equivalent to a correlation of -1 in a long/short portfolio, because there is only one trend in both cases. Therefore, the best case is when the correlation is equal to zero, because we have two independent trends. In fact, the concept of diversification is more complex for momentum strategies than for long-only investment portfolios. In particular, we must distinguish time-series momentum and cross-section momentum. A time-series momentum strategy prefers independent assets rather than (positively or negatively) correlated assets. It also prefers a small number of assets with a significant Sharpe ratio in absolute value to a large number of assets with a low Sharpe ratio. In contrast, a cross-section momentum prefers highly correlated assets to independent assets. The absolute level of Sharpe ratios is not important, because a cross-section momentum is more sensitive to the dispersion of Sharpe ratios. In the multivariate case, the allocation matrix becomes a key parameter for understanding the performance. For a time-series momentum strategy, weight diversification reduces the expected gain. For a cross-section momentum strategy, weight diversification improves the expected gain. The reason is that there are few big trends in financial markets. When a big trend appears, the time-series strategy should concentrate its exposure on this bet rather than diversify the bets. This is not the case of the cross-section strategy, because it should be exposed to many relative bets. The choice of the universe is therefore essential when considering a trend-following strategy. Generally, time-series momentum is implemented with a multi-asset universe in order to have decorrelated assets and absolute bets, whereas cross-section momentum is implemented within a single-asset class in order to have correlated assets and relative bets.

For a long time, investors perceived trend-following strategies in a pure alpha portfolio,

because they were mainly managed and proposed by hedge funds. The analysis of these strategies was therefore done on a standalone basis, in order to verify that they have a good risk/return profile. After this period, investors started to consider trend-following strategies as a building block in a diversified allocation, and not as an absolute return portfolio. Indeed, they realized that such strategies have locally a lot of beta. In the long-run, their beta is close to zero, because they dynamically manage these exposures, but this result is purely statistical. They understood that their diversification power comes from the short exposure and depends on the market regime. In particular, they observed that they have the tendency to perform well in a period of stressed equity markets (Fung and Hsieh, 2001). Since the concepts of diversification and hedging are related, some asset owners and asset managers then considered that trend-following strategies could be hedging strategies. It is true that they share common properties with option and overlay strategies (Dao *et al.*, 2016). As expected, our results confirm that trend-following strategies can be used to manage downside protection. However, our theoretical model shows that it is less obvious when we consider the multivariate case, when the hedged asset is a multi-asset diversified portfolio. Another important point concerns the definition of downside protection. Our simulations demonstrate that trend-following strategies are not able to manage the tail risk, and the momentum risk premium may suffer when skewness risks occur. Therefore, downside protection is not the same as tail risk protection, but must be seen as volatility risk protection. When the market downturn is gradual, momentum strategies may be hedging tools, but they are inefficient when skewness events drive sharp falls in asset prices. This is the story behind the performance of CTAs in January 2015.

Readers of this paper might think that harvesting the momentum risk premium is relatively straightforward. Indeed, we have shown that we can easily replicate the SG CTA Index using our theoretical model. However, we must warn investors that our backtest does not take into account transaction costs, and the simulated performance is calculated without applying management and performance fees. In reality, building a robust trend-following strategy is much more complex than the theoretical model we have developed in this paper. This model is enough to understand the behavior of the momentum risk premium, but it remains a toy model if the objective is to build an investment product that aims to fully capture the momentum risk premium. The reason is that three issues are not modeled in our study. The first issue is the portfolio turnover and the associated transaction costs. In our model, we do not manage turnover, because we assume that we continuously rebalance the portfolio. The second issue concerns the allocation. In our model, it is assumed to be given and is not dynamic. Finally, the third issue is the dynamics of asset prices. In our model, the dynamics are known and relatively simple. Therefore, we have no statistical problems for estimating trends. In the real world, asset prices are not geometric Brownian motions, but they incorporate jumps and are discontinuous. Trend estimation is then a challenge for professionals. In conclusion, our experience shows that considerable expertise is needed to harvest the momentum risk premium, but these recipes are out of the scope of this article.

References

- [1] ANG, A. (2014), *Asset Management – A Systematic Approach to Factor Investing*, Oxford University Press.
- [2] ASNESS, C.S., MOSKOWITZ, T.J., and PEDERSEN, L.H. (2013), Value and Momentum Everywhere, *Journal of Finance*, 68(3), pp. 929-985.
- [3] BLACK, F., and PEROULD, A. (1992), Theory of Constant Proportion Portfolio Insurance, *Journal of Economic Dynamics and Control*, 16(3-4), pp. 403-426.
- [4] BROCKWELL, P.J. (2001), Lévy-driven CARMA Processes, *Annals of the Institute of Statistical Mathematics*, 53(1), pp. 113-124.
- [5] BROCKWELL, P.J. (2004), Representations of Continuous-time ARMA Processes, *Journal of Applied Probability*, 41(A), pp. 375-382.
- [6] BRUDER, B., DAO, T.L., RICHARD, J.C., and RONCALLI, T. (2011), Trend Filtering Methods for Momentum Strategies, *SSRN*, www.ssrn.com/abstract=2289097.
- [7] BRUDER, B., and GAUSSEL, N. (2011), Risk-Return Analysis of Dynamic Investment Strategies, *SSRN*, www.ssrn.com/abstract=2465623.
- [8] CARHART, M.M. (1997), On Persistence in Mutual Fund Performance, *Journal of Finance*, 52(1), pp. 57-82.
- [9] CAZALET, Z., and RONCALLI, T. (2014), Facts and Fantasies About Factor Investing, *SSRN*, www.ssrn.com/abstract=2524547.
- [10] CVITANIĆ, J., and KARATZAS, I. (1995), On Portfolio Optimization under Drawdown Constraints, *IMA Volumes in Mathematics and its Applications*, 65, pp. 35-45.
- [11] CVITANIĆ, J., and KARATZAS, I. (1999), On Dynamic Measures of Risk, *Finance & Stochastics*, 3(4), pp. 451-482.
- [12] DANIEL, K.D., and MOSKOWITZ, T.J. (2016), Momentum Crashes, *Journal of Financial Economics*, 122(2), pp. 221-247.
- [13] DAO, T-L., NGUYEN, T.T., DEREMBLE, C., LEMPÉRIÈRE, Y., BOUCHAUD, J-P., and POTTERS, M. (2016), Tail Protection for Long Investors: Trend Convexity at Work, *SSRN*, www.ssrn.com/abstract=2777657.
- [14] EL KAROUI, N., JEANBLANC, M., and SHREVE, S.E. (1998), Robustness of the Black and Scholes Formula, *Mathematical Finance*, 8(2), pp. 93-126.
- [15] ELTON, E.J., GRUBER, M.J., and RENTZLER, J.C. (1987), Professionally Managed, Publicly Traded Commodity Funds, *Journal of Business*, 60(2), pp. 175-199.
- [16] ESTEP, T., and KRITZMAN, M. (1988), TIPP: Insurance without Complexity, *Journal of Portfolio Management*, 14(4), pp. 38-42.
- [17] FAMA, E.F., and FRENCH, K.R. (2012), Size, Value, and Momentum in International Stock Returns, *Journal of Financial Economics*, 105(3), pp. 457-472.
- [18] FUNG, W., and HSIEH, D.A. (1997), Empirical Characteristics of Dynamic Trading Strategies: the Case of Hedge Funds, *Review of Financial Studies*, 10(2), pp. 275-302.

- [19] FUNG, W., and HSIEH, D.A. (2001), The Risk in Hedge Fund Strategies: Theory and Evidence from Trend Followers, *Review of Financial studies*, 14(2), pp. 313-341.
 - [20] GORTON, G.B., HAYASHI, F., and ROUWENHORST, K.G. (2013), The Fundamentals of Commodity Futures Returns, 17(1), *Review of Finance*, pp. 35-105.
 - [21] GREBENKOV, D.S., and SERROR, J. (2014), Following a Trend with an Exponential Moving Average: Analytical Results for a Gaussian Model, *Physica A: Statistical Mechanics and its Applications*, 394, pp. 288-303.
 - [22] GRINBLATT, M., TITMAN, S., and WERMERS, R. (1995), Momentum Investment Strategies, Portfolio Performance, and Herding: A Study of Mutual Fund Behavior, *American Economic Review*, 85(5), pp. 1088-1105.
 - [23] GROSSMAN, S. J., and ZHOU, Z. (1993), Optimal Investment Strategies for Controlling Drawdowns, *Mathematical Finance*, 3(3), pp. 241-276.
 - [24] GRUNDY, B.D., and MARTIN, J.S.M. (2001), Understanding the Nature of the Risks and the Source of the Rewards to Momentum Investing, *Review of Financial Studies*, 14(1), pp. 29-78.
 - [25] GURLAND, J. (1955), Distribution of Definite and of Indefinite Quadratic Forms, *Annals of Mathematical Statistics*, 26(1), pp. 122-127.
 - [26] HAMDAN, R., PAVLOWSKY, F., RONCALLI, T., and ZHENG, B. (2016), A Primer on Alternative Risk Premia, *SSRN*, www.ssrn.com/abstract=2766850.
 - [27] HAMIDI, B., MAILLET, B., and Prigent, J.L. (2014), A Dynamic Autoregressive Expectile for Time-invariant Portfolio Protection Strategies, *Journal of Economic Dynamics and Control*, 46, pp. 1-29.
 - [28] HARVEY, A.C. (1990), Forecasting, Structural Time Series Models and the Kalman Filter, Cambridge University Press.
 - [29] HASANHODZIC, J., and LO, A. (2007), Can Hedge-fund Returns be Replicated?: The Linear Case, *Journal of Investment Management*, 5(2), pp. 5-45.
 - [30] HOCQUARD, A, NG, S., and PAPAGEORGIOU, N. (2013), A Constant-Volatility Framework for Managing Tail Risk, *Journal of Portfolio Management*, 39(2), pp. 28-40.
 - [31] HOU, K., XUE, C., and ZHANG, L. (2015), Digesting Anomalies: An Investment Approach, *Review of Financial Studies*, 28(3), pp. 650-705.
 - [32] HURST, B., OOI, Y.H., and Pedersen, L.H. (2014), A Century of Evidence on Trend-following Investing, *SSRN*, www.ssrn.com/abstract=2993026.
 - [33] IMHOF, J.P.(1961), Computing the Distribution of Quadratic Forms in Normal Variables, *Biometrika*, 48(3-4), pp. 419-426.
 - [34] JEGADEESH, N., and TITMAN, S. (1993), Returns to Buying Winners and Selling Losers: Implications for Stock Market Efficiency, *Journal of Finance*, 48(1), pp. 65-91.
 - [35] KALMAN, R.E., and BUCY, R.S. (1961), New Results in Linear Filtering and Prediction Theory, *Journal of Basic Engineering*, 83(3), pp. 95-108.
-

- [36] KOTZ, S., JOHNSON, N.L., and BOYD, D.W. (1967), Series Representations of Distributions of Quadratic Forms in Normal Variables II. Non-central Case, *Annals of Mathematical Statistics*, 38(3), pp. 838-848.
 - [37] LELAND, H.E. (1980), Who Should Buy Portfolio Insurance?, *Journal of Finance*, 35(2), pp. 581-594.
 - [38] LEMPÉRIÈRE, Y., DEREMBLE, C., NGUYEN, T.T., SEAGER, P., POTTERS, M., and BOUCHAUD, J-P. (2014), Risk Premia: Asymmetric Tail Risks and Excess Returns, *SSRN*, www.ssrn.com/abstract=2502743
 - [39] LEMPÉRIÈRE, Y., DEREMBLE, C., SEAGER, P., POTTERS, M., and BOUCHAUD, J-P. (2014b), Two Centuries of Trend Following, *Journal of Investment Strategies*, 3(3), pp. 41-61.
 - [40] LIU, H., TANG, Y., and ZHANG, H.H. (2009), A New Chi-square Approximation to the Distribution of Non-negative Definite Quadratic Forms in Non-central Normal Variables, *Computational Statistics & Data Analysis*, 53(4), pp. 853-856.
 - [41] LUKAC, L.P., BRORSEN, B.W., and IRWIN, S.H. (1988), A Test of Futures Market Disequilibrium using Twelve Different Technical Trading Systems, *Applied Economics*, 20(5), pp. 623-639.
 - [42] MARKOWITZ, H. (1952), Portfolio Selection, *Journal of Finance*, 7(1), pp. 77-91.
 - [43] MARTIN, R.J., and ZOU, D. (2012), Momentum Trading: 'Skews Me, *Risk*, 25(8), pp. 40-45.
 - [44] MERTON, R.C. (1971). Optimum Consumption and Portfolio Rules in a Continuous-time Model, *Journal of Economic Theory*, 3(4), pp. 373-413.
 - [45] MIFFRE, J., and RALLIS, G. (2007), Momentum Strategies in Commodity Futures Markets, *Journal of Banking & Finance*, 31(6), pp. 1863-1886.
 - [46] MOSKOWITZ, T.J., OOI, Y.H., and PEDERSEN, L.H. (2012), Time Series Momentum, *Journal of Financial Economics*, 104(2), pp. 228-250.
 - [47] PEROLD, A.F., and SHARPE, W.F. (1995), Dynamic Strategies for Asset Allocation, *Financial Analysts Journal*, 51(1), pp. 149-160.
 - [48] POTTERS, M., and BOUCHAUD, J-P. (2006), Trend Followers Lose More Often Than They Gain, *Wilmott Magazine*, 26, pp. 58-63.
 - [49] PROVOST, S.B., and RUDIUK, E.M. (1996), The Exact Distribution of Indefinite Quadratic Forms in Noncentral Normal Vectors, *Annals of the Institute of Statistical Mathematics*, 48(2), pp. 381-394.
 - [50] RONCALLI, T. (2013), *Introduction to Risk Parity and Budgeting*, Chapman & Hall/CRC Financial Mathematics Series.
 - [51] RONCALLI, T. (2017), Alternative Risk Premia: What Do We Know?, in Jurczenko, E. (Ed.), *Factor Investing and Alternative Risk Premia*, ISTE Press – Elsevier.
 - [52] RONCALLI, T., and TEILETCHE, J. (2008), An Alternative Approach to Alternative Beta, *Journal of Financial Transformation*, 24, pp. 43-52.
-

- [53] RONCALLI, T., and WEISANG, G. (2011), Tracking Problems, Hedge Fund Replications and Alternative Beta, *Journal of Financial Transformation*, 31, pp. 19-30.
- [54] ROUWENHORST, K.G. (1998), International Momentum Strategies, *Journal of Finance*, 53(1), pp. 267-284.
- [55] RUBEN, H. (1962), Probability Content of Regions Under Spherical Normal Distributions, IV: The Distribution of Homogeneous and Non-Homogeneous Quadratic Functions of Normal Variables, *Annals of Mathematical Statistics*, 33(2), pp. 542-570.
- [56] RUBEN, H. (1963), A New Result on the Distribution of Quadratic Forms, *Annals of Mathematical Statistics*, 34(4), pp. 1582-1584.
- [57] RUBINSTEIN, M., and LELAND, H.E. (1981), Replicating Option with Positions in Stock and Cash, *Financial Analysts Journal*, 37(4), pp. 63-72.
- [58] SHAH, B.K. (1963), Distribution of Definite and of Indefinite Quadratic Forms from a Non-Central Normal Distribution, *Annals of Mathematical Statistics*, 34(1), pp. 186-190.
- [59] SHAH, B.K., and KHATRI, C.G. (1961), Distribution of a Definite Quadratic Form for Non-Central Normal Variates, *Annals of Mathematical Statistics*, 32(3), pp. 883-887.
- [60] SOUPÉ, F., HECKEL, T., and DE CARVALHO, R.L. (2016), Portfolio Insurance with Adaptive Protection, *Journal of Investment Strategies*, 5(3), pp. 1-15.
- [61] SZAKMARY, A.C., SHEN, Q., and SHARMA, S.C. (2010), Trend-following Trading Strategies in Commodity Futures: A Re-examination, *Journal of Banking & Finance*, 34(2), pp. 409-426.
- [62] TAYLOR, S.J., and TARI, A. (1989), Further Evidence Against the Efficiency of Futures Markets, in Guimarães, R.M.C, Kingsman, B.G. and Taylor, S.J. (Eds), *A Reappraisal of the Efficiency of Financial Markets*, NATO ASI Series, 54, pp. 577-601, Springer.
- [63] WHALEY, R.E. (2013), Trading Volatility: At What Cost?, *Journal of Portfolio Management*, 40(1), pp. 95-108.
- [64] WHITTLE, P. (1953), The Analysis of Multiple Stationary Time Series, *Journal of the Royal Statistical Society B*, 15(1), pp. 125-139.
- [65] YU, Y. (2011), The Shape of the Noncentral Chi-square Density, *Statistics Theory (arXiv preprint)*, arXiv:1106.5241.

A Mathematical results

A.1 Kalman-Bucy filtering

A.1.1 Continuous-time modeling

We consider the state space model:

$$\begin{cases} dY_t = A_t X_t dt + B_t dW_t \\ dX_t = C_t X_t dt + D_t dW_t^* \end{cases}$$

where Y_t is the observed vector process and X_t is the hidden vector process. We assume that the multi-dimensional Brownian processes W_t and W_t^* are uncorrelated, and A_t , B_t , C_t and D_t are non-random matrices⁶⁰. The filtering problem consists in calculating the best estimate of X_t given the observed path $\{Y_s | s \leq t\}$. Let \hat{X}_t be the conditional mean:

$$\hat{X}_t = \mathbb{E}[X_t | \mathcal{F}_t]$$

We denote \hat{P}_t the error covariance matrix:

$$\hat{P}_t = \mathbb{E} \left[(X_t - \hat{X}_t) (X_t - \hat{X}_t)^\top \right]$$

The solution is given by the Kalman-Bucy filter⁶¹:

$$d\hat{X}_t = C_t \hat{X}_t dt + \hat{P}_t A_t^\top (B_t B_t^\top)^{-1} d\hat{W}_t$$

and:

$$d\hat{P}_t = \left(C_t \hat{P}_t + \hat{P}_t C_t^\top - \hat{P}_t A_t^\top (B_t B_t^\top)^{-1} A_t \hat{P}_t + D_t D_t^\top \right) dt$$

where \hat{W}_t is the innovation process:

$$d\hat{W}_t = dY_t - A_t \hat{X}_t dt$$

In the case of constant matrices, the error covariance matrix satisfies:

$$d\hat{P}_t = \left(C \hat{P}_t + \hat{P}_t C^\top - \hat{P}_t A^\top (B B^\top)^{-1} A \hat{P}_t + D D^\top \right) dt$$

and the steady-state \hat{P}_∞ is the solution of the algebraic Riccati equation:

$$C \hat{P}_\infty + \hat{P}_\infty C^\top - \hat{P}_\infty A^\top (B B^\top)^{-1} A \hat{P}_\infty + D D^\top = \mathbf{0}$$

A.1.2 Discrete-time modeling

We now consider the discrete-time state space model:

$$\begin{cases} Y_k = A_k X_k + a_k + B_k \epsilon_k \\ X_k = C_k X_{k-1} + c_k + D_k \epsilon_k^* \end{cases}$$

⁶⁰The matrix dimensions are respectively $(n \times 1)$ for Y_t , $(m \times 1)$ for X_t , $(p \times 1)$ for W_t , $(q \times 1)$ for W_t^* , $(n \times m)$ for A_t , $(n \times p)$ for B_t , $(m \times m)$ for C_t and $(m \times q)$ for D_t .

⁶¹See Kalman and Bucy (1961) for the derivation of these equations.

where Y_k is the observed vector process and X_k is the hidden vector process. Here, the time is indexed by $k \in \mathbb{N}$. We assume that $\epsilon_k \sim \mathcal{N}(\mathbf{0}, S_k)$ and $\epsilon_k^* \sim \mathcal{N}(\mathbf{0}, S_k^*)$ are two uncorrelated processes⁶². We note:

$$\hat{X}_k = \mathbb{E}[X_k | \mathcal{F}_k]$$

and:

$$\hat{X}_{k|k-1} = \mathbb{E}[X_k | \mathcal{F}_{k-1}]$$

The corresponding error covariance matrices are:

$$\hat{P}_k = \mathbb{E} \left[(X_k - \hat{X}_k) (X_k - \hat{X}_k)^\top \right]$$

and:

$$\hat{P}_{k|k-1} = \mathbb{E} \left[(X_k - \hat{X}_{k|k-1}) (X_k - \hat{X}_{k|k-1})^\top \right]$$

Let $X_0 \sim \mathcal{N}(\hat{X}_0, \hat{P}_0)$ be the initial position of the state vector. The estimates of \hat{X}_k and \hat{P}_k can be obtained by using the recursive Kalman filter⁶³:

$$\begin{cases} \hat{X}_{k|k-1} = C_k \hat{X}_{k-1} + c_k \\ \hat{P}_{k|k-1} = C_k \hat{P}_{k-1} C_k^\top + D_k S_k^* D_k^\top \\ v_k = A_k \hat{X}_{k|k-1} + a_k - Y_k \\ F_k = A_k \hat{P}_{k|k-1} A_k^\top + B_k S_k B_k^\top \\ \hat{X}_k = \hat{X}_{k|k-1} + \hat{P}_{k|k-1} A_k^\top F_k^{-1} v_k \\ \hat{P}_k = (I_m - \hat{P}_{k|k-1} A_k^\top F_k^{-1} A_k) \hat{P}_{k|k-1} \end{cases}$$

We notice that v_k is the innovation process at time k :

$$v_k = \mathbb{E}[Y_k | \mathcal{F}_{k-1}] - Y_k$$

Since we have $v_k \sim \mathcal{N}(\mathbf{0}, F_k)$, the log-likelihood function for observation k is equal to:

$$\ell_k = -\frac{n}{2} \ln 2\pi - \frac{1}{2} \ln |F_k| - \frac{1}{2} v_k^\top F_k^{-1} v_k$$

A.2 The noncentral chi-square distribution

A.2.1 Definition

Let (Y_1, \dots, Y_ν) be a set of independent Gaussian random variables such that $Y_i \sim \mathcal{N}(\mu_i, \sigma_i^2)$. The noncentral chi-square random variable is defined as follows:

$$X = \sum_{i=1}^{\nu} \frac{Y_i^2}{\sigma_i^2}$$

We write $X \sim \chi_\nu^2(\zeta)$ where ν is the number of degrees of freedom and ζ is the noncentrality parameter:

$$\zeta = \sum_{i=1}^{\nu} \frac{\mu_i^2}{\sigma_i^2}$$

When μ_i is equal to zero, X becomes a central chi-square distribution $\chi_\nu^2(0)$.

⁶²The matrix dimensions are respectively $(n \times 1)$ for Y_k , $(m \times 1)$ for X_k , $(p \times 1)$ for ϵ_k , $(q \times 1)$ for ϵ_k^* , $(n \times m)$ for A_k , $(n \times 1)$ for a_k , $(n \times p)$ for B_k , $(m \times m)$ for C_k , $(m \times 1)$ for c_k , $(m \times q)$ for D_k , $(p \times p)$ for S_k and $(q \times q)$ for S_k^* .

⁶³See Harvey (1990) for the derivation of these equations.

A.2.2 Statistical properties

The cumulative distribution function of X is defined as:

$$\mathbb{F}(x; \nu, \zeta) = \Pr\{X \leq x\} = \sum_{j=0}^{\infty} \frac{e^{-\zeta/2} \zeta^j}{2^j j!} \mathbb{F}(x; \nu + 2j, 0)$$

where $\mathbb{F}(x; \nu, 0)$ is the cumulative distribution function of the chi-square distribution with ν degrees of freedom. We have:

$$\mathbb{F}(x; \nu, 0) = \frac{\gamma(\nu/2, x/2)}{\Gamma(\nu/2)}$$

where $\gamma(a, b)$ is the lower incomplete Gamma function and $\Gamma(a)$ is the Gamma function. We deduce that the probability density function is:

$$f(x; \nu, \zeta) = \sum_{j=0}^{\infty} \frac{e^{-\zeta/2} \zeta^j}{2^j j!} f(x; \nu + 2j, 0)$$

where $f(x; \nu, 0)$ is the probability density function of the chi-square distribution:

$$f(x; \nu, 0) = \mathbf{1}\{x > 0\} \cdot \frac{x^{\nu/2-1} e^{-x/2}}{2^{\nu/2} \Gamma(\nu/2)}$$

We may also show that the mean and the variance of X are $\nu + \zeta$ and $2(\nu + 2\zeta)$, respectively. For the skewness and excess kurtosis coefficients, we obtain:

$$\begin{aligned} \gamma_1 &= (\nu + 3\zeta) \sqrt{\frac{2^3}{(\nu + 2\zeta)^3}} \\ \gamma_2 &= \frac{12(\nu + 4\zeta)}{(\nu + 2\zeta)^2} \end{aligned}$$

A.2.3 Conditional expectation of the noncentral chi-square random variable $\chi_1^2(\zeta)$

We note $Y \sim \mathcal{N}(\mu, \sigma^2)$ and:

$$X = \frac{Y^2}{\sigma^2} \sim \chi_1^2(\zeta)$$

Let $m^+(x, \zeta)$ be the conditional expectation of X given that $X \geq x$. We have:

$$\begin{aligned} m^+(x, \zeta) &= \mathbb{E}[X | X \geq x] \\ &= \mathbb{E}\left[\frac{Y^2}{\sigma^2} \middle| \frac{Y^2}{\sigma^2} \geq x\right] \\ &= \frac{\mathbb{E}[\mathbf{1}\{Y^2 \geq x\sigma^2\} \cdot Y^2]}{\sigma^2 \Pr\{X \geq x\}} \end{aligned}$$

It follows that⁶⁴:

$$\begin{aligned}
 \mathbb{E}[Y^2 | Y^2 \geq x\sigma^2] &= \int_{-\infty}^{-\sigma\sqrt{x}} \frac{y^2}{\sigma} \phi\left(\frac{y-\mu}{\sigma}\right) dy + \int_{\sigma\sqrt{x}}^{\infty} \frac{y^2}{\sigma} \phi\left(\frac{y-\mu}{\sigma}\right) dy \\
 &= \int_{-\infty}^{-\sqrt{x}-\sqrt{\zeta}} (\mu + \sigma z)^2 \phi(z) dz + \int_{\sqrt{x}-\sqrt{\zeta}}^{\infty} (\mu + \sigma z)^2 \phi(z) dz \\
 &= \int_{-\infty}^{-\sqrt{x}-\sqrt{\zeta}} (\mu^2 + 2\mu\sigma z + \sigma^2 z^2) \phi(z) dz + \\
 &\quad \int_{\sqrt{x}-\sqrt{\zeta}}^{\infty} (\mu^2 + 2\mu\sigma z + \sigma^2 z^2) \phi(z) dz
 \end{aligned}$$

Using the following results:

$$\begin{aligned}
 \int_a^b \phi(z) dz &= \Phi(b) - \Phi(a) \\
 \int_a^b z\phi(z) dz &= \phi(a) - \phi(b) \\
 \int_a^b z^2\phi(z) dz &= a\phi(a) - b\phi(b) + \Phi(b) - \Phi(a)
 \end{aligned}$$

we obtain:

$$\begin{aligned}
 \int_a^b (\mu^2 + 2\mu\sigma z + \sigma^2 z^2) \phi(z) dz &= (\mu^2 + \sigma^2)(\Phi(b) - \Phi(a)) + \\
 &\quad (2\mu\sigma + a\sigma^2)\phi(a) - \\
 &\quad (2\mu\sigma + b\sigma^2)\phi(b)
 \end{aligned}$$

We deduce that:

$$\begin{aligned}
 \mathbb{E}[Y^2 | Y^2 \geq x\sigma^2] &= (\mu^2 + \sigma^2) \left(\Phi(-\sqrt{x} - \sqrt{\zeta}) + 1 - \Phi(\sqrt{x} - \sqrt{\zeta}) \right) + \\
 &\quad (\mu\sigma + \sqrt{x}\sigma^2) \phi(\sqrt{x} - \sqrt{\zeta}\mu) - (\mu\sigma - \sqrt{x}\sigma^2) \phi(\sqrt{x} + \sqrt{\zeta})
 \end{aligned}$$

and:

$$\begin{aligned}
 m^+(x, \zeta) &= \frac{1}{1 - \mathbb{F}(x; 1, \zeta)} \left((1 + \zeta) \left(\Phi(-\sqrt{x} - \sqrt{\zeta}) + 1 - \Phi(\sqrt{x} - \sqrt{\zeta}) \right) + \right. \\
 &\quad \left. (\sqrt{\zeta} + \sqrt{x}) \phi(\sqrt{x} - \sqrt{\zeta}) + (\sqrt{x} - \sqrt{\zeta}) \phi(\sqrt{x} + \sqrt{\zeta}) \right)
 \end{aligned}$$

We also have:

$$\begin{aligned}
 m^-(x, \zeta) &= \mathbb{E}[X | X \leq x] \\
 &= \frac{1 + \zeta - (1 - \mathbb{F}(x; 1, \zeta)) m^+(x, \zeta)}{\mathbb{F}(x; 1, \zeta)} \\
 &= \frac{1}{1 - \mathbb{F}(x; 1, \zeta)} \left((1 + \zeta) \left(\Phi(\sqrt{x} + \sqrt{\zeta}) - \Phi(-\sqrt{x} + \sqrt{\zeta}) \right) - \right. \\
 &\quad \left. (\sqrt{\zeta} + \sqrt{x}) \phi(\sqrt{x} - \sqrt{\zeta}) - (\sqrt{x} - \sqrt{\zeta}) \phi(\sqrt{x} + \sqrt{\zeta}) \right)
 \end{aligned}$$

⁶⁴We have $\sqrt{\zeta} = \sigma^{-1}\mu$.

A.3 Distribution of Gaussian quadratic forms

A.3.1 The case of uncorrelated Gaussian random variables

Let (Z_1, \dots, Z_n) be a set of independent standardized Gaussian random variables. We consider the quadratic form \mathcal{Q}_1 defined by:

$$\mathcal{Q}_1(a, b) = \sum_{i=1}^n a_i (Z_i + b_i)^2$$

where $a_i > 0$. According to Ruben (1962, 1963) and Kotz *et al.* (1967), the cumulative density function⁶⁵ of \mathcal{Q}_1 admits a series expansion based on the chi-square distribution:

$$\begin{aligned} \mathbb{Q}_1(q; a, b) &= \Pr\{\mathcal{Q}_1(a, b) \leq q\} \\ &= \sum_{j=0}^{\infty} c_j \mathbb{F}\left(\frac{q}{\beta}; n + 2j, 0\right) \end{aligned}$$

Here, β is an arbitrary constant such that $0 < \beta \leq \min_i a_i$, $\mathbb{F}(x; \nu, 0)$ is the $\chi_\nu^2(0)$ cumulative distribution function and the coefficients c_j are given by:

$$\begin{cases} c_0 = e^{-\zeta/2} \prod_{i=1}^n (\beta/a_i)^{1/2} \\ c_j = j^{-1} \sum_{k=0}^{j-1} g_{j-k} c_k \end{cases}$$

where:

$$\zeta = \sum_{i=1}^n b_i^2$$

and:

$$g_m = \frac{1}{2} \left(\sum_{i=1}^n \left(1 - \frac{\beta}{a_i}\right)^m + m\beta \sum_{i=1}^n \frac{b_i^2}{a_i} \left(1 - \frac{\beta}{a_i}\right)^{m-1} \right)$$

Remark 12 We could also compute the cumulative density function of \mathcal{Q}_1 using the series expansion of Kotz *et al.* (1967) based on the noncentral chi-square distribution:

$$\mathbb{Q}_1(q; a, b) = \sum_{j=0}^{\infty} d_j \mathbb{F}\left(\frac{q}{\beta}; n + 2j, \zeta\right)$$

where the noncentrality parameter is:

$$\zeta = \sum_{i=1}^n b_i^2$$

Here, the coefficients d_j are given by:

$$d_j = e^{\zeta/2} \sum_{k=0}^j h_{j-k} c_k$$

with:

$$h_m = \frac{(-\zeta/2)^m}{m!}$$

⁶⁵If we are interested by the probability density function, we obtain:

$$f(q) = \frac{1}{\beta} \sum_{j=0}^{\infty} c_j f\left(\frac{q}{\beta}; n + 2j, 0\right)$$

We now consider the calculation of the four moments. We have:

$$\begin{aligned}\mathcal{Q}_1(a, b) &= \sum_{i=1}^n a_i (Z_i + b_i)^2 \\ &= \sum_{i=1}^n a_i (Z_i^2 + 2b_i Z_i + b_i^2)\end{aligned}$$

It follows that:

$$\mathbb{E}[\mathcal{Q}_1(a, b)] = \sum_{i=1}^n a_i (1 + b_i^2)$$

and:

$$\begin{aligned}\text{var}(\mathcal{Q}_1(a, b)) &= \mathbb{E} \left[\left(\sum_{i=1}^n a_i (Z_i^2 - 1 + 2b_i Z_i) \right)^2 \right] \\ &= 2 \sum_{i=1}^n a_i^2 (1 + 2b_i^2)\end{aligned}$$

For order $k \geq 3$, the direct computation of $\mathbb{E}[X^k]$ is tricky. However, we can show that the k^{th} cumulant of $\mathcal{Q}_1(a, b)$ is equal to:

$$\kappa_k(\mathcal{Q}_1(a, b)) = \frac{\partial^k K(0)}{\partial t^k}$$

where $K(t)$ is the cumulant generating function:

$$\begin{aligned}K(t) &= \ln \mathbb{E}[\exp(t\mathcal{Q}_1(a, b))] \\ &= \ln \mathbb{E} \left[\exp \left(t \sum_{i=1}^n a_i (Z_i + b_i)^2 \right) \right] \\ &= \sum_{i=1}^n \ln \mathbb{E} \left[\exp \left(t a_i (Z_i + b_i)^2 \right) \right]\end{aligned}$$

By linearity of the derivation, we obtain:

$$\kappa_k(\mathcal{Q}_1(a, b)) = \sum_{i=1}^n \kappa_k(a_i (Z_i + b_i)^2)$$

Since we have $\kappa_k(aX) = a^k \kappa_k(X)$, it follows that:

$$\kappa_k(a_i (Z_i + b_i)^2) = a_i^k 2^{k-1} (k-1)! (1 + kb_i^2)$$

and:

$$\kappa_k(\mathcal{Q}_1(a, b)) = 2^{k-1} (k-1)! \left(\sum_{i=1}^n a_i^k (1 + kb_i^2) \right)$$

We deduce that:

$$\gamma_1(\mathcal{Q}_1(a, b)) = \frac{2\sqrt{2} \sum_{i=1}^n a_i^3 (1 + 3b_i^2)}{(\sum_{i=1}^n a_i^2 (1 + 2b_i^2))^{3/2}}$$

and:

$$\gamma_2(\mathcal{Q}_1(a, b)) = \frac{12 \sum_{i=1}^n a_i^4 (1 + 4b_i^2)}{(\sum_{i=1}^n a_i^2 (1 + 2b_i^2))^2}$$

A.3.2 The case of correlated Gaussian random variables

Let $X \sim \mathcal{N}(\mu, \Sigma)$ be a Gaussian random vector and Q be a symmetric non-negative definite matrix. We define the quadratic form \mathcal{Q}_2 as follows:

$$\mathcal{Q}_2(\mu, \Sigma, Q) = X^\top Q X$$

Following Imhof (1961), Liu *et al.* (2009) show that the k^{th} cumulant of $\mathcal{Q}_2(\mu, \Sigma, Q)$ is equal to:

$$\kappa_k(\mathcal{Q}_2(\mu, \Sigma, Q)) = 2^{k-1} (k-1)! \left(\text{tr}(Q\Sigma)^k + k\mu^\top (Q\Sigma)^{k-1} Q\mu \right)$$

It follows that the mean and the variance of $\mathcal{Q}_2(\mu, \Sigma, Q)$ are κ_1 and κ_2 . For the skewness and excess kurtosis coefficients, we obtain:

$$\gamma_1 = \frac{\kappa_3}{\kappa_2^{3/2}} = \sqrt{8}s_1$$

and:

$$\gamma_2 = \frac{\kappa_4}{\kappa_2^2} = 12s_2$$

Liu *et al.* (2009) suggest approximating the GQF probability distribution by a linear transformation of a non-central chi-square distribution:

$$\begin{aligned} \mathbb{Q}_2(q; \mu, \Sigma, Q) &= \Pr\{\mathcal{Q}_2(\mu, \Sigma, Q) \leq q\} \\ &= \mathbb{F}(\mu^* + \sigma^* q^*; \nu, \zeta) \end{aligned}$$

where:

$$\begin{aligned} q^* &= \frac{q - \kappa_1}{\sqrt{\kappa_2}} \\ \mu^* &= \nu + \zeta \\ \sigma^* &= \sqrt{2\nu + 4\zeta} \end{aligned}$$

If $s_1^2 > s_2$, we obtain:

$$\begin{cases} \zeta = s_1 \omega^3 - \omega^2 \\ \nu = \omega^2 - 2\zeta \end{cases}$$

where:

$$\omega = \frac{1}{s_1 - \sqrt{s_1^2 - s_2}}$$

If $s_1^2 \leq s_2$, the solution becomes:

$$\begin{cases} \zeta = 0 \\ \nu = 1/s_1^2 \end{cases}$$

A.3.3 Relationship between the two Gaussian quadratic forms

\mathcal{Q}_1 is related to \mathcal{Q}_2 as follows:

$$\begin{aligned} \mathcal{Q}_1(a, b) &= \sum_{i=1}^n a_i (Z_i + b_i)^2 \\ &= \mathcal{Q}_2(\mu, \Sigma, Q) \end{aligned}$$

where $\mu = b$, $\Sigma = \mathbf{I}_n$ and $Q = \text{diag}(a_1, \dots, a_n)$.

If we consider \mathcal{Q}_2 , Liu *et al.* (2009) show that⁶⁶:

$$\begin{aligned}\mathcal{Q}_2(\mu, \Sigma, Q) &= X^\top Q X \\ &= Y^\top D Y\end{aligned}$$

where $Y \sim \mathcal{N}(m, \mathbf{I}_n)$, $D = \text{diag}(d_1, \dots, d_n)$ and U are the eigenvalue and eigenvector matrices of $\Sigma^{1/2} Q \Sigma^{1/2}$, and $m = U^\top \Sigma^{-1/2} \mu$. We deduce that:

$$\begin{aligned}\mathcal{Q}_2(\mu, \Sigma, Q) &= \sum_{i=1}^n d_i Y_i^2 \\ &= \sum_{i=1}^n d_i (Z_i + m_i)^2 \\ &= \mathcal{Q}_1(d, m)\end{aligned}$$

where $d = (d_1, \dots, d_n)$.

A.3.4 The case of indefinite quadratic forms

In the general case where Q is a symmetric matrix, which is not necessarily positive definite, we have:

$$Q = Q_1 - Q_2$$

where Q_1 and Q_2 are two symmetric positive semi-definite matrices. It follows that:

$$\begin{aligned}\mathcal{Q}_2(\mu, \Sigma, Q) &= X^\top Q X \\ &= X^\top Q_1 X - X^\top Q_2 X \\ &= \mathcal{Q}_2(\mu, \Sigma, Q_1) - \mathcal{Q}_2(\mu, \Sigma, Q_2)\end{aligned}$$

Any indefinite quadratic form may then be written as the difference of two definite quadratic forms. We deduce that:

$$\begin{aligned}\mathcal{Q}_2(q; \mu, \Sigma, Q) &= \Pr\{\mathcal{Q}_2(\mu, \Sigma, Q) \leq q\} \\ &= \Pr\{\mathcal{Q}_2(\mu, \Sigma, Q_1) - \mathcal{Q}_2(\mu, \Sigma, Q_2) \leq q\}\end{aligned}$$

The exact computation of $\mathcal{Q}_2(q; \mu, \Sigma, Q)$ is more complicated than in the definite case since it requires the convolution of $\mathcal{Q}_2(\mu, \Sigma, Q_1)$ and $\mathcal{Q}_2(\mu, \Sigma, Q_2)$ (Gurland, 1955; Provost and Rudiuk, 1996). However, we can find an upper bound:

$$\begin{aligned}\mathcal{Q}_2(q; \mu, \Sigma, Q) &= \Pr\{\mathcal{Q}_2(\mu, \Sigma, Q_1) \leq q + \mathcal{Q}_2(\mu, \Sigma, Q_2)\} \\ &\leq \Pr\{\mathcal{Q}_2(\mu, \Sigma, Q_1) \leq q\} \\ &= \mathcal{Q}_2(q; \mu, \Sigma, Q_1)\end{aligned}$$

because $\mathcal{Q}_2(\mu, \Sigma, Q_2) \geq 0$. In particular, this upper bound can be used as an approximation if:

$$\sum_{i=1}^n d_i(Q_1) \gg \sum_{i=1}^n d_i(Q_2)$$

where $d_i(Q)$ is the i^{th} eigenvalue of Q .

⁶⁶We note $\Omega = \Sigma^{1/2} Q \Sigma^{1/2}$. We have $\Omega = UDU^\top$, $D = U^\top \Omega U$ and $U^{-1} = U^\top$. The random vector $Y = U^\top \Sigma^{-1/2} X$ is normally distributed $\mathcal{N}(U^\top \Sigma^{-1/2} \mu, \mathbf{I}_n)$. Since we have $X = \Sigma^{1/2} U Y$, it follows that:

$$\begin{aligned}X^\top Q X &= Y^\top U^\top \Sigma^{1/2} Q \Sigma^{1/2} U Y \\ &= Y^\top U^\top \Omega U Y \\ &= Y^\top D Y\end{aligned}$$

A.4 The Bruder-Gaussel model

A.4.1 Derivation and statistical properties of the EWMA estimator

We assume that:

$$\begin{cases} dS_t = \mu_t S_t dt + \sigma S_t dW_t \\ d\mu_t = \gamma dW_t^* \end{cases}$$

Let $dy_t = dS_t/S_t$. We have:

$$\begin{cases} dy_t = \mu_t dt + \sigma dW_t \\ d\mu_t = \gamma dW_t^* \end{cases}$$

We denote $\hat{\mu}_t = \mathbb{E}[\mu_t | \mathcal{F}_t]$ the estimator of the trend μ_t with respect to the filtration \mathcal{F}_t , and $v_t = \mathbb{E}[(\hat{\mu}_t - \mu_t)^2 | \mathcal{F}_t]$ the variance of the estimation error. The Kalman-Bucy filter equations are:

$$d\hat{\mu}_t = \frac{v_t}{\sigma^2} (dy_t - \hat{\mu}_t dt)$$

and:

$$\frac{dv_t}{dt} = \gamma^2 - \frac{1}{\sigma^2} v_t^2$$

We verify that $v_\infty = \gamma\sigma$, implying that⁶⁷:

$$d\hat{\mu}_t = \lambda (dy_t - \hat{\mu}_t dt)$$

where the parameter λ is equal to $\gamma\sigma^{-1}$. Finally, Bruder and Gaussel (2011) deduce that $\hat{\mu}_t$ is an exponential weighted moving average (EWMA) estimator:

$$\hat{\mu}_t = \lambda \int_0^t e^{-\lambda(t-u)} dy_u + e^{-\lambda t} \hat{\mu}_0$$

We also verify that the sum of EWMA weights are equal to one, because we have:

$$\lambda \int_0^t e^{-\lambda(t-u)} du = \left[e^{-\lambda(t-u)} \right]_0^t = 1 - e^{-\lambda t}$$

If the asset volatility σ is larger than the trend volatility γ , the EWMA parameter λ is less than one. Otherwise, it is more than one.

A.4.2 P&L of the trend-following strategy

We recall that the Kalman filtering equation is:

$$d\hat{\mu}_t = \lambda (dy_t - \hat{\mu}_t dt)$$

meaning that:

$$dy_t = \frac{1}{\lambda} d\hat{\mu}_t + \hat{\mu}_t dt$$

It follows that:

$$\begin{aligned} \frac{dV_t}{V_t} &= e_t \frac{dS_t}{S_t} \\ &= \frac{\alpha}{\lambda} \hat{\mu}_t d\hat{\mu}_t + \alpha \hat{\mu}_t^2 dt \end{aligned}$$

⁶⁷We assume here that the Kalman filter has sufficiently converged in order to replace v_t by its limit v_∞ .

We deduce that⁶⁸:

$$\begin{aligned} d\langle V, V \rangle_t &= \frac{\alpha^2}{\lambda^2} V_t^2 \hat{\mu}_t d\langle \hat{\mu}, \hat{\mu} \rangle_t \hat{\mu}_t \\ &= \alpha^2 V_t^2 \hat{\mu}_t^2 \sigma^2 dt \end{aligned}$$

If we apply Ito's formula to $W_t = \ln V_t$, we obtain:

$$\begin{aligned} dW_t &= \frac{dV_t}{V_t} - \frac{1}{2V_t^2} d\langle V, V \rangle_t \\ &= \frac{\alpha}{\lambda} \hat{\mu}_t d\hat{\mu}_t + \alpha \hat{\mu}_t^2 \left(1 - \frac{\alpha \sigma^2}{2}\right) dt \end{aligned}$$

Since we have:

$$\begin{aligned} d\hat{\mu}_t^2 &= 2\hat{\mu}_t d\hat{\mu}_t + d\langle \hat{\mu}, \hat{\mu} \rangle_t \\ &= 2\hat{\mu}_t d\hat{\mu}_t + \lambda^2 \sigma^2 dt \end{aligned}$$

we obtain the following expression:

$$\begin{aligned} dW_t &= \frac{\alpha}{2\lambda} (d\hat{\mu}_t^2 - \lambda^2 \sigma^2 dt) + \alpha \hat{\mu}_t^2 \left(1 - \frac{\alpha \sigma^2}{2}\right) dt \\ &= \frac{\alpha}{2\lambda} d\hat{\mu}_t^2 + \left(\alpha \hat{\mu}_t^2 \left(1 - \frac{\alpha \sigma^2}{2}\right) - \frac{\lambda \alpha \sigma^2}{2}\right) dt \end{aligned}$$

Therefore, the P&L of the trend-following strategy is equal to:

$$\ln \frac{V_T}{V_0} = \frac{\alpha}{2\lambda} (\hat{\mu}_T^2 - \hat{\mu}_0^2) + \alpha \sigma^2 \int_0^T \left(\frac{\hat{\mu}_t^2}{\sigma^2} \left(1 - \frac{\alpha \sigma^2}{2}\right) - \frac{\lambda}{2}\right) dt$$

A.4.3 Probability distribution of the trend-following strategy

By definition, the Sharpe ratio of the asset is equal to:

$$s_t = \frac{\mu_t}{\sigma}$$

The Sharpe ratio estimator is then equal to:

$$\hat{s}_t = \frac{\hat{\mu}_t}{\sigma}$$

Using Kalman filter, we have $\hat{\mu}_t \sim \mathcal{N}(\mu_t, v_t)$. Since we have made the approximation $v_t = v_\infty$, we deduce that:

$$\hat{s}_t \sim \mathcal{N}\left(s_t, \frac{v_\infty}{\sigma^2}\right)$$

where:

$$\frac{v_\infty}{\sigma^2} = \frac{\gamma \sigma}{\sigma^2} = \lambda$$

⁶⁸We have:

$$\begin{aligned} d\langle \hat{\mu}, \hat{\mu} \rangle_t &= \langle d\hat{\mu}, d\hat{\mu} \rangle_t \\ &= \gamma^2 dt \\ &= \lambda^2 \sigma^2 dt \end{aligned}$$

It follows that \hat{s}_t^2/λ is a noncentral chi-square random variable $\chi_1^2(\zeta)$ with:

$$\zeta = \frac{\hat{s}_t^2}{\lambda}$$

Let us now consider the trading impact g_t :

$$\begin{aligned} g_t &= \alpha\sigma^2 \left(\hat{s}_t^2 \left(1 - \frac{\alpha\sigma^2}{2} \right) - \frac{\lambda}{2} \right) \\ &= \frac{\alpha\sigma^2}{2} (2 - \alpha\sigma^2) \hat{s}_t^2 - \frac{\lambda\alpha\sigma^2}{2} \end{aligned}$$

We deduce that g_t is an affine transformation of a noncentral chi-square random variable:

$$\begin{aligned} \Pr\{g_t \leq g\} &= \Pr\left\{ \frac{\alpha\sigma^2}{2} (2 - \alpha\sigma^2) \hat{s}_t^2 - \frac{\lambda\alpha\sigma^2}{2} \leq g \right\} \\ &= \Pr\left\{ \hat{s}_t^2 \leq \frac{2g + \lambda\alpha\sigma^2}{\alpha\sigma^2 (2 - \alpha\sigma^2)} \right\} \\ &= \mathbb{F}\left(\frac{2g + \lambda\alpha\sigma^2}{\lambda\alpha\sigma^2 (2 - \alpha\sigma^2)}; 1, \zeta \right) \end{aligned}$$

where $\mathbb{F}(x; \nu, \zeta)$ is the cumulative distribution function of the noncentral chi-square distribution, whose degree of freedom is ν and noncentrality parameter is ζ .

A.4.4 Average duration of the EWMA estimator

In order to better understand the parameter λ , we compute the average duration of the EWMA estimator:

$$\tau = \lim_{t \rightarrow \infty} \frac{\lambda}{1 - e^{-\lambda t}} \int_0^t e^{-\lambda(t-u)} (t-u) du$$

We have:

$$\begin{aligned} \int_0^t e^{-\lambda(t-u)} (t-u) du &= t \int_0^t e^{-\lambda(t-u)} du - \int_0^t e^{-\lambda(t-u)} u du \\ &= t \left(\frac{1 - e^{-\lambda t}}{\lambda} \right) - \left(\frac{t}{\lambda} - \frac{1 - e^{-\lambda t}}{\lambda^2} \right) \\ &= \frac{-te^{-\lambda t}}{\lambda} + \frac{1 - e^{-\lambda t}}{\lambda^2} \end{aligned}$$

We deduce that:

$$\begin{aligned} \tau &= \lim_{t \rightarrow \infty} \frac{\lambda}{1 - e^{-\lambda t}} \left(\frac{-te^{-\lambda t}}{\lambda} + \frac{1 - e^{-\lambda t}}{\lambda^2} \right) \\ &= \frac{1}{\lambda} \end{aligned}$$

The average duration of the EWMA estimator is then equal to the inverse of the frequency parameter λ .

A.4.5 Hit ratio

We note:

$$\hat{s}_t = s_t + \sqrt{\lambda}X$$

where $X \sim \mathcal{N}(0, 1)$. We deduce that the hit ratio \mathcal{H} is equal to:

$$\begin{aligned}\mathcal{H} &= \Pr\{g_t \geq 0\} \\ &= \Pr\left\{\hat{s}_t^2 \geq \frac{\lambda}{2 - \alpha\sigma^2}\right\} \\ &= \Pr\left\{\left(s_t + \sqrt{\lambda}X\right)^2 \geq \frac{\lambda}{2 - \alpha\sigma^2}\right\} \\ &= \Pr\left\{X \geq \sqrt{\frac{1}{2 - \alpha\sigma^2}} - \frac{s_t}{\sqrt{\lambda}}\right\} + \Pr\left\{X \leq -\sqrt{\frac{1}{2 - \alpha\sigma^2}} - \frac{s_t}{\sqrt{\lambda}}\right\} \\ &= 1 - \Phi\left(\sqrt{\frac{1}{2 - \alpha\sigma^2}} - \frac{s_t}{\sqrt{\lambda}}\right) + \Phi\left(-\sqrt{\frac{1}{2 - \alpha\sigma^2}} - \frac{s_t}{\sqrt{\lambda}}\right)\end{aligned}$$

The hit ratio depends then on four parameters: s_t , α , σ and λ . We verify that the sign of the Sharpe ratio does not change the value of the hit ratio:

$$\mathcal{H}(s_t; \alpha, \sigma, \lambda) = \mathcal{H}(-s_t; \alpha, \sigma, \lambda)$$

A.4.6 Expected loss and gain

We have:

$$\begin{aligned}\mathbb{E}[g_t | g_t \leq 0] &= \mathbb{E}\left[\alpha\sigma^2\left(\hat{s}_t^2\left(1 - \frac{\alpha\sigma^2}{2}\right) - \frac{\lambda}{2}\right) \middle| \alpha\sigma^2\left(\hat{s}_t^2\left(1 - \frac{\alpha\sigma^2}{2}\right) - \frac{\lambda}{2}\right) \leq 0\right] \\ &= \alpha\sigma^2\left(1 - \frac{\alpha\sigma^2}{2}\right) \mathbb{E}\left[\hat{s}_t^2 \middle| \hat{s}_t^2 \leq \frac{\lambda}{2 - \alpha\sigma^2}\right] - \frac{\lambda\alpha\sigma^2}{2}\end{aligned}$$

Since we have:

$$\frac{\hat{s}_t^2}{\lambda} \sim \chi_1^2(\zeta)$$

We deduce that the expected loss and gain are equal to:

$$\mathbb{E}[g_t | g_t \leq 0] = \alpha\sigma^2\left(1 - \frac{\alpha\sigma^2}{2}\right) m^-\left(\frac{1}{2 - \alpha\sigma^2}, \zeta\right) - \frac{\lambda\alpha\sigma^2}{2}$$

and:

$$\mathbb{E}[g_t | g_t \geq 0] = \alpha\sigma^2\left(1 - \frac{\alpha\sigma^2}{2}\right) m^+\left(\frac{1}{2 - \alpha\sigma^2}, \zeta\right) - \frac{\lambda\alpha\sigma^2}{2}$$

where $m^-(x, \zeta)$ and $m^+(x, \zeta)$ are the functions defined in Appendix A.2 on page 63.

A.5 The multivariate case

We now consider that:

$$\begin{cases} d\mathbf{S}_t = \mu_t \odot \mathbf{S}_t dt + (\sigma \odot \mathbf{S}_t) \odot dW_t \\ d\mu_t = \sigma^\star \odot dW_t^\star \end{cases}$$

where \mathbf{S}_t , μ_t , σ and σ^\star are four $n \times 1$ vectors. We also assume that $\mathbb{E}[W_t W_t^\top] = \mathcal{C}\mathbf{I}_n$ and $\mathbb{E}[W_t^\star W_t^{\star\top}] = \mathcal{C}^\star\mathbf{I}_n$ where \mathcal{C} and \mathcal{C}^\star are two square matrices, and $\mathbb{E}[W_t^\star W_t^\top] = 0$. We denote Σ the covariance matrix of asset returns and Γ the covariance matrix of trends⁶⁹.

⁶⁹We have $\Sigma_{i,j} = \mathcal{C}_{i,j}\sigma_i\sigma_j$ and $\Gamma_{i,j} = \mathcal{C}_{i,j}^\star\sigma_i^\star\sigma_j^\star$.

A.5.1 Derivation of the EWMA estimator

Let $dy_t = d\mathbf{S}_t/\mathbf{S}_t$. We denote $\hat{\mu}_t = \mathbb{E}[\mu_t | \mathcal{F}_t]$ the estimator of the trend μ_t , and $\Upsilon_t = \mathbb{E}[(\hat{\mu}_t - \mu_t)(\hat{\mu}_t - \mu_t)^\top]$ the error covariance matrix. The Kalman-Bucy filter gives:

$$d\hat{\mu}_t = \Upsilon_t \Sigma^{-1} (dy_t - \hat{\mu}_t dt)$$

and:

$$d\Upsilon_t = (\Gamma - \Upsilon_t \Sigma^{-1} \Upsilon_t) dt$$

At the steady state Υ_∞ , we have:

$$d\hat{\mu}_t = \Lambda (dy_t - \hat{\mu}_t dt)$$

where $\Lambda = \Upsilon_\infty \Sigma^{-1}$. We deduce that $\hat{\mu}_t$ is a multi-dimensional exponential moving average estimator (Brockwell, 2004):

$$\hat{\mu}_t = \int_0^t e^{-\Lambda(t-u)} \Lambda dy_u + e^{-\Lambda t} \hat{\mu}_0$$

Remark 13 *The steady state Υ_∞ is obtained by solving the continuous algebraic Riccati equation:*

$$\Gamma - \Upsilon_\infty \Sigma^{-1} \Upsilon_\infty = \mathbf{0}$$

In some special cases, we obtain the following analytical solution:

$$\Upsilon_\infty = \Gamma^{1/2} \Sigma^{1/2}$$

In this case, we have $\Lambda = \Gamma^{1/2} \Sigma^{-1/2}$. However, this equation is only valid when the matrices $\Gamma^{1/2}$ and $\Sigma^{1/2}$ commute. Indeed, we verify that $\Gamma^{1/2} \Sigma^{1/2}$ is always one solution of the equation $\Gamma - \Upsilon_\infty \Sigma^{-1} \Upsilon_\infty = \mathbf{0}$, but it does not necessarily define a symmetric matrix.

A.5.2 Expression of the P&L

The P&L of the momentum strategy is given by:

$$\frac{dV_t}{V_t} = \mathbf{e}_t^\top \frac{d\mathbf{S}_t}{\mathbf{S}_t}$$

We assume that:

$$\mathbf{e}_t = A \hat{\mu}_t$$

where A is a squared matrix and $\hat{\mu}_t = (\hat{\mu}_{1,t}, \dots, \hat{\mu}_{n,t})$ is the vector of estimated trends. It follows that:

$$\frac{dV_t}{V_t} = \hat{\mu}_t^\top A^\top (\Lambda^{-1} d\hat{\mu}_t + \hat{\mu}_t dt)$$

and⁷⁰:

$$\begin{aligned} d\langle V, V \rangle_t &= V_t^2 \hat{\mu}_t^\top A^\top \Lambda^{-1} d\langle \hat{\mu}, \hat{\mu} \rangle_t (\Lambda^\top)^{-1} A \hat{\mu}_t \\ &= V_t^2 \hat{\mu}_t^\top A^\top \Lambda^{-1} \Lambda \Sigma \Lambda^\top (\Lambda^\top)^{-1} A \hat{\mu}_t dt \\ &= V_t^2 \hat{\mu}_t^\top A^\top \Sigma A \hat{\mu}_t dt \end{aligned}$$

⁷⁰We have:

$$\begin{aligned} d\langle \hat{\mu}, \hat{\mu} \rangle_t &= \langle d\hat{\mu}, d\hat{\mu} \rangle_t \\ &= \Lambda \left\langle \frac{d\mathbf{S}}{\mathbf{S}}, \frac{d\mathbf{S}}{\mathbf{S}} \right\rangle_t \Lambda^\top \\ &= \Lambda \Sigma \Lambda^\top dt \end{aligned}$$

If we apply Itô's lemma to $W_t = \ln V_t$, we obtain:

$$\begin{aligned} dW_t &= \frac{dV_t}{V_t} - \frac{1}{2V_t^2} d\langle V, V \rangle_t \\ &= \hat{\mu}_t^\top A^\top (\Lambda^{-1} d\hat{\mu}_t + \hat{\mu}_t dt) - \frac{1}{2} \hat{\mu}_t^\top A^\top \Sigma A \hat{\mu}_t dt \\ &= \hat{\mu}_t^\top A^\top \Lambda^{-1} d\hat{\mu}_t + \hat{\mu}_t^\top A^\top \left(\mathbf{I}_n - \frac{1}{2} \Sigma A \right) \hat{\mu}_t dt \end{aligned}$$

Since we have⁷¹:

$$\begin{aligned} d(\hat{\mu}_t^\top A^\top \Lambda^{-1} \hat{\mu}_t) &= 2\hat{\mu}_t^\top A^\top \Lambda^{-1} d\hat{\mu}_t + \text{tr}(A^\top \Lambda^{-1} d\langle \hat{\mu}, \hat{\mu} \rangle_t) \\ &= 2\hat{\mu}_t^\top A^\top \Lambda^{-1} d\hat{\mu}_t + \text{tr}(A^\top \Sigma \Lambda^\top) dt \end{aligned}$$

we obtain the following expression:

$$dW_t = \frac{1}{2} d(\hat{\mu}_t^\top A^\top \Lambda^{-1} \hat{\mu}_t) + \left(\hat{\mu}_t^\top A^\top \left(\mathbf{I}_n - \frac{1}{2} \Sigma A \right) \hat{\mu}_t - \frac{1}{2} \text{tr}(A^\top \Sigma \Lambda^\top) \right) dt$$

We finally conclude that the P&L of the momentum strategy is given by:

$$\begin{aligned} \ln \frac{V_T}{V_0} &= \frac{1}{2} (\hat{\mu}_T^\top A^\top \Lambda^{-1} \hat{\mu}_T - \hat{\mu}_0^\top A^\top \Lambda^{-1} \hat{\mu}_0) + \\ &\quad \int_0^T \left(\hat{\mu}_t^\top A^\top \left(\mathbf{I}_n - \frac{1}{2} \Sigma A \right) \hat{\mu}_t - \frac{1}{2} \text{tr}(A^\top \Sigma \Lambda^\top) \right) dt \end{aligned}$$

A.5.3 The case of uncorrelated assets

In the case where the matrix A is diagonal⁷², the exposure of Asset i is given by:

$$e_{i,t} = \alpha_i \hat{\mu}_{i,t}$$

If we assume that the assets are uncorrelated ($\mathcal{C} = \mathbf{0}$ and $\mathcal{C}^* = \mathbf{0}$), the EWMA matrix Λ becomes a diagonal matrix:

$$\Lambda = \text{diag}(\lambda_1, \dots, \lambda_n)$$

Therefore, the expression of the P&L is reduced to:

$$\ln \frac{V_T}{V_0} = \sum_{i=1}^n \frac{\alpha_i}{2\lambda_i} (\hat{\mu}_{i,T}^2 - \hat{\mu}_{i,0}^2) + \sum_{i=1}^n \alpha_i \sigma_i^2 \int_0^T \left(\frac{\hat{\mu}_{i,t}^2}{\sigma_i^2} \left(1 - \frac{\alpha_i \sigma_i^2}{2} \right) - \frac{\lambda_i}{2} \right) dt$$

We see the previous decomposition between the option profile and the trading impact:

$$\ln \frac{V_T}{V_0} = G_{0,T} + \int_0^T g_t dt$$

where:

$$G_{0,T} = \sum_{i=1}^n \frac{\alpha_i}{2\lambda_i} (\hat{\mu}_{i,T}^2 - \hat{\mu}_{i,0}^2)$$

⁷¹This result is only valid if $A^\top \Lambda^{-1}$ is a symmetric matrix.

⁷²We have:

$$A = \text{diag}(\alpha_1, \dots, \alpha_n)$$

and:

$$g_t = \sum_{i=1}^n \alpha_i \sigma_i^2 \left(\frac{\hat{\mu}_{i,t}^2}{\sigma_i^2} \left(1 - \frac{\alpha_i \sigma_i^2}{2} \right) - \frac{\lambda_i}{2} \right)$$

Another expression of the trading impact g_t is:

$$\begin{aligned} g_t &= \sum_{i=1}^n w_i \left(\left(\frac{\hat{\mu}_{i,t}}{\sigma_i} \right)^2 - \frac{\bar{\lambda}_i}{2} \right) \\ &= \sum_{i=1}^n w_i \left(\frac{\hat{\mu}_{i,t}^2}{\sigma_i^2} \right) - \frac{\bar{\lambda}}{2} \end{aligned}$$

where:

$$w_i = \alpha_i \sigma_i^2 \left(1 - \frac{\alpha_i \sigma_i^2}{2} \right)$$

and:

$$\bar{\lambda}_i = \frac{2\lambda_i}{2 - \alpha_i \sigma_i^2}$$

The parameter $\bar{\lambda}$ is defined as follows:

$$\bar{\lambda} = \sum_{i=1}^n w_i \bar{\lambda}_i$$

If we would like to find the probability distribution of g_t , we have:

$$g_t = \sum_{i=1}^n w_i \hat{s}_{i,t}^2 - \frac{\bar{\lambda}}{2}$$

where $\hat{s}_{i,t} \sim \mathcal{N}(s_{i,t}, \lambda_i)$. Let $\mathbf{Z} \sim \mathcal{N}(\mathbf{0}, \mathbf{I}_n)$. We have:

$$\begin{aligned} g_t &= \sum_{i=1}^n w_i \left(\sqrt{\lambda_i} Z_i + s_{i,t} \right)^2 - \frac{\bar{\lambda}}{2} \\ &= \sum_{i=1}^n w_i \lambda_i \left(Z_i + \frac{s_{i,t}}{\sqrt{\lambda_i}} \right)^2 - \frac{\bar{\lambda}}{2} \\ &= \mathcal{Q}_1(a, b) - \frac{\bar{\lambda}}{2} \end{aligned}$$

where $a = (a_i)$, $a_i = w_i \lambda_i$, $b = (b_i)$ and $b_i = s_{i,t}/\sqrt{\lambda_i}$. We deduce that:

$$\begin{aligned} \Pr\{g_t \leq g\} &= \Pr\left\{\mathcal{Q}_1(a, b) - \frac{\bar{\lambda}}{2} \leq g\right\} \\ &= \Pr\left\{\mathcal{Q}_1(a, b) \leq g + \frac{\bar{\lambda}}{2}\right\} \\ &= \mathbb{Q}_1\left(g + \frac{\bar{\lambda}}{2}; a, b\right) \end{aligned}$$

If we are interested in the statistical moments of g_t , we have:

$$\begin{cases} \mathbb{E}[g_t] = \sum_{i=1}^n a_i (1 + b_i^2) - \frac{\bar{\lambda}}{2} \\ \text{var}(g_t) = 2 \sum_{i=1}^n a_i^2 (1 + 2b_i^2) \\ \gamma_1(g_t) = \frac{2\sqrt{2} \sum_{i=1}^n a_i^3 (1 + 3b_i^2)}{(\sum_{i=1}^n a_i^2 (1 + 2b_i^2))^{3/2}} \\ \gamma_2(g_t) = \frac{12 \sum_{i=1}^n a_i^4 (1 + 4b_i^2)}{(\sum_{i=1}^n a_i^2 (1 + 2b_i^2))^2} \end{cases}$$

A.5.4 Probability distribution of the trend-following strategy

Using the Kalman filter, we have $\hat{\mu}_t \sim \mathcal{N}(\mu_t, \Upsilon_t)$. At the steady state, we can then use the following approximation:

$$\hat{\mu}_t \sim \mathcal{N}(\mu_t, \Upsilon_\infty)$$

It follows that:

$$\hat{\mu}_t^\top A^\top \left(\mathbf{I}_n - \frac{1}{2} \Sigma A \right) \hat{\mu}_t \sim Q_2 \left(\mu_t, \Upsilon_\infty, A^\top \left(\mathbf{I}_n - \frac{1}{2} \Sigma A \right) \right)$$

and:

$$\begin{aligned} \Pr\{g_t \leq g\} &= \Pr \left\{ \hat{\mu}_t^\top A^\top \left(\mathbf{I}_n - \frac{1}{2} \Sigma A \right) \hat{\mu}_t - \frac{1}{2} \text{tr}(A^\top \Sigma \Lambda^\top) \leq g \right\} \\ &= \Pr \left\{ Q_2 \left(\mu_t, \Upsilon_\infty, A^\top \left(\mathbf{I}_n - \frac{1}{2} \Sigma A \right) \right) \leq g + \frac{1}{2} \text{tr}(A^\top \Sigma \Lambda^\top) \right\} \\ &= Q_2 \left(g + \frac{1}{2} \text{tr}(A^\top \Sigma \Lambda^\top); \mu_t, \Upsilon_\infty, A^\top \left(\mathbf{I}_n - \frac{1}{2} \Sigma A \right) \right) \end{aligned}$$

Therefore, we can compute the distribution function of g_t by using the approximation of Liu *et al.* (2009) or the Ruben formula:

$$\Pr\{g_t \leq g\} = Q_1 \left(g + \frac{1}{2} \text{tr}(A^\top \Sigma \Lambda^\top); a, b \right)$$

where $a = \text{diag}(D)$, $b = U^\top \Upsilon_\infty^{-1/2} \mu_t$, D and U are the eigenvalue and eigenvector matrices of $\Omega = \Upsilon_\infty^{1/2} A^\top (\mathbf{I}_n - \frac{1}{2} \Sigma A) \Upsilon_\infty^{1/2}$.

A.5.5 Hit ratio

We have:

$$\begin{aligned} \mathcal{H} &= \Pr\{g_t \geq 0\} \\ &= \Pr \left\{ \hat{\mu}_t^\top A^\top \left(\mathbf{I}_n - \frac{1}{2} \Sigma A \right) \hat{\mu}_t - \frac{1}{2} \text{tr}(A^\top \Sigma \Lambda^\top) \geq 0 \right\} \\ &= \Pr \left\{ Q_2 \left(\mu_t, \Upsilon_\infty, A^\top \left(\mathbf{I}_n - \frac{1}{2} \Sigma A \right) \right) \geq \frac{1}{2} \text{tr}(A^\top \Sigma \Lambda^\top) \right\} \\ &= 1 - Q_2 \left(\frac{1}{2} \text{tr}(A^\top \Sigma \Lambda^\top); \mu_t, \Upsilon_\infty, A^\top \left(\mathbf{I}_n - \frac{1}{2} \Sigma A \right) \right) \end{aligned}$$

In the case where $A = n^{-1}\mathbf{I}_n$ and $\Lambda = \lambda\mathbf{I}_n$, we obtain:

$$\mathcal{H} = 1 - \mathbb{Q}_2 \left(\frac{\lambda}{2n} \sum_{i=1}^n \sigma_i^2; \mu_t, \lambda\Sigma, \frac{2n\mathbf{I}_n - \Sigma}{2n^2} \right)$$

A.5.6 Statistical moments of g_t

We have:

$$g_t = Q_2 \left(\mu_t, \Upsilon_\infty, A^\top \left(\mathbf{I}_n - \frac{1}{2}\Sigma A \right) \right) - \frac{1}{2} \text{tr}(A^\top \Sigma \Lambda^\top)$$

Using Appendix A.3.2 on page 68, we deduce that:

$$\begin{aligned} \mu(g_t) &= \text{tr}(Q\Lambda\Sigma) + \mu_t^\top Q\mu_t - \frac{1}{2} \text{tr}(A^\top \Sigma \Lambda^\top) \\ \sigma(g_t) &= \sqrt{2 \left(\text{tr}(Q\Lambda\Sigma)^2 + 2\mu_t^\top Q\Lambda\Sigma Q\mu_t \right)} \\ \gamma_1(g_t) &= \sqrt{8} \frac{\left(\text{tr}(Q\Lambda\Sigma)^3 + 3\mu_t^\top (Q\Lambda\Sigma)^2 Q\mu_t \right)}{\left(\text{tr}(Q\Lambda\Sigma)^2 + 2\mu_t^\top Q\Lambda\Sigma Q\mu_t \right)^{3/2}} \\ \gamma_2(g_t) &= 12 \frac{\left(\text{tr}(Q\Lambda\Sigma)^4 + 4\mu_t^\top (Q\Lambda\Sigma)^3 Q\mu_t \right)}{\left(\text{tr}(Q\Lambda\Sigma)^2 + 2\mu_t^\top Q\Lambda\Sigma Q\mu_t \right)^2} \end{aligned}$$

where:

$$Q = A^\top \left(\mathbf{I}_n - \frac{1}{2}\Sigma A \right)$$

A.5.7 Covariance of the estimation error

We recall that the Kalman-Bucy filter defines an optimal EWMA estimator. In this case, the EWMA matrix Λ is given by:

$$\Lambda = \Upsilon_\infty \Sigma^{-1}$$

where Υ_∞ is the solution of the algebraic Riccati solution:

$$\Gamma - \Upsilon_\infty \Sigma^{-1} \Upsilon_\infty = \mathbf{0}$$

When the matrices $\Gamma^{1/2}$ and $\Sigma^{1/2}$ commute, the solution becomes $\Upsilon_\infty = \Gamma^{1/2}\Sigma^{1/2}$ and we have $\Lambda = \Gamma^{1/2}\Sigma^{-1/2}$.

We now assume that the EWMA matrix is a given matrix, which is not necessarily equal to $\Upsilon_\infty \Sigma^{-1}$. We denote $\tilde{\Lambda}$ this matrix and $\tilde{\Upsilon}_t$ the associated covariance matrix of estimation errors. We always have:

$$d\hat{\mu}_t = \tilde{\Lambda} (dy_t - \hat{\mu}_t dt)$$

However, the dynamics of the covariance matrix $\tilde{\Upsilon}_t$ is not given by the Kalman-Bucy filter. It follows that⁷³:

$$\begin{aligned} d(\hat{\mu}_t - \mu_t) &= \tilde{\Lambda} (dy_t - \hat{\mu}_t dt) - d\mu_t \\ &= -\tilde{\Lambda} (\hat{\mu}_t - \mu_t) dt + \tilde{\Lambda} \Sigma^{1/2} dZ_t - \Gamma^{1/2} dZ_t^* \end{aligned}$$

⁷³We recall that:

$$\begin{cases} dy_t = \mu_t dt + \Sigma^{1/2} dZ_t \\ d\mu_t = \Gamma^{1/2} dZ_t^* \end{cases}$$

where Z_t and Z_t^* are two uncorrelated vectors of independent Brownian motions.

and:

$$\begin{aligned} d \left((\hat{\mu}_t - \mu_t) (\hat{\mu}_t - \mu_t)^\top \right) &= d(\hat{\mu}_t - \mu_t) \cdot (\hat{\mu}_t - \mu_t)^\top + (\hat{\mu}_t - \mu_t) \cdot d(\hat{\mu}_t - \mu_t)^\top + \\ &\quad d \left\langle (\hat{\mu}_t - \mu_t) (\hat{\mu}_t - \mu_t)^\top \right\rangle \\ &= -\tilde{\Lambda} (\hat{\mu}_t - \mu_t) (\hat{\mu}_t - \mu_t)^\top dt - (\hat{\mu}_t - \mu_t) (\hat{\mu}_t - \mu_t)^\top \tilde{\Lambda}^\top dt + \\ &\quad (\Gamma + \tilde{\Lambda} \Sigma \tilde{\Lambda}^\top) dt + dM_t \end{aligned}$$

where M_t is a local martingale. We deduce that:

$$\begin{aligned} d\tilde{\Upsilon}_t &= \mathbb{E} \left[d \left((\hat{\mu}_t - \mu_t) (\hat{\mu}_t - \mu_t)^\top \right) \right] \\ &= \left(-\tilde{\Lambda} \tilde{\Upsilon}_t - \tilde{\Upsilon}_t \tilde{\Lambda}^\top + \Gamma + \tilde{\Lambda} \Sigma \tilde{\Lambda}^\top \right) dt \\ &= \varrho \left(\tilde{\Upsilon}_t; \tilde{\Lambda} \right) dt \end{aligned}$$

We obtain a Lyapunov equation and the solution is:

$$\tilde{\Upsilon}_t = \int_0^t e^{-\tilde{\Lambda}(t-u)} \left(\Gamma + \tilde{\Lambda} \Sigma \tilde{\Lambda}^\top \right) e^{-\tilde{\Lambda}^\top(t-u)} du + e_0^{-\tilde{\Lambda} t} \tilde{\Upsilon}_0 e^{-\tilde{\Lambda}^\top t}$$

The covariance matrix $\tilde{\Upsilon}_t$ tends exponentially to the solution of $\varrho \left(\tilde{\Upsilon}_t; \tilde{\Lambda} \right) = 0$. By the implicit function theorem, the equation $\varrho \left(\tilde{\Upsilon}_t; \tilde{\Lambda} \right) = 0$ defines a curve $\tilde{\Upsilon}_t = g \left(\tilde{\Lambda} \right)$, and $d g \left(\tilde{\Lambda} \right) / d \tilde{\Lambda} = 0$ is equivalent to $\partial \varrho \left(\tilde{\Upsilon}_t; \tilde{\Lambda} \right) / \partial \tilde{\Lambda} = 0$. We have⁷⁴:

$$\frac{\partial \varrho \left(\tilde{\Upsilon}_t; \tilde{\Lambda} \right)}{\partial \tilde{\Lambda}} = -2\tilde{\Upsilon}_t + 2\tilde{\Lambda}\Sigma = 0$$

We deduce that the optimal solution is:

$$\tilde{\Lambda}^* = \tilde{\Upsilon}_t \Sigma^{-1} = \Lambda$$

In this case, we retrieve the Kalman-Bucy filter:

$$\begin{aligned} d\tilde{\Upsilon}_t &= \left(-\Lambda \tilde{\Upsilon}_t - \tilde{\Upsilon}_t \Lambda^\top + \Gamma + \Lambda \Sigma \Lambda^\top \right) dt \\ &= \left(\Gamma - \tilde{\Upsilon}_t \Sigma^{-1} \tilde{\Upsilon}_t^\top \right) dt \end{aligned}$$

We confirm that the Kalman-Bucy solution $\Lambda = \Upsilon_t \Sigma^{-1}$ minimizes the estimation error.

A.5.8 Probability distribution of the cross-section momentum strategy

We recall that:

$$A = \text{diag}(\alpha) - \frac{1}{n} \alpha \otimes \mathbf{1}_n^\top$$

Another expression of A is:

$$A = \text{diag}(\alpha) \left(\mathbf{I}_n - \frac{1}{n} \mathbf{1}_n \mathbf{1}_n^\top \right)$$

⁷⁴We need $\tilde{\Lambda}$ to commute with $\tilde{\Upsilon}_t$.

The eigenvalues of $\mathbf{I}_n - \frac{1}{n}\mathbf{1}_n\mathbf{1}_n^\top$ are all equal to one, except the last eigenvalue, which is equal to zero. It follows that $\text{rank}(A) = n - 1$. If we consider the matrix $Q = A^\top (\mathbf{I}_n - \frac{1}{2}\Sigma A)$, we deduce that $\text{rank}(Q) \leq n - 1$. In the cross-section momentum, the quadratic form $Q_2(\mu_t, \Upsilon_\infty, Q)$ is then a sum of $n - 1$ independent noncentral chi-square random variables. This is why we can compute the distribution of g_t by using the parametrization \mathbb{Q}_1 with the first $n - 1$ eigenvalues.

A.6 The hedged strategy

A.6.1 The univariate case

We now assume that the portfolio is both long on the underlying asset and the trend-following strategy, meaning that the allocation is as follows:

$$e_t = \alpha\hat{\mu}_t + \beta$$

where $\beta \geq 0$ is the buy-and-hold exposure on the asset S_t .

P&L of the strategy We have:

$$\frac{dV_t}{V_t} = (\alpha\hat{\mu}_t + \beta) dy_t$$

and:

$$d\ln V_t = (\alpha\hat{\mu}_t + \beta) dy_t - \frac{1}{2}(\alpha\hat{\mu}_t + \beta)^2 \sigma^2 dt$$

Since we have $dy_t = \lambda^{-1} d\hat{\mu}_t + \hat{\mu}_t dt$, we deduce that⁷⁵:

$$\begin{aligned} d\ln V_t &= (\alpha\hat{\mu}_t + \beta) \lambda^{-1} d\hat{\mu}_t + (\alpha\hat{\mu}_t + \beta) \hat{\mu}_t dt - \frac{1}{2}(\alpha\hat{\mu}_t + \beta)^2 \sigma^2 dt \\ &= \frac{d(\alpha\hat{\mu}_t + \beta)^2}{2\alpha\lambda} + \left((\alpha\hat{\mu}_t + \beta) \hat{\mu}_t - \frac{1}{2}(\alpha\hat{\mu}_t + \beta)^2 \sigma^2 - \frac{1}{2}\alpha\lambda\sigma^2 \right) dt \\ &= \frac{d(\alpha\hat{\mu}_t + \beta)^2}{2\alpha\lambda} + \left(\alpha\hat{\mu}_t^2 + \beta\hat{\mu}_t - \frac{1}{2}(\alpha^2\hat{\mu}_t^2 + 2\alpha\beta\hat{\mu}_t + \beta^2)\sigma^2 - \frac{1}{2}\alpha\lambda\sigma^2 \right) dt \\ &= \frac{\alpha}{2\lambda} d\hat{\mu}_t^2 + \frac{\beta}{\lambda} d\hat{\mu}_t + \left(\alpha\hat{\mu}_t^2 - \frac{1}{2}\alpha^2\sigma^2\hat{\mu}_t^2 - \frac{1}{2}\alpha\lambda\sigma^2 \right) dt + \\ &\quad \beta \left(\hat{\mu}_t - \frac{\sigma^2}{2}(2\alpha\hat{\mu}_t + \beta) \right) dt \end{aligned}$$

We conclude that:

$$d\ln V_t = dG_t + g_t dt + h_t$$

⁷⁵We have:

$$\begin{aligned} d(\alpha\hat{\mu}_t + \beta)^2 &= 2\alpha(\alpha\hat{\mu}_t + \beta) d\hat{\mu}_t + \alpha^2 d\langle \hat{\mu}, \hat{\mu} \rangle_t \\ &= 2\alpha(\alpha\hat{\mu}_t + \beta) d\hat{\mu}_t + \alpha^2\lambda^2\sigma^2 dt \end{aligned}$$

and:

$$(\alpha\hat{\mu}_t + \beta) d\hat{\mu}_t = \frac{d(\alpha\hat{\mu}_t + \beta)^2 - \alpha^2\lambda^2\sigma^2 dt}{2\alpha}$$

where:

$$\begin{aligned} G_t &= \frac{\alpha}{2\lambda} \hat{\mu}_t^2 \\ g_t &= \alpha \hat{\mu}_t^2 \left(1 - \frac{\alpha\sigma^2}{2}\right) - \frac{1}{2} \alpha \lambda \sigma^2 = \alpha \sigma^2 \left(\frac{\hat{\mu}_t^2}{\sigma^2} \left(1 - \frac{\alpha\sigma^2}{2}\right) - \frac{\lambda}{2}\right) \end{aligned}$$

and:

$$h_t = \beta \lambda^{-1} d\hat{\mu}_t + \beta \left(\hat{\mu}_t \left(1 - \alpha\sigma^2\right) - \frac{\beta\sigma^2}{2} \right) dt$$

Therefore, the P&L of the portfolio is composed of three terms:

$$\ln \frac{V_T}{V_0} = G_{0,T} + \int_0^T g_t dt + \int_0^T h_t$$

The hedging cost As previously, we can derive a closed formula of the P&L, where we identify both the P&L of the buy-and-hold strategy and the P&L of the trend-following plus an additional term, which may be interpreted as the cost of the hedge. Indeed, we have:

$$\begin{aligned} h_t &= \beta \lambda^{-1} d\hat{\mu}_t + \beta \left(\hat{\mu}_t \left(1 - \alpha\sigma^2\right) - \frac{\beta\sigma^2}{2} \right) dt \\ &= \beta (\lambda^{-1} d\hat{\mu}_t + \hat{\mu}_t dt) - \beta \left(\alpha \sigma^2 \hat{\mu}_t - \frac{\beta\sigma^2}{2} \right) dt \\ &= \left(\beta dy_t - \frac{\beta^2 \sigma^2}{2} dt \right) - \alpha \beta \sigma^2 \hat{\mu}_t dt \\ &= d(\beta \ln S_t) - \alpha \beta \sigma^2 \hat{\mu}_t dt \end{aligned}$$

The new term h_t is decomposed into a usual asset price term and an additional term, coming from the aggregation of trend following and long-only positions. We obtain:

$$d \ln V_t = d(G_t + \beta \ln S_t) + g_t dt - c_t dt$$

where $c_t = \alpha \beta \sigma^2 \hat{\mu}_t$. Since we have:

$$\begin{cases} c_t \geq 0 \Leftrightarrow \hat{\mu}_t \geq 0 \\ c_t \leq 0 \Leftrightarrow \hat{\mu}_t \leq 0 \end{cases}$$

c_t is the price of hedging in a bullish market (when $\hat{\mu}_t \geq 0$). In return, the strategy benefits from out-performance when the market is down.

The option profile We have:

$$\begin{aligned} d \ln V_t &= \frac{d(\alpha \hat{\mu}_t + \beta)^2}{2\alpha\lambda} + \left((\alpha \hat{\mu}_t + \beta) \hat{\mu}_t - \frac{1}{2} (\alpha \hat{\mu}_t + \beta)^2 \sigma^2 - \frac{1}{2} \alpha \lambda \sigma^2 \right) dt \\ &= d\tilde{G}_t + \tilde{g}_t dt \end{aligned}$$

where:

$$\tilde{G}_t = \frac{(\alpha \hat{\mu}_t + \beta)^2}{2\alpha\lambda}$$

It follows that the option profile of the hedged strategy is:

$$\begin{aligned}\tilde{G}_{0,T} &= \frac{(\alpha\hat{\mu}_T + \beta)^2 - (\alpha\hat{\mu}_0 + \beta)^2}{2\alpha\lambda} \\ &= \frac{\alpha}{2\lambda} (\hat{\mu}_T^2 - \hat{\mu}_0^2) + \frac{\beta}{\lambda} (\hat{\mu}_T - \hat{\mu}_0) \\ &= G_{0,T} + \frac{\beta}{\lambda} (\hat{\mu}_T - \hat{\mu}_0)\end{aligned}$$

This is the shifted option profile of the trend-following strategy.

Probability distribution of the hedged strategy The trading impact of the hedged strategy has the following expression:

$$\begin{aligned}\tilde{g}_t &= (\alpha\hat{\mu}_t + \beta)\hat{\mu}_t - \frac{1}{2}(\alpha\hat{\mu}_t + \beta)^2\sigma^2 - \frac{1}{2}\alpha\lambda\sigma^2 \\ &= \alpha\left(1 - \frac{\alpha\sigma^2}{2}\right)\left(\hat{\mu}_t - \frac{\beta(\alpha\sigma^2 - 1)}{\alpha(2 - \alpha\sigma^2)}\right)^2 - \left(\frac{\beta^2(1 - \alpha\sigma^2)^2}{\alpha(4 - 2\alpha\sigma^2)} + \frac{\beta^2\sigma^2}{2} + \frac{1}{2}\alpha\lambda\sigma^2\right) \\ &= \alpha\sigma^2\left(1 - \frac{\alpha\sigma^2}{2}\right)\left(\hat{s}_t - \frac{\beta(\alpha\sigma^2 - 1)}{\alpha\sigma(2 - \alpha\sigma^2)}\right)^2 - \left(\frac{\beta^2(1 - \alpha\sigma^2)^2}{\alpha(4 - 2\alpha\sigma^2)} + \frac{\beta^2\sigma^2}{2} + \frac{1}{2}\alpha\lambda\sigma^2\right) \\ &= a(\hat{s}_t - b)^2 - c\end{aligned}$$

We notice that:

$$\hat{s}_t - b \sim \mathcal{N}(s_t - b, \lambda)$$

It follows that $\lambda^{-1}(\hat{s}_t - b)^2$ is a noncentral chi-square random variable $\chi_1^2(\zeta)$ with $\zeta = \lambda^{-1}(s_t - b)^2$. We deduce that \tilde{g}_t is an affine transformation of a noncentral chi-square random variable:

$$\begin{aligned}\Pr\{\tilde{g}_t \leq g\} &= \Pr\left\{a(\hat{s}_t - b)^2 - c \leq g\right\} \\ &= \Pr\left\{(\hat{s}_t - b)^2 \leq \frac{g + c}{a}\right\} \\ &= \mathbb{F}\left(\frac{g + c}{\lambda a}; 1, \zeta\right)\end{aligned}$$

where $\mathbb{F}(x; \nu, \zeta)$ is the cumulative noncentral chi-square probability distribution.

Remark 14 Another expression of the probability distribution is:

$$\begin{aligned}\Pr\{\tilde{g}_t \leq g\} &= \Pr\left\{-\frac{g + c}{a} \leq \hat{s}_t - b \leq \frac{g + c}{a}\right\} \\ &= \Phi\left(\frac{b + a^{-1}(g + c) - s_t}{\sqrt{\lambda}}\right) - \Phi\left(\frac{b - a^{-1}(g + c) - s_t}{\sqrt{\lambda}}\right)\end{aligned}$$

We now compute the statistical moments. Since $\tilde{g}_t = a\lambda\chi_1^2(\zeta) - c$, we have:

$$\begin{aligned}\mu(\tilde{g}_t) &= a\lambda(1 + \zeta) - c \\ &= \frac{\lambda\alpha\sigma^2(2 - \alpha\sigma^2)(1 + \zeta)}{2} - \frac{1}{2}\alpha\lambda\sigma^2 - \frac{\beta^2(1 - \alpha\sigma^2)^2}{\alpha(4 - 2\alpha\sigma^2)} - \frac{\beta^2\sigma^2}{2}\end{aligned}$$

where:

$$\zeta = \lambda^{-1} \left(s_t - \frac{\beta(\alpha\sigma^2 - 1)}{\alpha\sigma(2 - \alpha\sigma^2)} \right)^2$$

For the second moment, we obtain:

$$\sigma(\tilde{g}_t) = \left| \frac{\lambda\alpha\sigma^2(2 - \alpha\sigma^2)}{2} \right| \sqrt{2 + 4\zeta}$$

We also have:

$$\gamma_1(\tilde{g}_t) = (1 + 6\zeta) \sqrt{\frac{2}{(1 + 2\zeta)^3}}$$

and:

$$\gamma_2(\tilde{g}_t) = \frac{12 + 48\zeta}{(1 + 2\zeta)^2}$$

A.6.2 The multivariate case

In the multivariate case, the allocation becomes:

$$\mathbf{e}_t = A\hat{\mu}_t + B$$

P&L of the strategy Using some technical assumptions⁷⁶, we obtain:

$$\frac{dV_t}{dt} = \mathbf{e}_t^\top dy_t$$

and:

$$\begin{aligned} d\ln V_t &= (A\hat{\mu}_t + B)^\top dy_t - \frac{1}{2} (A\hat{\mu}_t + B)^\top \Sigma (A\hat{\mu}_t + B) dt \\ &= (A\hat{\mu}_t + B)^\top \Lambda^{-1} d\hat{\mu}_t + \left((A\hat{\mu}_t + B)^\top \hat{\mu}_t - \frac{1}{2} (A\hat{\mu}_t + B)^\top \Sigma (A\hat{\mu}_t + B) \right) dt \end{aligned}$$

Since we have:

$$(A\hat{\mu}_t + B)^\top \Lambda^{-1} d\hat{\mu}_t = \frac{1}{2} d(\hat{\mu}_t^\top A^\top \Lambda^{-1} \hat{\mu}_t) + d(B^\top \Lambda^{-1} \hat{\mu}_t) - \frac{1}{2} \text{tr}(A^\top \Sigma \Lambda^\top) dt$$

we deduce that:

$$d\ln V_t = d\tilde{G}_t + \tilde{g} dt$$

where:

$$\begin{aligned} \tilde{G}_t &= \frac{1}{2} \hat{\mu}_t^\top A^\top \Lambda^{-1} \hat{\mu}_t + B^\top \Lambda^{-1} \hat{\mu}_t \\ &= G_t + B^\top \Lambda^{-1} \hat{\mu}_t \end{aligned}$$

and:

$$\begin{aligned} \tilde{g}_t &= (A\hat{\mu}_t + B)^\top \hat{\mu}_t - \frac{1}{2} (A\hat{\mu}_t + B)^\top \Sigma (A\hat{\mu}_t + B) - \frac{1}{2} \text{tr}(A^\top \Sigma \Lambda^\top) \\ &= \hat{\mu}_t^\top A^\top \left(\mathbf{I}_n - \frac{1}{2} \Sigma A \right) \hat{\mu}_t - \frac{1}{2} \text{tr}(A^\top \Sigma \Lambda^\top) + \\ &\quad (B^\top - B^\top \Sigma A) \hat{\mu}_t - \frac{1}{2} B^\top \Sigma B \\ &= g_t + (B^\top - B^\top \Sigma A) \hat{\mu}_t - \frac{1}{2} B^\top \Sigma B \end{aligned}$$

⁷⁶We recall that the matrices (A, Σ) and (Λ, B) commute, and $A\Sigma^{-1}$ is symmetric.

The hedging cost Another expression of the P&L is:

$$d \ln V_t = dG_t + g_t dt + h_t$$

where:

$$\begin{aligned} h_t &= B^\top \Lambda^{-1} d\hat{\mu}_t + \left((B^\top - B^\top \Sigma A) \hat{\mu}_t - \frac{1}{2} B^\top \Sigma B \right) dt \\ &= B^\top dy_t - \left(B^\top \Sigma A \hat{\mu}_t + \frac{1}{2} B^\top \Sigma B \right) dt \\ &= d \ln (B^\top \mathbf{S}_t) - B^\top \Sigma A \hat{\mu}_t dt \end{aligned}$$

We deduce that:

$$d \ln V_t = d(G_t + \ln(B^\top \mathbf{S}_t)) + g_t dt - c_t dt$$

where $c_t = B^\top \Sigma A \hat{\mu}_t$.

A.6.3 The shape of the hedged strategy

Shape of noncentral chi-square distribution Let X be a noncentral chi-square random variable with ν degrees of freedom and noncentrality parameter ζ . We define the function $g(\zeta)$ as follows:

$$g(\zeta) = \frac{I_{\nu/2}(\sqrt{\zeta(\zeta + \nu - 4)})}{I_{\nu/2-1}(\sqrt{\zeta(\zeta + \nu - 4)})} - \frac{\zeta - 2}{\sqrt{\zeta(\zeta + \nu - 4)}}$$

where $I_\nu(x)$ denotes the modified Bessel function of the first kind. Let $\zeta^* \in (4 - \nu, \infty)$ be the unique solution of the equation $g(\zeta) = 0$. Yu (2011) shows the following results:

- the density of X is log-concave iff $\nu \geq 2$;
- the density of X is decreasing iff $0 < \nu \leq 2$ and $\zeta \leq \zeta^*$;
- the density of X is bi-modal iff $0 < \nu < 2$ and $\zeta > \zeta^*$.

In Figure 46, we represent the density for some parameters. The parameters $(\nu = 1, \zeta = 1)$ produce a decreasing function, the bi-modal shape is obtained for the parameters $(\nu = 1, \zeta = 1)$, whereas the parameters $(\nu = 3, \zeta = 5)$ correspond to a log-concave density. Figure 47 shows the critical value ζ^* that splits noncentral chi-square densities between decreasing curves and bi-modal curves.

Application to the trading impact \tilde{g}_t In the one-dimension case, we recall that the degree of freedom ν is equal to one and the noncentral parameter is defined by:

$$\zeta = \frac{(\alpha\sigma(2 - \alpha\sigma^2)s_t - \beta(\alpha\sigma^2 - 1))^2}{\alpha^2\lambda\sigma^2(2 - \alpha\sigma^2)^2}$$

The solution ζ^* of the equation $g(\zeta) = 0$ is equal to 4.2166. We deduce that a low exposure α produces a bi-modal density for \tilde{g}_t . This property holds as long as $\zeta \geq \zeta^*$. Then, we obtain a decreasing density function. An illustration is given in Figure 48 with $\beta = 1$, $\sigma = 30\%$ and $\lambda = 2$.

Figure 46: Noncentral chi-square probability density functions

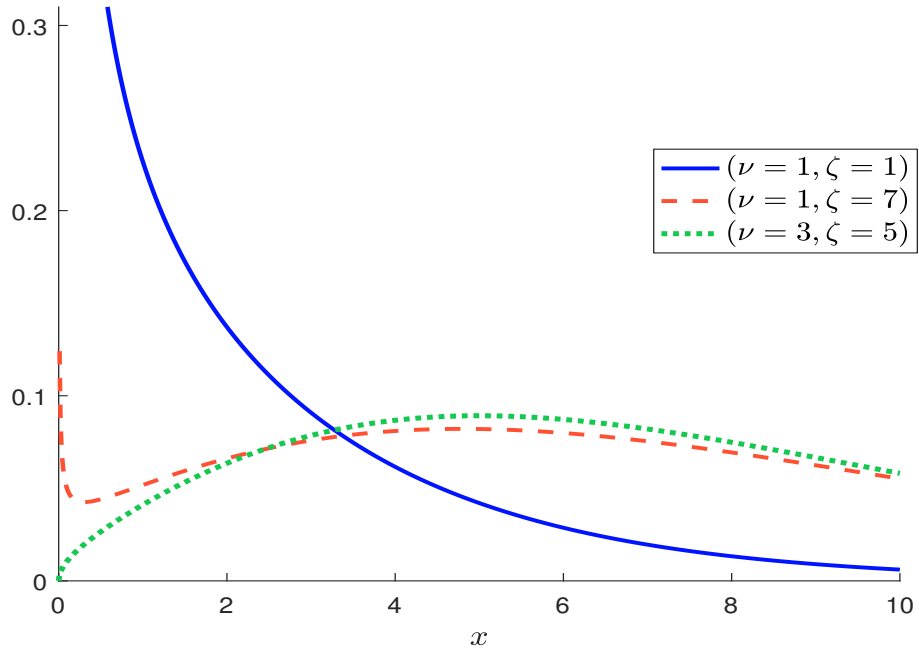


Figure 47: Critical value ζ^*

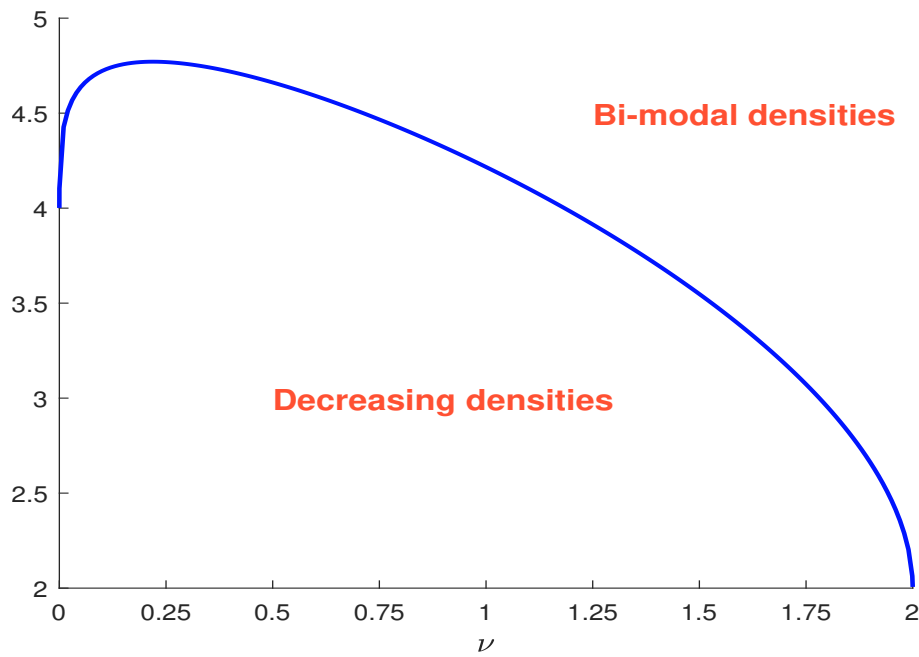
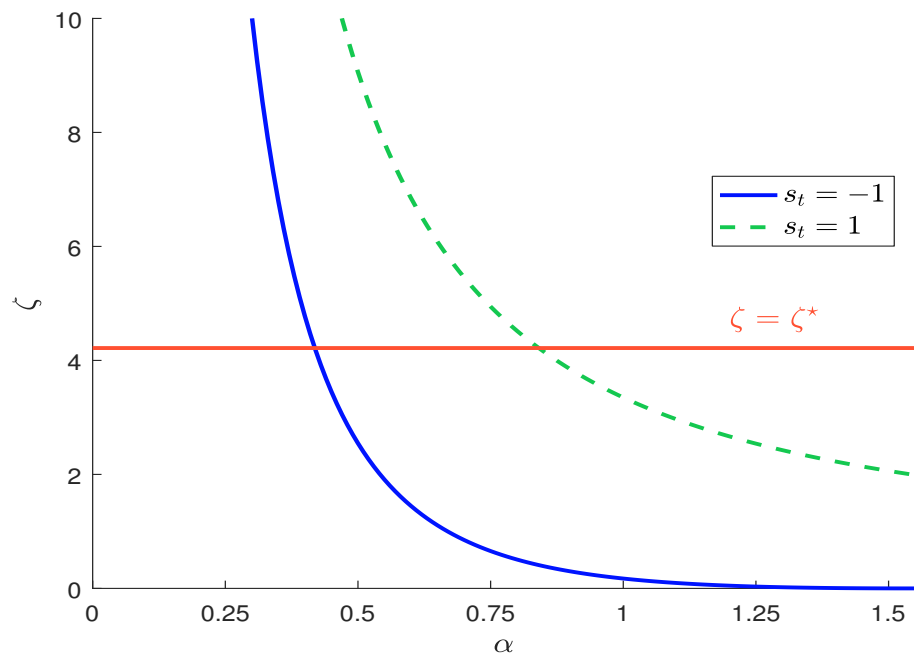


Figure 48: Noncentral parameter ζ



B Additional tables

 Table 4: Difference between naive and Riccati solutions ($\rho = \rho^* = 30\%$)

	Naive solution	Riccati solution
Υ_∞	$\Upsilon_\infty = \Gamma^{1/2}\Sigma^{1/2}$ $\begin{pmatrix} 0.0199 & 0.0069 & 0.0074 \\ 0.0101 & 0.0399 & 0.0131 \\ 0.0137 & 0.0161 & 0.0598 \end{pmatrix}$	$\Upsilon_\infty\Sigma^{-1}\Upsilon_\infty = \Gamma$ $\begin{pmatrix} 0.0197 & 0.0078 & 0.0089 \\ 0.0078 & 0.0396 & 0.0140 \\ 0.0089 & 0.0140 & 0.0592 \end{pmatrix}$
Λ	$\Lambda = \Upsilon_\infty\Sigma^{-1} = \Gamma^{1/2}\Sigma^{1/2}$ $\begin{pmatrix} 0.4828 & 0.0160 & 0.0358 \\ -0.0611 & 1.0027 & 0.0452 \\ -0.1118 & -0.0253 & 1.5367 \end{pmatrix}$	$\Lambda = \Upsilon_\infty\Sigma^{-1}$ $\begin{pmatrix} 0.4600 & 0.0346 & 0.0745 \\ -0.1325 & 1.0045 & 0.0872 \\ -0.2314 & -0.0516 & 1.5661 \end{pmatrix}$

 Table 5: Difference between naive and Riccati solutions ($\rho = \rho^* = 90\%$)

	Naive solution	Riccati solution
Υ_∞	$\Upsilon_\infty = \Gamma^{1/2}\Sigma^{1/2}$ $\begin{pmatrix} 0.0193 & 0.0186 & 0.0197 \\ 0.0321 & 0.0386 & 0.0367 \\ 0.0451 & 0.0487 & 0.0578 \end{pmatrix}$	$\Upsilon_\infty\Sigma^{-1}\Upsilon_\infty = \Gamma$ $\begin{pmatrix} 0.0137 & 0.0160 & 0.0186 \\ 0.0160 & 0.0276 & 0.0286 \\ 0.0186 & 0.0286 & 0.0416 \end{pmatrix}$
Λ	$\Lambda = \Upsilon_\infty\Sigma^{-1} = \Gamma^{1/2}\Sigma^{1/2}$ $\begin{pmatrix} 0.1965 & 0.0233 & 0.2939 \\ -0.6139 & 1.0178 & 0.5553 \\ -0.9087 & -0.0101 & 2.2731 \end{pmatrix}$	$\Lambda = \Upsilon_\infty\Sigma^{-1}$ $\begin{pmatrix} -0.4572 & 0.1145 & 0.7745 \\ -1.7999 & 1.0921 & 1.3524 \\ -2.4824 & 0.0099 & 3.2662 \end{pmatrix}$

 Table 6: Difference between naive and Riccati solutions ($\mathcal{C} = \mathcal{C}^* \neq \mathcal{C}_3(\rho)$)

	Naive solution	Riccati solution
Υ_∞	$\Upsilon_\infty = \Gamma^{1/2}\Sigma^{1/2}$ $\begin{pmatrix} 0.0196 & 0.0194 & 0 \\ 0.0317 & 0.0392 & 0 \\ 0 & 0 & 0.0600 \end{pmatrix}$	$\Upsilon_\infty\Sigma^{-1}\Upsilon_\infty = \Gamma$ $\begin{pmatrix} 0.0165 & 0.0198 & 0 \\ 0.0198 & 0.0330 & 0 \\ 0 & 0 & 0.0600 \end{pmatrix}$
Λ	$\Lambda = \Upsilon_\infty\Sigma^{-1} = \Gamma^{1/2}\Sigma^{1/2}$ $\begin{pmatrix} 0.2783 & 0.2346 & 0 \\ -0.4692 & 1.4011 & 0 \\ 0 & 0 & 1.5000 \end{pmatrix}$	$\Lambda = \Upsilon_\infty\Sigma^{-1}$ $\begin{pmatrix} -0.1734 & 0.6503 & 0 \\ -1.3007 & 1.9944 & 0 \\ 0 & 0 & 1.5000 \end{pmatrix}$

Table 7: Difference between Riccati and Lyapunov solutions ($\rho = \rho^* = 30\%$)

Riccati solution	Lyapunov solution for $\tilde{\Lambda}_1$
$\Upsilon_\infty = \begin{pmatrix} 0.0197 & 0.0078 & 0.0089 \\ 0.0078 & 0.0396 & 0.0140 \\ 0.0089 & 0.0140 & 0.0592 \end{pmatrix}$	$\tilde{\Upsilon}_\infty = \begin{pmatrix} 0.0200 & 0.0080 & 0.0090 \\ 0.0080 & 0.0400 & 0.0144 \\ 0.0090 & 0.0144 & 0.0600 \end{pmatrix}$
Lyapunov solution for $\tilde{\Lambda}_2$	Lyapunov solution for $\tilde{\Lambda}_3$
$\tilde{\Upsilon}_\infty = \begin{pmatrix} 0.0250 & 0.0135 & 0.0195 \\ 0.0135 & 0.0850 & 0.0375 \\ 0.0195 & 0.0375 & 0.1850 \end{pmatrix}$	$\tilde{\Upsilon}_\infty = \begin{pmatrix} 0.0250 & 0.0090 & 0.0105 \\ 0.0090 & 0.0400 & 0.0150 \\ 0.0105 & 0.0150 & 0.0650 \end{pmatrix}$

Table 8: Difference between Riccati and Lyapunov solutions ($\rho = \rho^* = 90\%$)

Riccati solution	Lyapunov solution for $\tilde{\Lambda}_1$
$\Upsilon_\infty = \begin{pmatrix} 0.0137 & 0.0160 & 0.0186 \\ 0.0160 & 0.0276 & 0.0286 \\ 0.0186 & 0.0286 & 0.0416 \end{pmatrix}$	$\tilde{\Upsilon}_\infty = \begin{pmatrix} 0.0200 & 0.0240 & 0.0270 \\ 0.0240 & 0.0400 & 0.0432 \\ 0.0270 & 0.0432 & 0.0600 \end{pmatrix}$
Lyapunov solution for $\tilde{\Lambda}_2$	Lyapunov solution for $\tilde{\Lambda}_3$
$\tilde{\Upsilon}_\infty = \begin{pmatrix} 0.0250 & 0.0405 & 0.0585 \\ 0.0405 & 0.0850 & 0.1125 \\ 0.0585 & 0.1125 & 0.1850 \end{pmatrix}$	$\tilde{\Upsilon}_\infty = \begin{pmatrix} 0.0250 & 0.0270 & 0.0315 \\ 0.0270 & 0.0400 & 0.0450 \\ 0.0315 & 0.0450 & 0.0650 \end{pmatrix}$

Table 9: Difference between Riccati and Lyapunov solutions ($\mathcal{C} = \mathcal{C}^* \neq \mathcal{C}_3(\rho)$)

Riccati solution	Lyapunov solution for $\tilde{\Lambda}_1$
$\Upsilon_\infty = \begin{pmatrix} 0.0165 & 0.0198 & 0 \\ 0.0198 & 0.0330 & 0 \\ 0 & 0 & 0.0600 \end{pmatrix}$	$\tilde{\Upsilon}_\infty = \begin{pmatrix} 0.0200 & 0.0240 & 0 \\ 0.0240 & 0.0400 & 0 \\ 0 & 0 & 0.0600 \end{pmatrix}$
Lyapunov solution for $\tilde{\Lambda}_2$	Lyapunov solution for $\tilde{\Lambda}_3$
$\tilde{\Upsilon}_\infty = \begin{pmatrix} 0.0250 & 0.0405 & 0 \\ 0.0405 & 0.0850 & 0 \\ 0 & 0 & 0.1850 \end{pmatrix}$	$\tilde{\Upsilon}_\infty = \begin{pmatrix} 0.0250 & 0.0270 & 0 \\ 0.0270 & 0.0400 & 0 \\ 0 & 0 & 0.0650 \end{pmatrix}$

C Additional figures

Figure 49: Impact of using two moving averages on the option profile

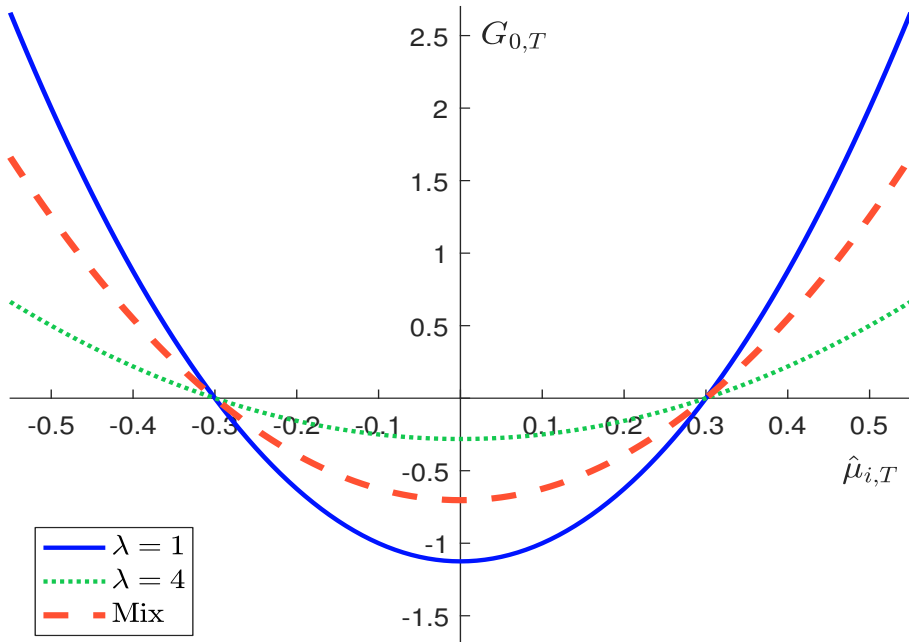


Figure 50: Evolution of the $\omega(s)$ matrix (optimal estimator)

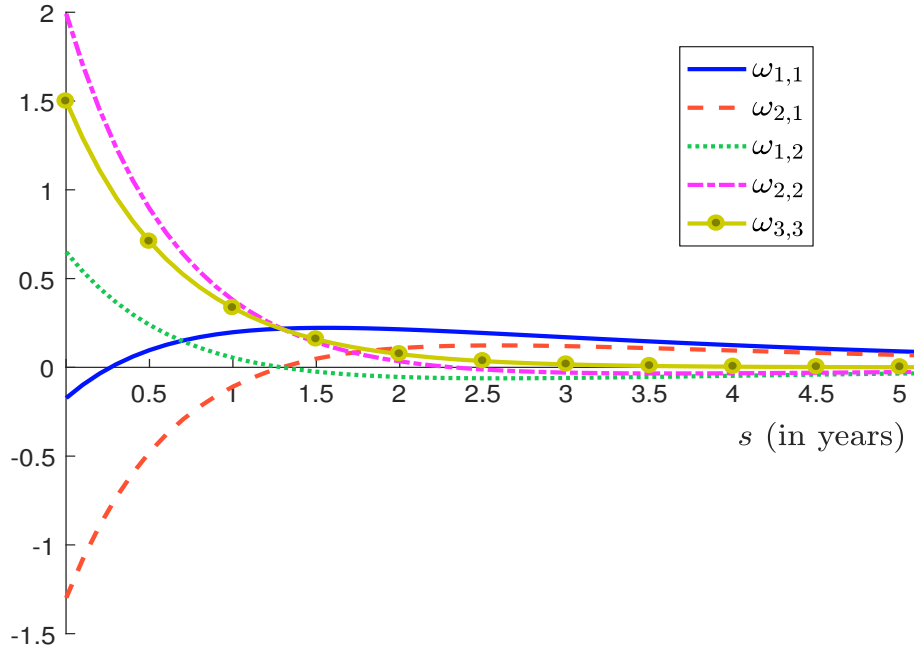


Figure 51: Evolution of the $\omega(s)$ matrix (naive estimator)

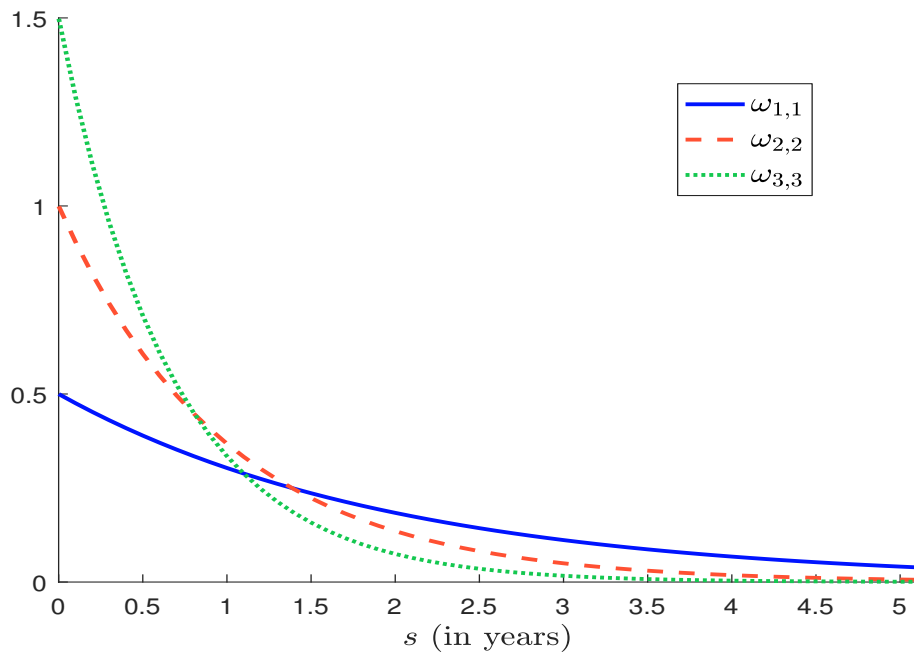


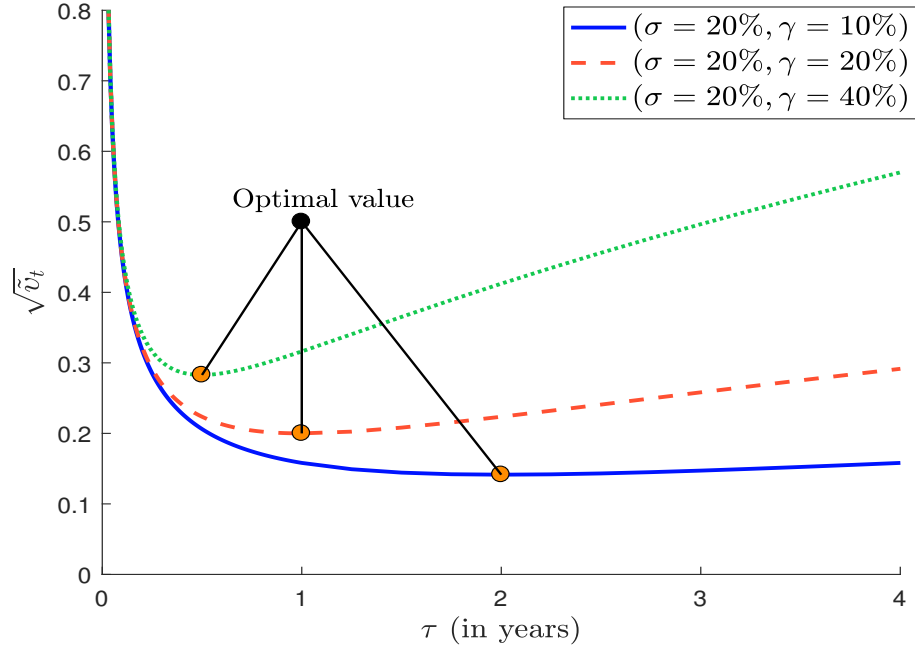
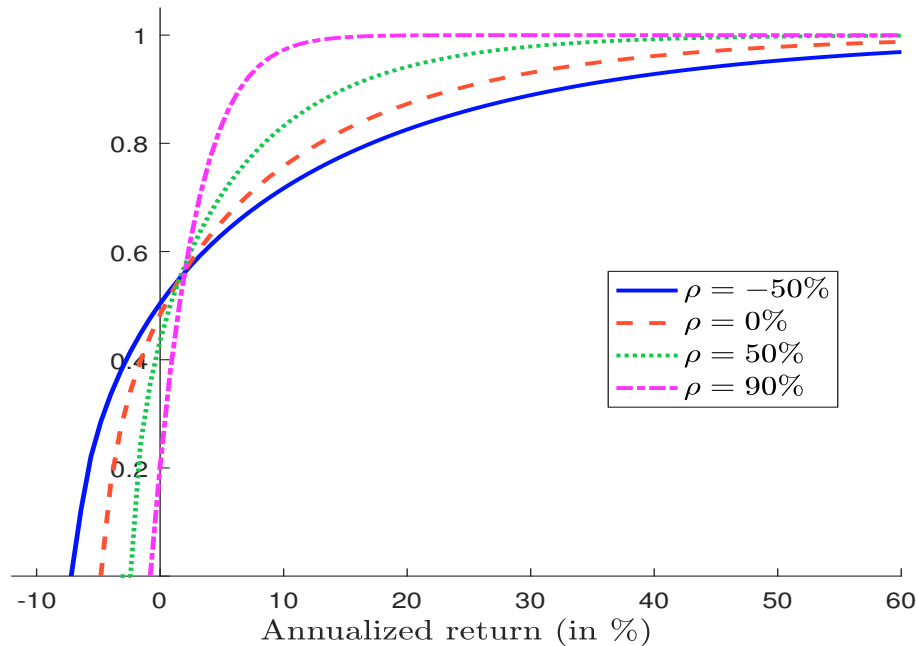
Figure 52: Evolution of the volatility $\sqrt{\tilde{v}_t}$ with respect to the duration τ

 Figure 53: Cumulative distribution function of g_t (cross-section, $n = 2$)
 $(\alpha = 1, \lambda = 1, \mu_{1,t} = 30\%, \mu_{2,t} = 10\% \text{ and } \sigma_{1,t} = \sigma_{2,t} = 30\%)$


Figure 54: Sharpe ratio of the trading impact g_t (cross-section, $n = 2$)
 $(\alpha = 1, \lambda = 1$ and $\sigma_{1,t} = \sigma_{2,t} = 30\%$)

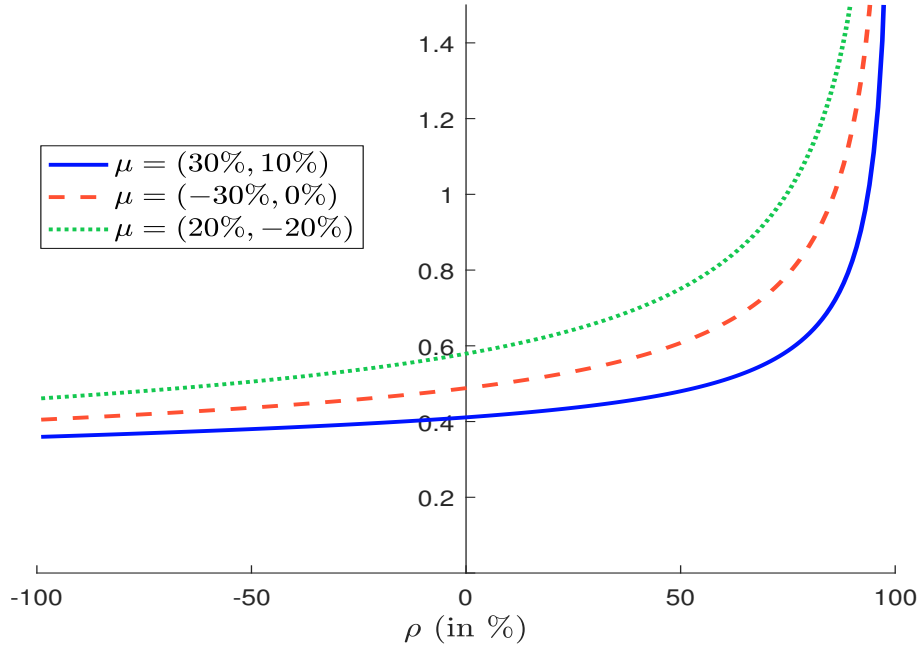


Figure 55: Cumulative distribution function of g_t (cross-section, $n = 4$)
 $(\alpha = 0.5, \lambda = 1, \mu_t = (30\%, 10\%, -30\%, 0\%)$ and $\sigma_{i,t} = 30\%$)

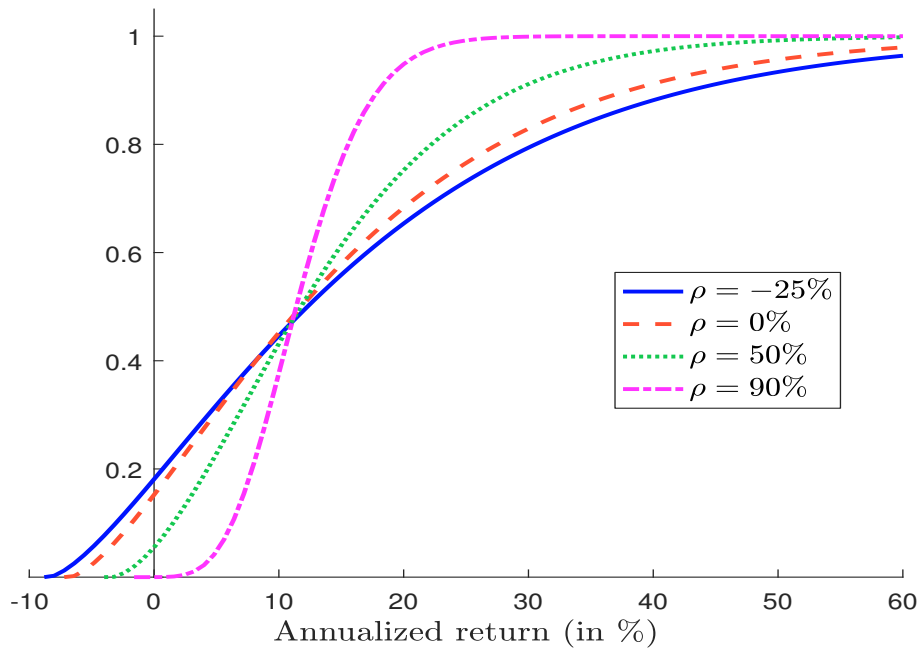


Figure 56: Statistical moments of g_t with respect to the correlation ρ (cross-section, $n = 4$)
 $(\alpha = 0.5, \lambda = 1$ and $\sigma_{i,t} = 30\%$)

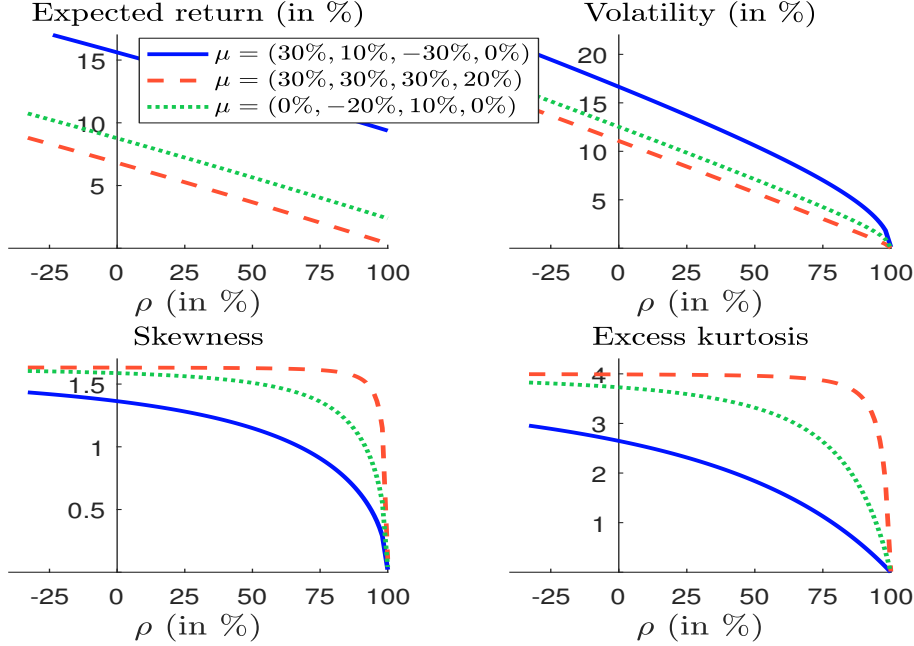


Figure 57: Sharpe ratio of the trading impact g_t (cross-section, $n = 4$)
 $(\alpha = 0.5, \lambda = 1$ and $\sigma_{i,t} = 30\%$)

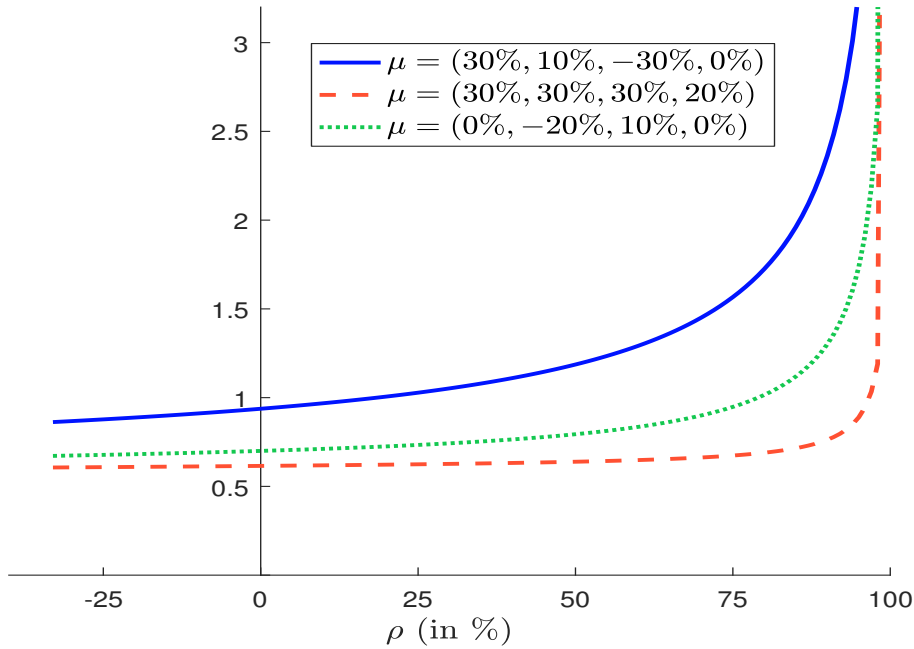


Figure 58: Comparison of the strategy performance V_t and the model performance \tilde{V}_t when the underlying asset is a simulated geometric Brownian motion

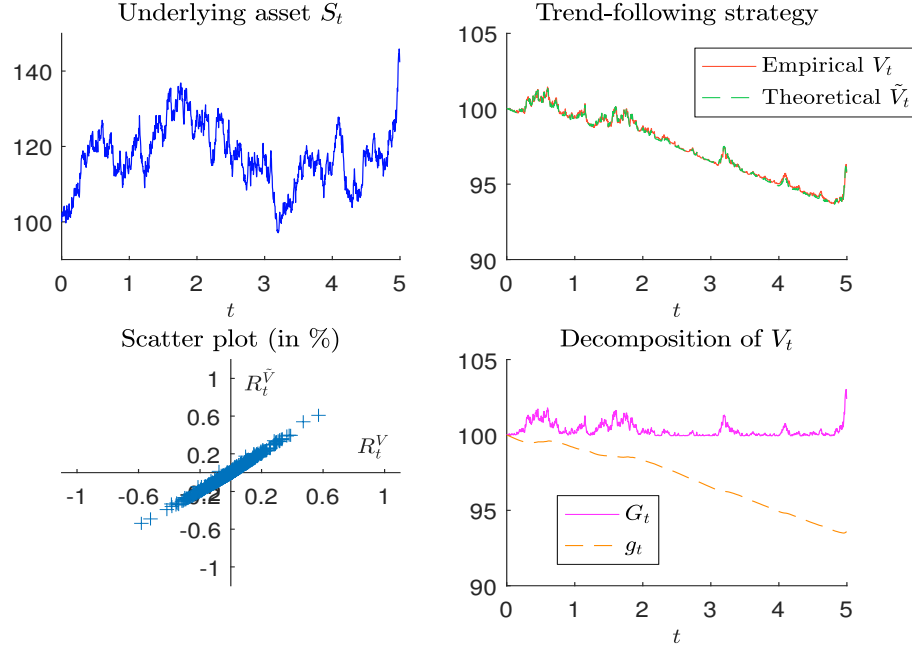


Figure 59: Comparison of the strategy performance V_t and the model performance \tilde{V}_t when the underlying asset is a simulated geometric Brownian motion

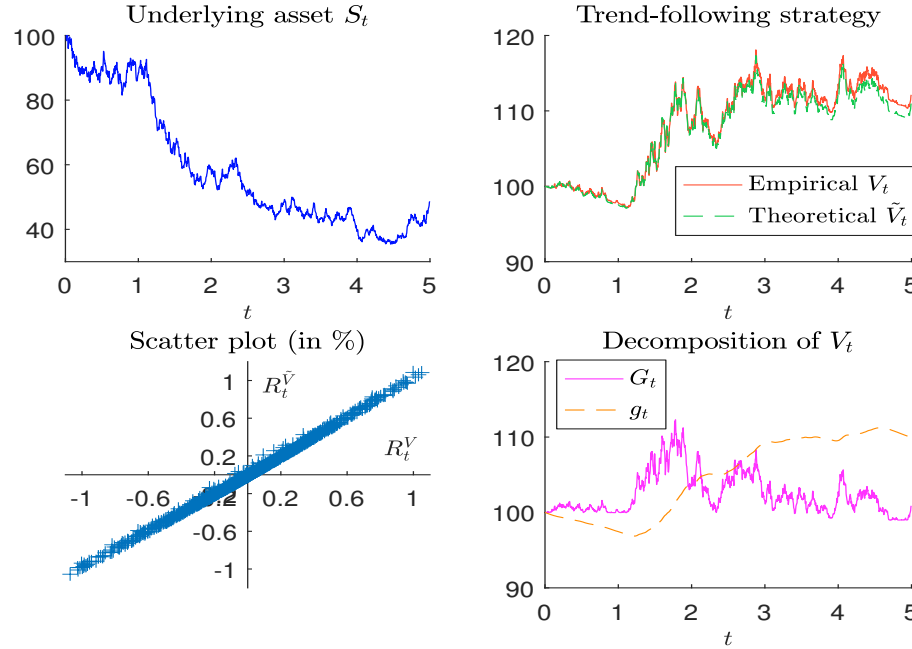


Figure 60: Decomposition of the trend-following strategy (S&P 500)

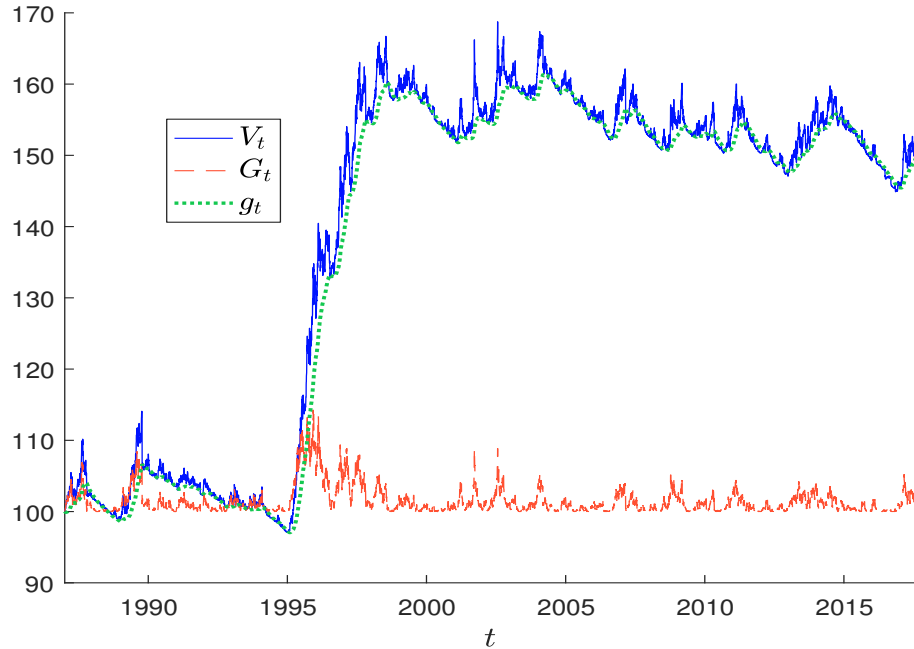


Figure 61: Scatterplot between asset returns and momentum returns (S&P 500)

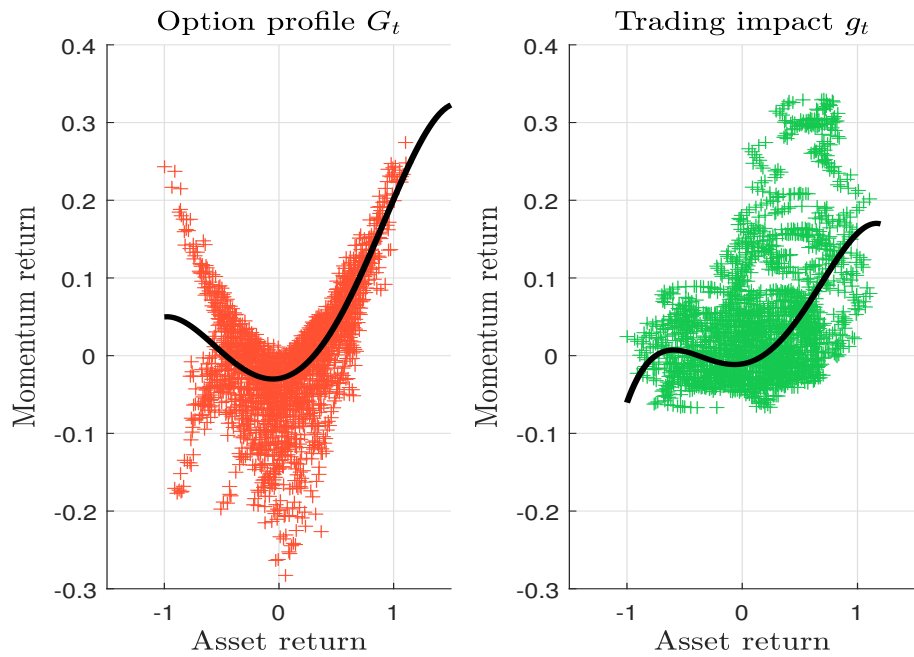


Figure 62: Decomposition of the trend-following strategy (Nikkei 225)

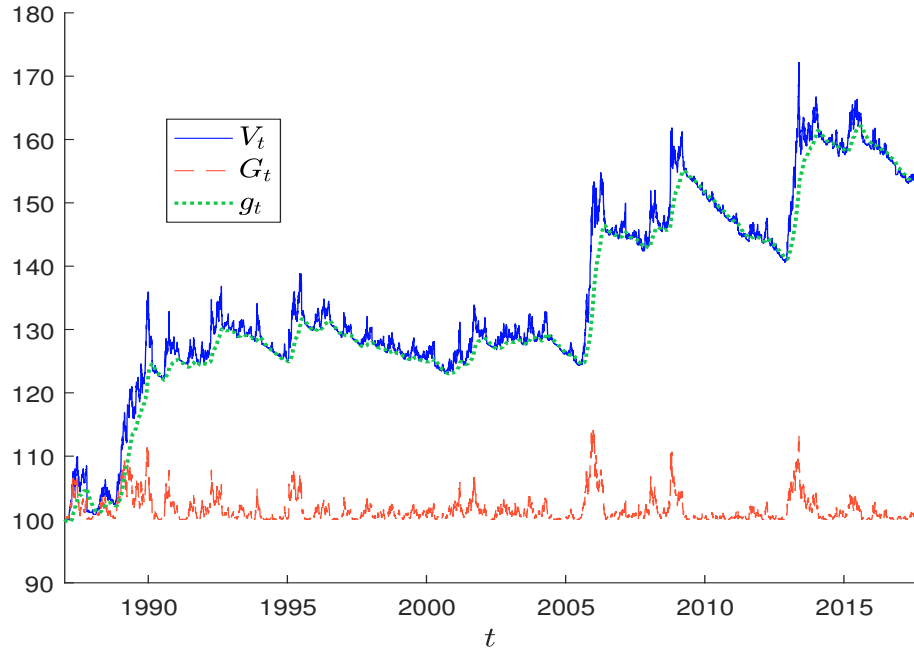


Figure 63: Scatterplot between asset returns and momentum returns (Nikkei 225)

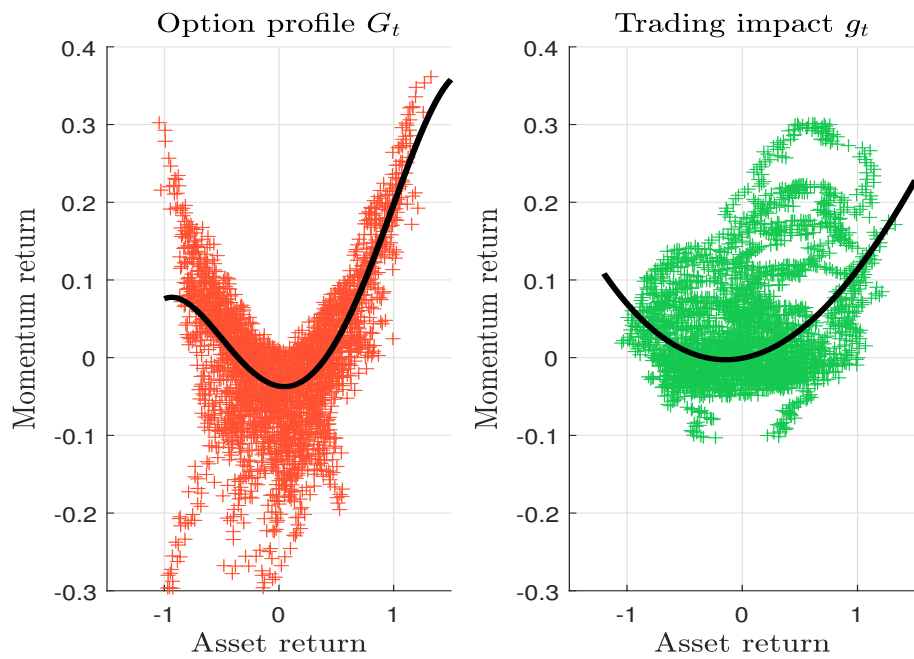


Figure 64: Correlation between the asset class trend-following strategy and the SG CTA Index

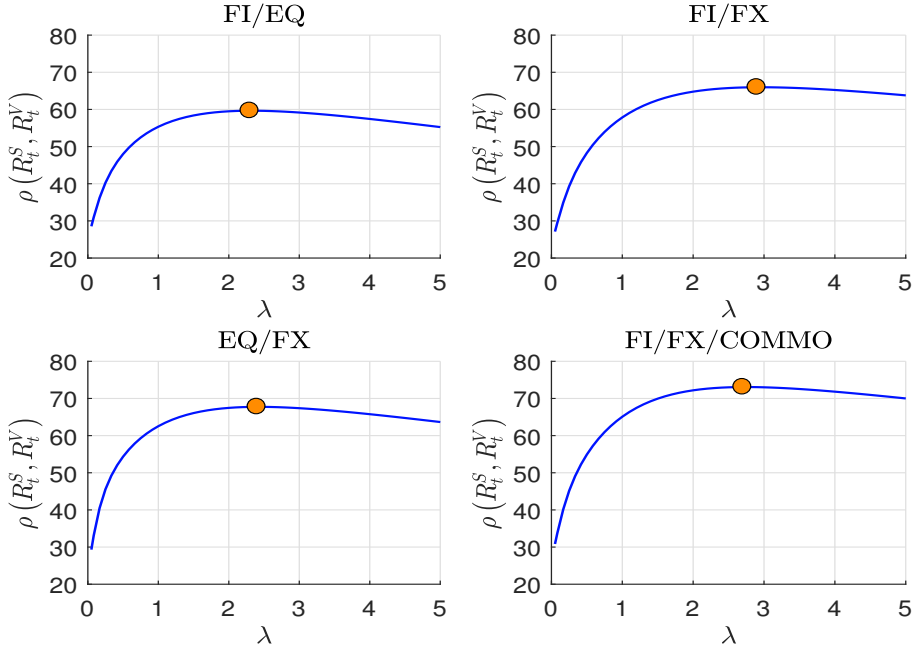


Figure 65: Comparison between the cumulative performance of the asset class trend-following strategy and the SG CTA Index

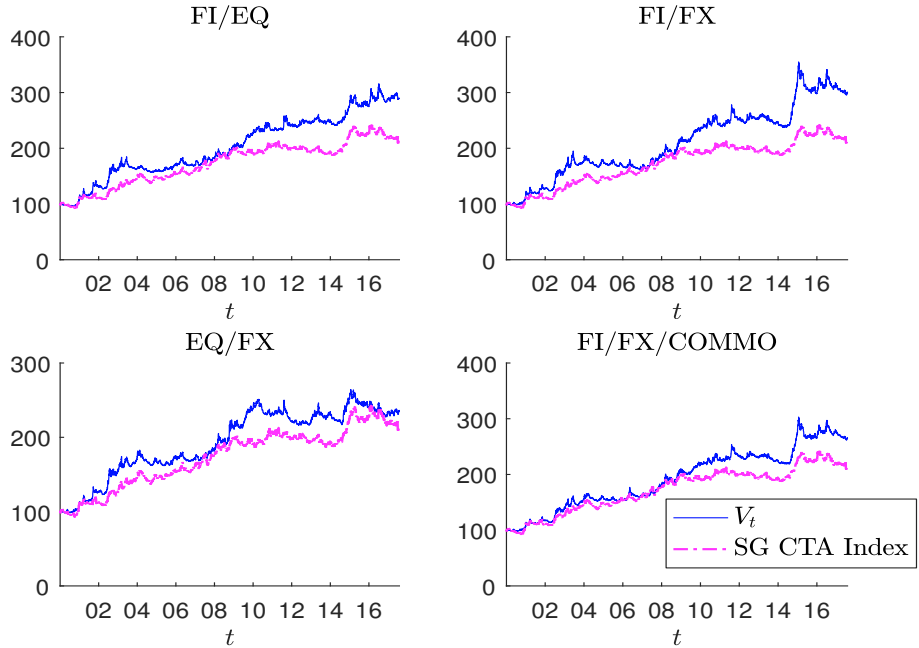


Figure 66: Option profile of the hedged strategy ($\alpha = 5, \hat{\mu}_0 = -30\%$)

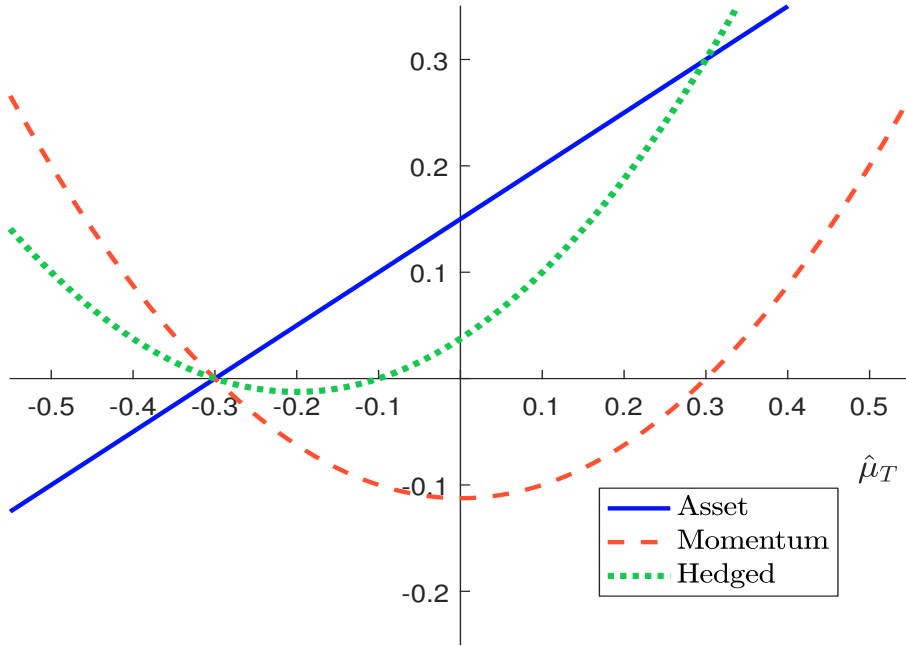


Figure 67: Option profile of the hedged strategy ($\alpha = 5, \hat{\mu}_0 = 30\%$)

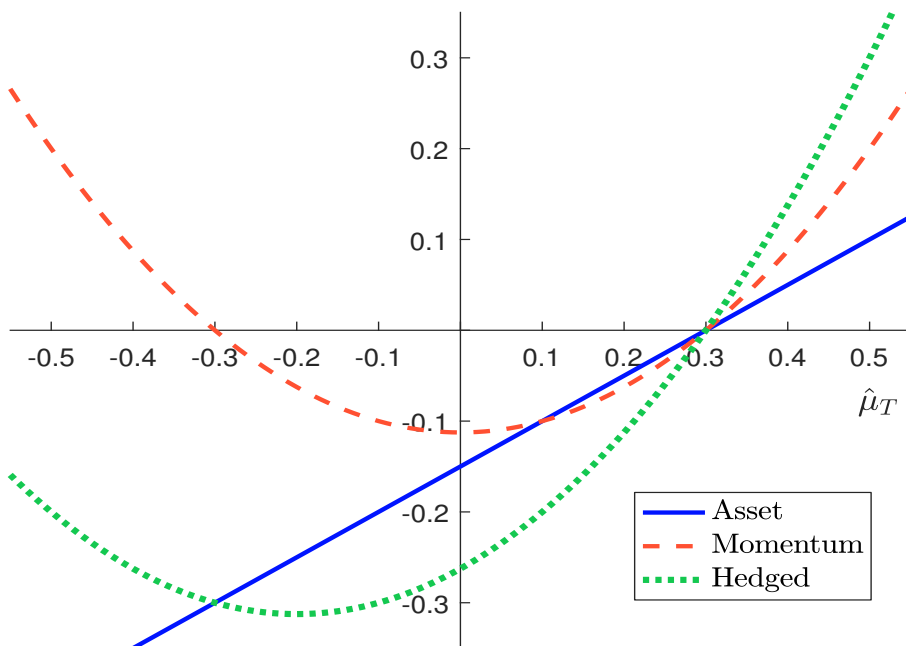


Figure 68: Probability density function of \tilde{g}_t ($s_t = -1$, $\alpha = 0.5$, $\lambda = 1$)

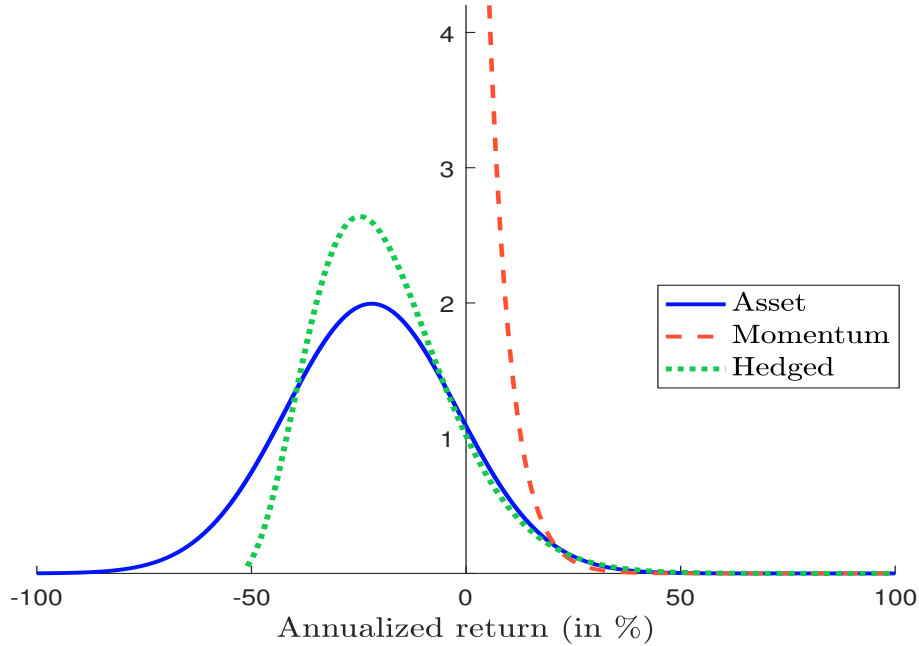


Figure 69: Cumulative distribution function of \tilde{g}_t ($s_t = -1$, $\alpha = 0.5$, $\lambda = 1$)

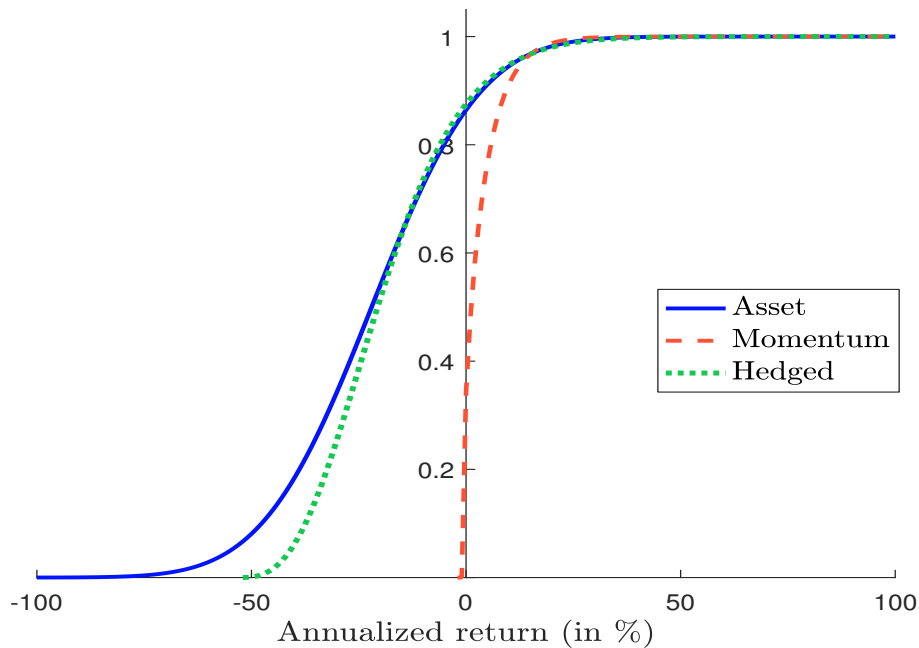


Figure 70: Probability density function of \tilde{g}_t ($s_t = 1$, $\alpha = 1.0$, $\lambda = 2$)

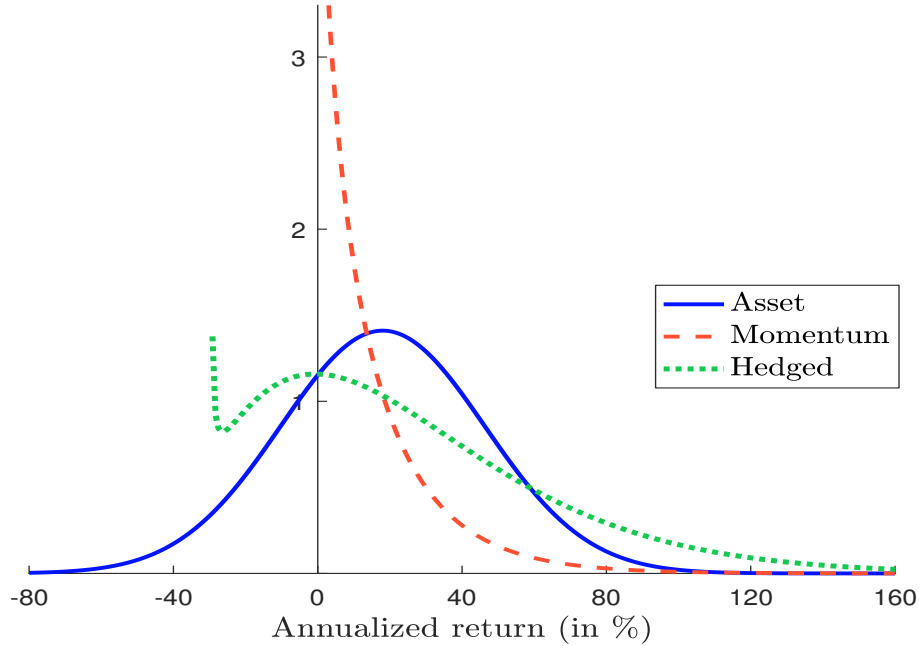


Figure 71: Cumulative distribution function of \tilde{g}_t ($s_t = 1$, $\alpha = 1.0$, $\lambda = 2$)

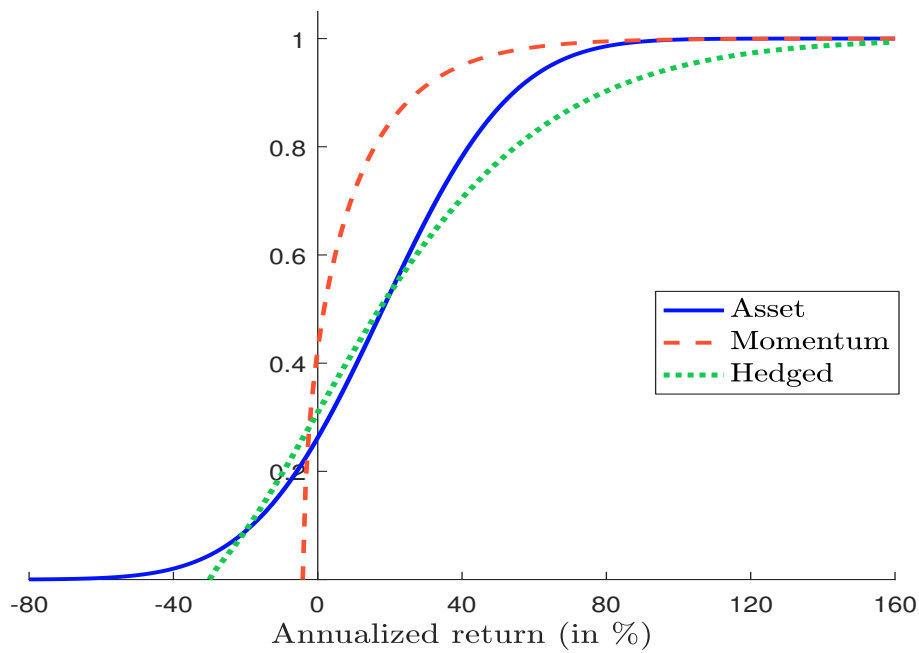


Figure 72: Probability density function of \tilde{g}_t ($s_t = 1$, $\alpha = 0.5$, $\lambda = 2$)

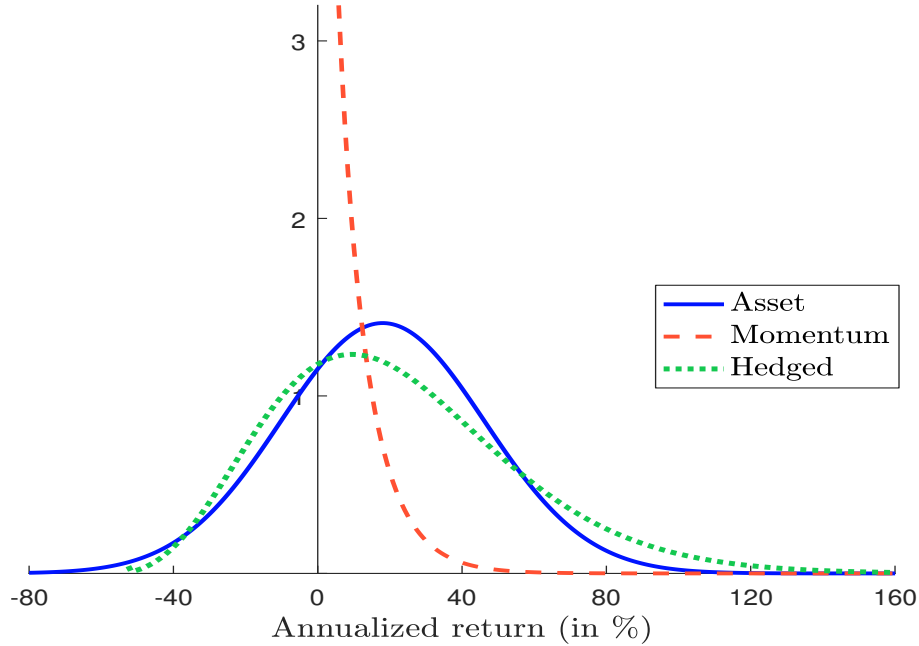


Figure 73: Cumulative distribution function of \tilde{g}_t ($s_t = 1$, $\alpha = 0.5$, $\lambda = 2$)

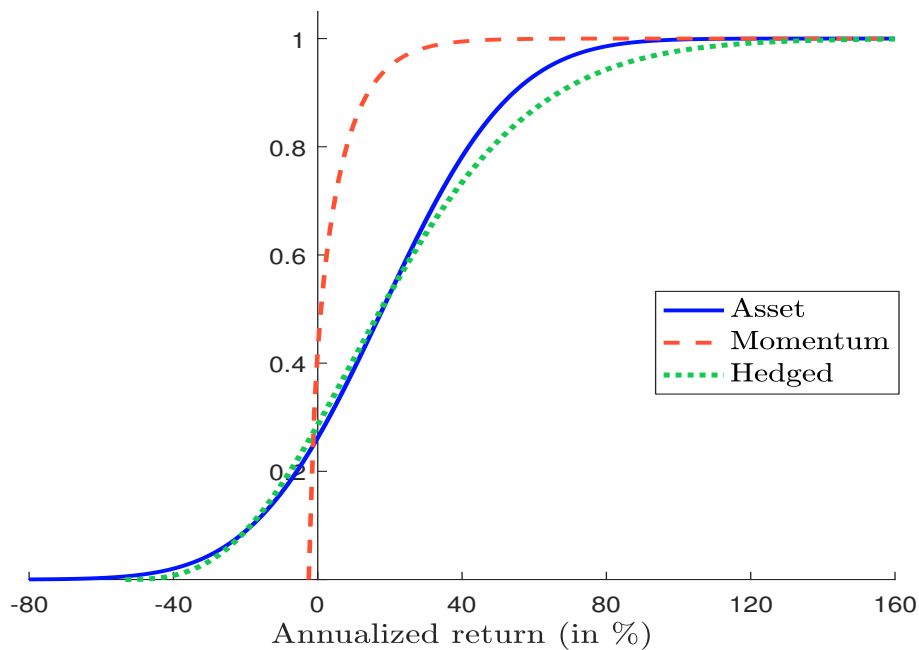
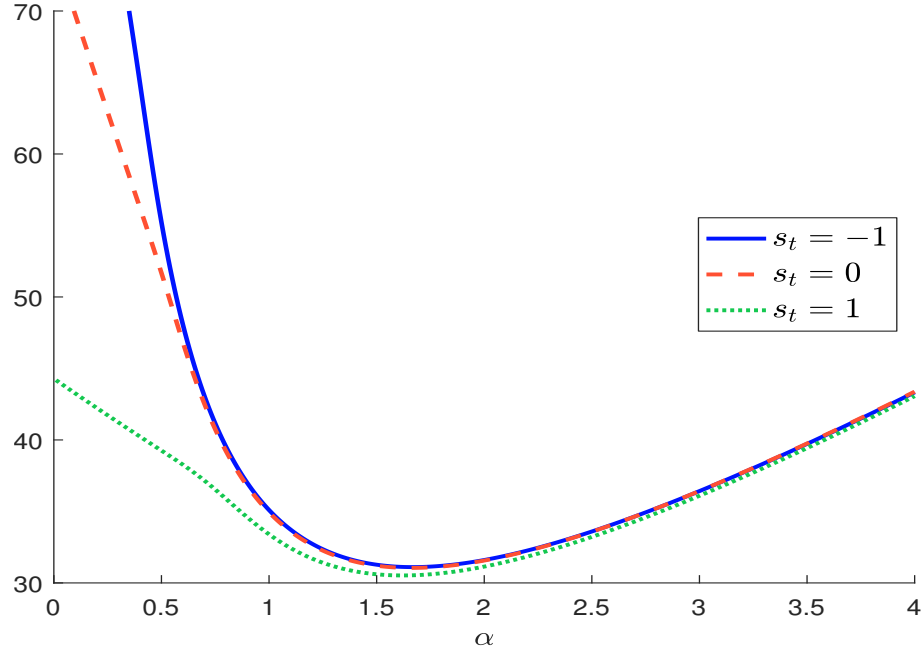


Figure 74: 95% Value-at-risk of the hedged strategy ($\sigma = 30\%$, $\lambda = 2$)

 Figure 75: Simulation of the cross-hedging strategy ($\delta = 0.40$)
